University of Hamburg,
Germany

European Organization for
Nuclear Research, Geneva,
Switzerland

Emittance Preservation at the LHC

Maria Kuhn
born October 17, 1987

MASTER THESIS

University of Hamburg

March 2013

supervised by:

Prof. Dr. Jörg Rossbach (University of Hamburg, Germany)

Dr. Verena Kain (CERN, Geneva, Switzerland)

CERN-THESIS-2013-031
05/04/2013

Abstract

The Large Hadron Collider (LHC) at CERN is a high energy storage ring that provides proton and heavy ion collisions to study fundamental particle processes. The luminosity production is tightly linked to emittance preservation in the accelerator. During the 2012 LHC proton run about 30 % of the potential luminosity performance was lost through the different phases of the LHC cycle, mainly due to blow-up of the transverse emittance. At the LHC design stage the total allowed emittance increase through the cycle was set to 7 %. A breakdown of the growth through the various phases in the LHC cycle is given, as well as a comparison with the data from the LHC experiments for the transverse beam size. In 2012 a number of possible causes and solutions of emittance blow-up in the LHC have been studied. Among the sources are intra-beam scattering and 50 Hz noise. A possible remedy for some of the growth is higher transverse damper gain. The results of the investigations are summarized in this thesis. Measuring the emittance growth is a difficult task with high intensity beams and changing energies. Accuracy and limitations of the LHC transverse profile monitors will be discussed. An outlook for future LHC upgrade scenarios with low emittance beams will be given.

Kurzfassung

Der Large Hadron Collider (LHC) am CERN ist ein Hochenergie Speicherring, in dem Protonen und Schwerionen kollidieren um Elementarteilchen zu studieren. Die Luminositätsproduktion ist eng mit der Emittanzerhaltung in dem Beschleuniger verbunden. Während des LHC Protonen Runs 2012 gingen ungefähr 30 % der potenziellen Luminositätsleistung in den verschiedenen Phasen des LHC Zyklus verloren. Dies wurde hauptsächlich durch das Aufblasen der transversalen Emittanz verursacht. Der Designwert für den gesamten erlaubten Emittanzanstieg durch den Zyklus ist 7 %. Eine Aufschlüsselung des Wachstums durch die verschiedenen Phasen des LHC Zyklus sowie ein Vergleich mit den Daten aus den LHC Experimenten für die transversale Strahlgrösse werden dargelegt. In 2012 wurde eine Reihe von möglichen Ursachen und Lösungen des Emittanzaufblasen im LHC untersucht. Unter den Gründen sind Intra-Beam Scattering und 50 Hz Rauschen. Eine mögliche Abhilfe für einen Teil des Wachstums ist höherer transversaler Damper Gain. Die Ergebnisse der Untersuchungen werden in dieser Arbeit zusammengefasst. Das Messen des Emittanzwachstums ist eine schwierige Aufgabe mit hohen Strahlintensitäten und sich ändernder Energie. Genauigkeit und Beschränkungen der transversalen Profilmonitore im LHC werden diskutiert. Es wird ein Ausblick auf zukünftige LHC Upgrade Szenarien mit kleinen Strahlemittanzen gegeben.

Acknowledgements

The measurements presented in this thesis would not have been possible without the help and advice from many colleagues. I am very grateful for our collaboration.

First and foremost, I would like to thank my supervisor at CERN, Verena Kain, for her support and encouragement. Her determination and competence carried this thesis. I appreciate her suggestions and contributions to this work. She always welcomes my ideas. Her supervision is magnificent.

I extend my gratitude to Jörg Rossbach, my supervisor at the University of Hamburg, for his wisdom and support. I am very thankful that he encourages my personal and professional development and that he shares his knowledge with me. His guidance is outstanding.

Special thanks are dedicated to Bernd Dehning, Jonathan Emery, Ana Guerrero, Federico Roncarolo, Mariusz Sapinski and George Trad for their effort to improve the LHC transverse profile monitors. Their support during measurements and for the analysis is priceless.

I would also like to express my gratitude to Wolfgang Höfle and Daniel Valuch who are responsible for the LHC transverse damper system. They supported many emittance growth investigations.

I am thankful for the collaboration with Michaela Schaumann for IBS simulations.

The assistance from Philippe Baudrenghien and his colleagues concerning RF batch-by-batch blow-up questions is very much acknowledged.

Ralph Steinhagen guided the noise studies discussed in this thesis. With his competence a source of emittance growth could be revealed.

I would also like to thank Gianluigi Arduini for many fruitful discussions.

I further appreciate the input and training opportunities given by Jörg Wenninger and Mike Lamont.

The help from everybody who proofread this thesis is gratefully acknowledged.

Last but not least, I thank my family and friends for personal and emotional support in all circumstances.

Contents

1. Introduction

1.1. The Large Hadron Collider (LHC) at the CERN Accelerator Complex

The Large Hadron Collider (LHC) [1] is part of the CERN (European Organization for Nuclear Research) accelerator complex and its main purpose is to provide particle beam collisions at high energies to find answers for unresolved questions in fundamental particle physics [2]. Four large experiments are stationed in the LHC interaction points to benefit from the collisions:

- ATLAS: A Toroidal LHC ApparatuS
- CMS: Compact Muon Solenoid
- LHCb: Large Hadron Collider beauty
- ALICE: A Large Ion Collider Experiment

The Standard Model of particle physics describes fundamental particles and interactions that form the Universe. Some theories of the Standard Model still need to be proven experimentally. One of these questions is the origin of the particles' masses. The Higgs Field is the key mechanism to the concept of mass in the Standard Model. The two LHC experiments ATLAS and CMS are searching for the Higgs Boson to prove the existence of the Higgs Field. They could already record successful results [3]. The LHC was able to achieve outstanding milestones in fundamental particle physics in 2011 and 2012.

Another theory these experiments are testing is Supersymmetry, which could possibly explain dark matter and dark energy that make up 96 % of the universe and cannot be described by the Standard Model.

The third LHC experiment, called LHCb, investigates the properties of antimatter to explore the question of the Universe's existence, for instance why there is more matter than antimatter in the Universe.

Finally, the ALICE experiment uses the LHC beam collisions to detect the creation of a quark-gluon plasma as it is believed to have existed just after the Big Bang, a state of matter where no nuclei or nuclear particles exist.

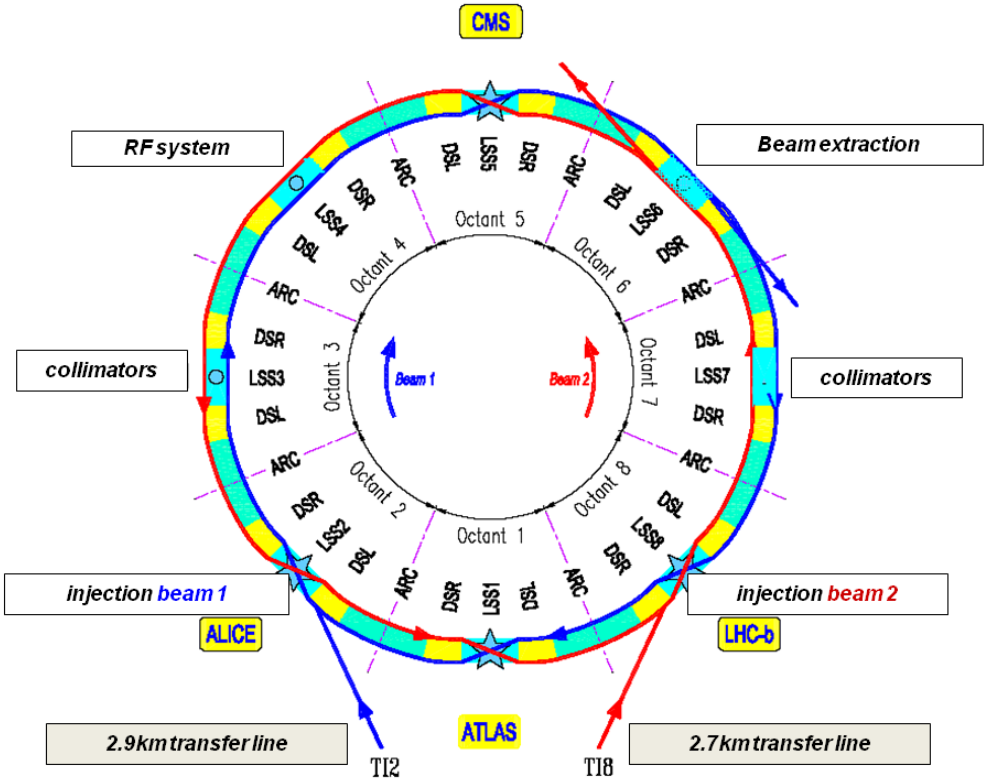

Figure 1.1.: LHC schematic layout [1]. Beam 1 circulates clockwise and Beam 2 counter-clockwise. The beams are injected through the transfer lines (TI) from the SPS. The four interaction points with detectors are ATLAS, ALICE, CMS and LHCb. The LHC is designed with eight identical arcs consisting in total of about 8000 superconducting magnets.

Moreover, all experiments look for clues of hidden dimensions of space as stated in the String Theory.

Figure 1.1 shows the LHC ring with the location of the four experiments ATLAS, CMS, LHCb and ALICE. The schematic displays the two counter-rotating beams and their four interaction points (IP). Beam 1 is circulating clockwise and beam 2 counter-clockwise.

The LHC has a circumference of about 27 km which makes it the world's largest accelerator. It is installed in the former LEP (Large Electron-Positron Collider) tunnel which is located 70 to 140 m below the earth's surface. The LHC is a hadron collider with a design energy of 7 TeV per charge. The two rings of the LHC are designed to be filled with protons (p) or ions (Pb). So far p-p, Pb-Pb and also p-Pb collisions have been produced in the LHC.

Superconducting magnets and accelerating cavities are installed in the LHC surrounded by a cryogenic system that makes the LHC the largest refrigerator in the world. For the cooling, superfluid Helium at 1.9 K is used. Inside the LHC the beam pipes are in a ultra-high vacuum with an internal pressure of 10^{-13} atm.

The LHC as part of the CERN accelerator complex is shown in Fig. 1.2. Most of the other CERN accelerators are combined to the LHC injector chain producing the beam for the LHC. This will be explained in the next section.

The LHC Injector Chain

The LHC cannot be run with beam energies below 450 GeV. The beam has to be pre-accelerated in the LHC injector chain [4]. In the following the production of high intensity proton bunches for the nominal case is explained. An overview is given in Table 1.1.

	Extraction energy [GeV]	**Number of bunches**
Booster	1.4	6
PS	26	72
SPS	450	288
LHC	7000	2808

Table 1.1.: Nominal LHC beam production scheme from the Booster to the LHC. The extraction energy (in the LHC: collision energy) and number of bunches for every accelerator is listed.

The protons are produced, bunched and pre-accelerated in the linear accelerator Linac2. Afterwards they enter the LHC injector chain with only circular accelerators. From Linac2 the protons are transferred to the Booster with an energy of 50 MeV.

The Booster has four identical rings that can be filled with two proton bunches each. For the nominal case only three rings are filled with one very high brightness bunch each. The Booster extraction energy is 1.4 GeV. The bunches are accelerated further to the Proton Synchrotron (PS). Two injections from the Booster (3 + 3 bunches) are needed to fill the PS ring with six bunches. Another nominal injection scheme suggests a single extraction of six bunches from the Booster to the PS at once with three rings of the Booster filled with two bunches. This single batch injection was used only in the early part of the first LHC run. Afterwards the filling scheme was changed to two batch injections from the Booster to the PS.

For the nominal bunch spacing of 25 ns the different radio frequency (RF) systems in the PS are used to split the bunches from the Booster. The six bunches are separated into 72 bunches, 25 ns spaced. The protons in the PS reach an extraction energy of about 26 GeV before they are injected into the Super Proton Synchrotron (SPS).

The SPS can be filled with four injections of 72 bunches from the PS. At flattop energy of the SPS, which is 450 GeV, the protons are extracted towards the LHC into two transfer lines (TI2 and TI8). The nominal batch consists of 288 bunches

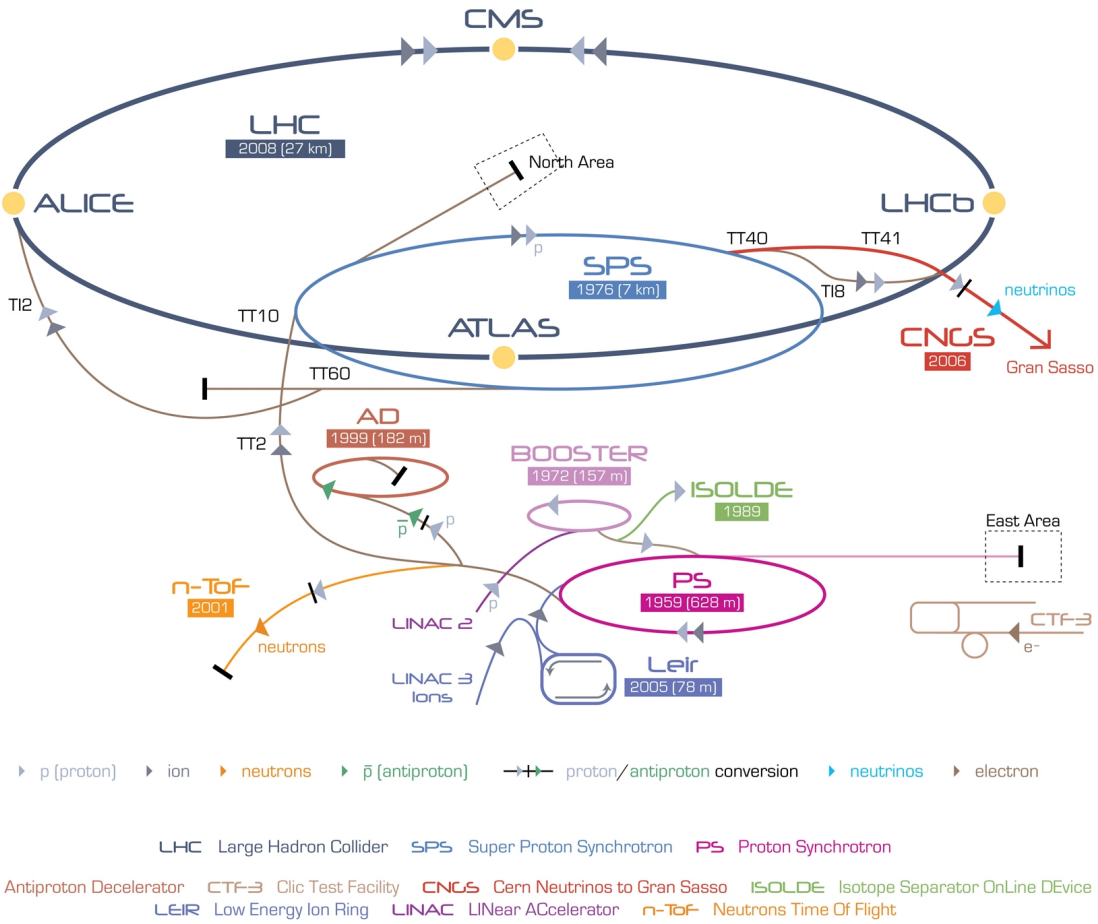

Figure 1.2.: The CERN accelerator complex [2]. All CERN accelerators and experiments with beam are shown. The acceleration chain of the protons to the LHC is: Linac2 $\longrightarrow$ Booster $\longrightarrow$ PS $\longrightarrow$ SPS $\longrightarrow$ LHC.

with an intensity of 1.15×10^{11} protons per bunch (ppb) and a transverse normalized emittance of 3.5 μm at 450 GeV injection energy.

For the nominal filling scheme 12 injections per ring are necessary to fill the LHC with 25 ns bunch spacing to get a total number of 2808 bunches per ring.

Due to limitations created by electron cloud effects the bunch spacing in 2011 and 2012 was increased to 50 ns [5]. That means the six bunches from the Booster are split into only 36 bunches in the PS instead of 72. The final number of bunches in the LHC for the filling scheme in 2012 was 1374.

Once the injection process into the LHC is completed, the proton bunches are accelerated to 7 TeV in the nominal case and the beta functions at the experiments are squeezed to a minimum. Then the beams go into collisions and the LHC becomes a high energy storage ring. The protons collide at four points in the ring, where the important LHC experiments are located: ATLAS, CMS, LHCb and ALICE.

The LHC is fully operational since 2010 [1] with reduced collision energy (3.5 TeV

[1]During the 2010 LHC proton run, the machine was commissioned with beam. First collisions at 3.5 TeV took place on March 30^{th}, 2010.

in 2011, 4 TeV in 2012). The design collision energy will be reached after the first long LHC maintenance period in 2013/14.

1.2. Collider Performance and Emittance

The main parameter to measure the performance of a collider is the luminosity L. The product of luminosity and interaction cross-section of the two beams σ_p is directly proportional to the collision rate $\frac{dN_p}{dt}$ and indirectly proportional to the transverse beam size at the interaction point:

$$\frac{dN_p}{dt} = \sigma_p L. \tag{1.2.1}$$

The machine parameters define the luminosity. In a first approximation the luminosity is given by:

$$L = \frac{f_{rev} n_b}{4\pi} \cdot \frac{N_1 N_2}{\sigma_1 \sigma_2} \propto f_{rev} n_b \cdot \frac{N_1 N_2}{\varepsilon}, \tag{1.2.2}$$

where f_{rev} is the revolution frequency, n_b is the number of bunches per beam, N_1 and N_2 are the number of protons per bunch for beam 1 and beam 2 and σ_1 and σ_2 are the transverse beam sizes of beam 1 and beam 2 at the interaction point, respectively.

The LHC design peak luminosity at the interaction points of ATLAS (IP1) and CMS (IP5) is 10^{34} cm^{-2}s^{-1} with a nominal collision rate of 19.02 events per bunch crossing for a total cross section of 100 mb [1].

The transverse beam size is proportional to the square root of a parameter called emittance ε. The concept of emittance will be introduced in detail in this thesis. To maximize luminosity, beams with a large number of bunches and high bunch intensities are required, as well as small transverse emittances. In an ideal synchrotron the normalized transverse emittance is preserved. Disturbing effects lead, in general, to emittance growth [6]. To achieve maximum performance, the LHC injectors have to produce beams with as small emittances as possible. The challenge of the LHC is to conserve the small emittances through the cycle until the beams are brought into collision.

In this thesis the LHC performance in terms of emittance preservation will be quantified. The different ways of measuring emittance will be introduced and the emittance evolution through the LHC cycle will be discussed. Finally, solutions to counteract the emittance growth in the LHC and an outlook to emittance blow-up for future LHC beams will be given.

2. Introduction to Basic Accelerator Physics and Concept of Emittance

This chapter is aimed at introducing the basic principles of high energy particle accelerators. The linear transverse motion in the accelerator and the concept of emittance will be discussed in detail.

2.1. Lorentz Forces

Charged particles gain energy by accelerating them in electromagnetic fields. The driving force is the Lorentz force [7]:

$$\vec{F} = e \cdot \left(\vec{E} + \vec{v} \times \vec{B} \right), \tag{2.1.1}$$

where e is the elementary charge, the vectors $\vec{E}$ and $\vec{B}$ are the electric and the magnetic field vectors, respectively, and $\vec{v}$ is the velocity vector of the particle. Only electric fields lead to an increased energy with $\mathcal{E} = \int \vec{F} d\vec{r}$ [1] for a particle with charge e.

The construction of an accelerator determines the design orbit. To keep the particles on the reference path, which might be curved, bending and focusing magnets are needed. Both bending and focusing is accomplished by electromagnetic forces.

The particles in high energy accelerators have velocities $v \approx c$. In this case:

$$|\vec{E}| = c \cdot |\vec{B}|. \tag{2.1.2}$$

So that a magnetic field of 1 T corresponds to an electric field of 300 MV/m. Electric fields of this strength are technically not feasible. High energy accelerators therefore rely only on magnetic fields for bending and focusing.

Beam dynamics and optics describe the evolution of the particle orbit under the Lorentz forces. The main task in beam optics is to transport a charged particle from an arbitrary starting point to a final point along the beam line. The collection of bending and focusing magnets along the ideal path is called the magnet lattice.

[1] The particle's velocity $\vec{v}$ is parallel to $\vec{r}$, the vector of the longitudinal particle motion, thus $\vec{v} \times \vec{B}$ is perpendicular to $\vec{r}$. Therefore the magnetic term cancels out in the energy relation.

2.2. Betatron Oscillations

The coordinates in six-dimensional phase space describing the particle motion in an accelerator are [7]

$$\vec{X}(s) = \begin{pmatrix} x \\ x' \\ y \\ y' \\ l \\ \frac{\Delta p}{p} \end{pmatrix}. \tag{2.2.1}$$

The ideal orbit for the charged particle beam designed by the beam transport system is called the reference trajectory s. The deviation of a particle from the reference path in the deflecting plane is u. Where u can be either x or y. The derivatives $x' = \frac{dx}{ds}$ and $y' = \frac{dy}{ds}$ describe the horizontal and vertical slopes with respect to s. The coordinate l is the longitudinal displacement from the particle on the ideal path and $\frac{\Delta p}{p}$ is the relative momentum deviation from a particle with the ideal momentum p. The geometrical coordinate system is displayed in Fig. 2.1. The origin of the coordinate system (x, y, s) moves along the orbit of the longitudinal particle motion.

From Newton's second law the general equation of motion for a particle with charge e in a magnetic field without acceleration ($\vec{E} = 0$) is [6]

$$\vec{F} = \frac{d\vec{p}}{dt} = \frac{d}{dt}\left(m_0 \gamma \vec{v}\right) = e\left(\vec{v} \times \vec{B}\right). \tag{2.2.2}$$

Assuming a planar circular accelerator with a curvature in the horizontal plane, the coordinate system only rotates around the y-axis. The deflection angle is φ and the path element of a curved trajectory with radius R is $ds = Rd\varphi$.

If the magnetic field only has transverse components, $\vec{B} = (B_x, B_y, 0)$, the equation of motion can be written as

$$x'' = \frac{1}{R}\left(1 + \frac{x}{R}\right) - \left(1 + \frac{x}{R}\right)^2 \frac{eB_y}{p}, \tag{2.2.3}$$

$$y'' = \left(1 + \frac{x}{R}\right)\frac{eB_x}{p}. \tag{2.2.4}$$

The deduction can be found in [6]. With a small momentum deviation $\frac{\Delta p}{p}$ the evolution of the momentum to first order is

$$\frac{1}{p_d} = \frac{1}{p}\left(1 - \frac{\Delta p}{p}\right), \tag{2.2.5}$$

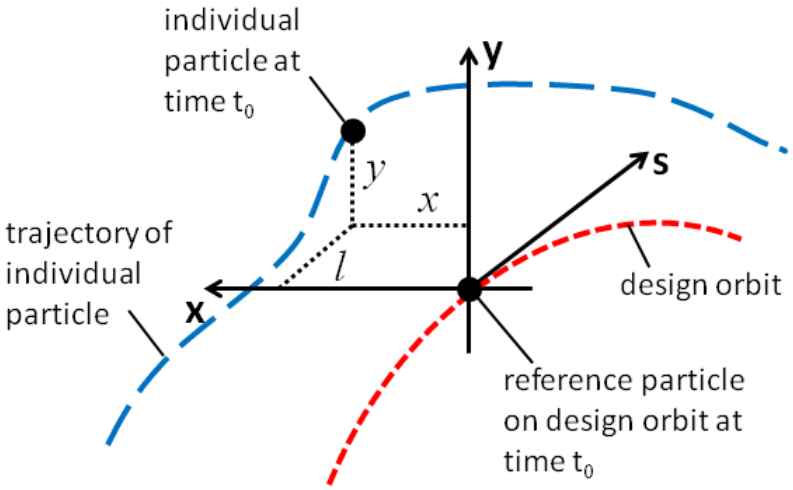

Figure 2.1.: Geometric coordinate system (x, y, s) with the design orbit (red) and a particle's trajectory (blue).

where p_d is the particle momentum which differs from the ideal momentum. Assuming only horizontal deflecting dipoles with a strength $\frac{1}{R}$ and quadrupoles with strength k the magnet field components can be written as

$$\frac{e}{p}B_y = \frac{1}{R} - kx, \qquad \frac{e}{p}B_x = -ky. \tag{2.2.6}$$

Then Eq. 2.2.3 and Eq. 2.2.4 transform to

$$x'' = \frac{1}{R}\left(1+\frac{x}{R}\right) - \left(1+\frac{x}{R}\right)^2\left(\frac{1}{R}-kx\right)\left(1-\frac{\Delta p}{p}\right) \tag{2.2.7}$$

$$y'' = -\left(1+\frac{x}{R}\right)^2 ky\left(1-\frac{\Delta p}{p}\right). \tag{2.2.8}$$

With $x \ll R$, $y \ll R$ and $\frac{\Delta p}{p} \ll 1$ the equations simplify to the linear equations of motion for a charged particle moving through the magnetic lattice depending on the longitudinal position s in the accelerator

$$x''(s) - x(s)\left(k(s) - \frac{1}{R^2(s)}\right) = \frac{1}{R(s)}\frac{\Delta p}{p} \tag{2.2.9}$$

$$y''(s) + k(s)y(s) = 0. \tag{2.2.10}$$

These are the basic equations to calculate the particle motion through linear beam optics [6].

In the special case where there is no bending of the beam, $\frac{1}{R} = 0$, and for a non-dispersive trajectory, $\frac{\Delta p}{p} = 0$, the linear equations of motion transforms to a

homogeneous differential equation [7]

$$u''(s) \mp k(s)u(s) = 0. \tag{2.2.11}$$

For any point s of the trajectory the solutions of Eq. 2.2.11 are

$$\begin{aligned} u(s) &= C(s)u_0 + S(s)u_0', \\ u'(s) &= C'(s)u_0 + S'(s)u_0', \end{aligned} \tag{2.2.12}$$

which can be written in matrix notation:

$$\begin{pmatrix} u(s) \\ u'(s) \end{pmatrix} = \underbrace{\begin{pmatrix} C(s) & S(s) \\ C'(s) & S'(s) \end{pmatrix}}_{\text{transfer matrix}} \begin{pmatrix} u_0 \\ u_0' \end{pmatrix}, \tag{2.2.13}$$

where the index 0 describes the initial parameters at $s = s_0$.

Solution of Hill's Equation

The particle trajectory in the horizontal plane is solution to the homogeneous differential Hill equation:

$$x''(s) - k(s)x(s) = 0. \tag{2.2.14}$$

The function $x(s)$ defines a transverse motion around the design orbit, called betatron oscillation. The oscillation amplitude and phase depend on the longitudinal position s in the accelerator. The Hill equation is solved with the ansatz:

$$x(s) = a \cdot q(s)\cos(\psi(s) + \phi), \tag{2.2.15}$$

where a is the constant amplitude of the oscillation and ϕ is the constant initial phase. Inserting this solution into Hill's equation, Eq. 2.2.14, yields

$$q''(s) - q(s)\psi'(s)^2 - k(s)q(s) = 0, \tag{2.2.16}$$

$$2q'(s)\psi'(s) + q(s)\psi''(s) = 0. \tag{2.2.17}$$

Integrating Eq. 2.2.17 leads to

$$\psi(s) = \int_0^s \frac{d\lambda}{q^2(\lambda)}. \tag{2.2.18}$$

Using this result for $\psi(s)$, Eq. 2.2.16 can be written as

$$q''(s) - \frac{1}{q^3(s)} - k(s)q(s) = 0, \tag{2.2.19}$$

with the definition

$$\beta(s) \equiv q^2(s). \tag{2.2.20}$$

Thus the solution to Hill's equation $x(s)$ and its derivative $x'(s)$ with respect to s, as well as the phase $\psi(s)$ are

$$\begin{aligned} x(s) &= a\sqrt{\beta(s)}\cos(\psi(s)+\phi), & (2.2.21)\\ x'(s) &= -\frac{a}{\sqrt{\beta(s)}}\left(\alpha(s)\cos(\psi(s)+\phi)+\sin(\psi(s)+\phi)\right), & (2.2.22)\\ \psi(s) &= \int_0^s \frac{d\lambda}{\beta(\lambda)}, & (2.2.23) \end{aligned}$$

where $\beta(s)$ is the well-known beta function. The definition of $\alpha(s)$ is:

$$\alpha(s) \equiv -\frac{\beta'(s)}{2}. \tag{2.2.24}$$

The derivative $\beta'(s)$ is taken with respect to s. The functions $\alpha(s)$, $\beta(s)$ and $\psi(s)$ are called lattice or optics functions. They are defined by the magnetic structure of the accelerator.

The number of betatron oscillations per revolution 2π is called the tune Q [6]:

$$Q = \frac{1}{2\pi}\int_0^L \frac{d\lambda}{\beta(\lambda)}, \tag{2.2.25}$$

where L is the circumference of the accelerator.

In matrix notation the transfer from a starting point s_0 with optical functions α_0 and β_0 to the end of the structure where the optical functions are $\alpha(s)$ and $\beta(s)$ is

$$\boldsymbol{M} = \begin{pmatrix} \sqrt{\frac{\beta}{\beta_0}}(\cos\Delta\psi + \alpha_0\sin\Delta\psi) & \sqrt{\beta\beta_0}\sin\Delta\psi \\ \frac{(\alpha-\alpha_0)\cos\Delta\psi - (1+\alpha_0\alpha)\sin\Delta\psi}{\sqrt{\beta\beta_0}} & \sqrt{\frac{\beta}{\beta_0}}(\cos\Delta\psi - \alpha\sin\Delta\psi) \end{pmatrix}, \tag{2.2.26}$$

with the phase advance $\Delta\psi$ of the betatron oscillation between s and s_0. In this way any point of the particle trajectory in the accelerator can be calculated.

2.3. Dispersion

In the six-dimensional phase space a particle on the design orbit also has the ideal momentum p. Inside a bending magnet with homogeneous magnet field and no gradient, however, particles with momentum offset move on different trajectories.

For a particle with a momentum offset $\frac{\Delta p}{p} \neq 0$ the equation of motion becomes

$$x'' + \frac{1}{R^2}x = \frac{1}{R}\frac{\Delta p}{p}, \tag{2.3.1}$$

where R is the radius of curvature of the particle trajectory. Introducing a dispersion function $D(s)$ for which $\frac{\Delta p}{p} = 1$ yields

$$D''(s) + \frac{1}{R^2}D(s) = \frac{1}{R}. \tag{2.3.2}$$

This is an inhomogeneous differential equation that can be solved with the already known solution of the homogeneous equation and any particular solution to the inhomogeneous equation. The deduction can be found in [6]. Finally the dispersion function can be written as

$$D(s) = D_0 \cos\left(\frac{s}{R}\right) + D_0' R \sin\left(\frac{s}{R}\right) + R\left(1 - \cos\left(\frac{s}{R}\right)\right), \tag{2.3.3}$$

$$D'(s) = -\frac{D_0}{R}\sin\left(\frac{s}{R}\right) + D_0' \cos\left(\frac{s}{R}\right) + \sin\left(\frac{s}{R}\right). \tag{2.3.4}$$

In regions with non-zero dispersion the transverse position of the particle with momentum deviation $\frac{\Delta p}{p}$ changes to

$$x_g(s) = x(s) + x_D(s) = x(s) + D(s)\frac{\Delta p}{p}, \tag{2.3.5}$$

with an offset $x_D(s)$ with respect to the position $x(s)$ of a particle with no dispersion. The dispersive trajectory is determined by $\frac{\Delta p}{p}$ [6].

2.4. Emittance and Emittance Preservation

The solution of the linear equation, Eq. 2.2.21, has the invariant of motion in phase space [6]

$$\gamma(s)x^2(s) + 2\alpha(s)x(s)x'(s) + \beta(s)x'^2(s) = a^2 = const., \tag{2.4.1}$$

where πa^2 is the area of the ellipse and α , β and γ are the optical functions, also referred to as twiss parameters. The relation between those three functions is:

$$\gamma \equiv \frac{1 + \alpha^2}{\beta}. \tag{2.4.2}$$

The invariant is called Courant-Snyder invariant. Equation 2.4.1 describes a skew ellipse in phase space (x, x') as shown in Fig. 2.2. For a periodic lattice, such as a circular machine, where $\beta(s + L) = \beta(s)$, $\alpha(s + L) = \alpha(s)$ and $\gamma(s + L) = \gamma(s)$, a particle's position and angle after one period must again lie on the same ellipse as

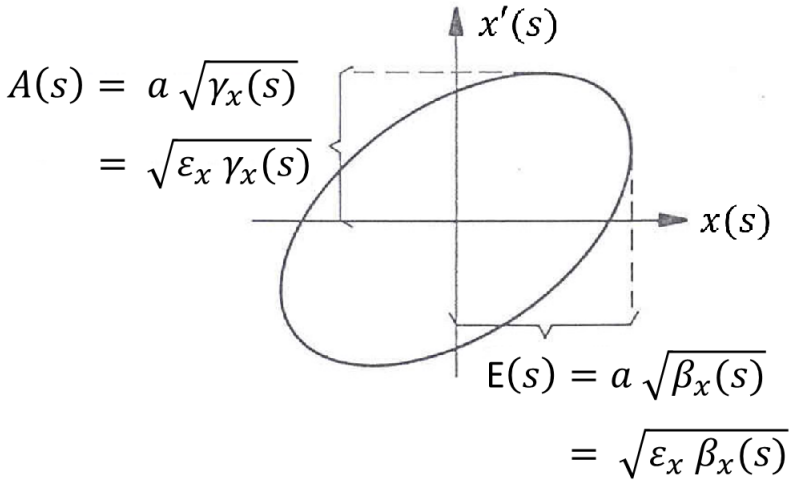

Figure 2.2.: A phase space ellipse in the horizontal plane. $E(s)$ is called beam envelope, $A(s)$ divergence.

on the previous pass.

For a beam of particles, there is a whole family of similar ellipses, centered around the origin. All ellipses have the same orientation. A particle which is contained inside an ellipse returns to a point inside the ellipse on a consecutive of the periodic motion through the accelerator. The emittance ε is defined as the ellipse

$$\gamma x^2 + 2\alpha x x' + \beta x'^2 = \varepsilon, \tag{2.4.3}$$

containing a fraction of particles of the beam. This ellipse will always contain the same fraction of beam on consecutive turns. In case of a Gaussian particle distribution

$$\rho(x,y) = \frac{Ne}{2\pi\sigma_x\sigma_y}\exp\left(-\frac{x^2}{2\sigma_x^2} - \frac{y^2}{2\sigma_y^2}\right), \tag{2.4.4}$$

with the horizontal and vertical beam sizes σ_x and σ_y, the emittance for a particular plane is defined as the ellipse with the fraction of beam contained within one σ_u $(u = x, y)$. The beam envelope $E(s)$ of this ellipse equals therefore

$$E(s) = \sigma_u = \sqrt{\varepsilon_u \beta_u(s)}. \tag{2.4.5}$$

Another important parameter of the phase space ellipse is the beam divergence $A(s)$:

$$A(s) = \sqrt{\varepsilon\left(\frac{1+\alpha_u^2(s)}{\beta_u(s)}\right)} = \sqrt{\varepsilon_u \gamma_u(s)}. \tag{2.4.6}$$

The emittance of the particle beam ε_{stat} is then defined in a statistical way: it is the ellipse which contains the particles within one standard deviation around the

mean of the Gaussian distribution such that its beam envelope yields [6]

$$\varepsilon_{stat} = \varepsilon = \frac{\sigma^2(s)}{\beta(s)}. \tag{2.4.7}$$

The emittance is energy dependent. The conserved quantity, the normalized emittance, is defined as:

$$\varepsilon_N = \left(\frac{p}{m_0 c}\right)\varepsilon, \tag{2.4.8}$$

where p is the momentum and m_0 is the particle's rest mass. As proven by Liouville's Theorem, the normalized emittance stays constant during acceleration for particles in an accelerator [8], as derived in the next section.

The unit of the emittance used in this thesis is [μm]. Note that other conventions sometimes use [mm·mrad].

2.4.1. Liouville's Theorem

The area of the ellipse containing always the same fraction of the beam, meaning the emittance, remains constant when the particle beam is transformed through the accelerator. This is the principle of Liouville's Theorem [8]. It postulates the conservation of a particle density in phase space for non-dissipative systems.

To prove this theorem, it has to be verified that the total time derivative, $\frac{d}{dt}$, of a particle phase space density vanishes, which means that the phase space density stays constant under the influence of conservative forces.

A conservative system with a general set of coordinates $(q_1(t), \ldots, q_n(t), p_1(t), \ldots, p_n(t))$ can be described by the Hamiltonian $H(q_1, \ldots, q_n, p_1, \ldots, p_n)$ and the Hamiltonian equations [7]:

$$\frac{\partial q_i}{\partial t} = \dot{q}_i = \frac{\partial H}{\partial p_i}, \qquad \frac{\partial p_i}{\partial t} = \dot{p}_i = -\frac{\partial H}{\partial q_i}. \tag{2.4.9}$$

First, the total derivative of the phase space density $\rho(q_1, \ldots, q_n, p_1, \ldots, p_n)$ is calculated:

$$\begin{aligned} \frac{d\rho}{dt} &= \frac{\partial \rho}{\partial t} + \sum_i \frac{\partial \rho}{\partial q_i}\frac{\partial q_i}{\partial t} + \sum_i \frac{\partial \rho}{\partial p_i}\frac{\partial p_i}{\partial t}, \\ &= \frac{\partial \rho}{\partial t} + \sum_i \frac{\partial \rho}{\partial q_i}\dot{q}_i + \sum_i \frac{\partial \rho}{\partial p_i}\dot{p}_i. \end{aligned} \tag{2.4.10}$$

To prove that $\dfrac{d\rho}{dt}$ vanishes, a phase space current $\vec{v}\cdot\rho$ is defined with $\vec{v}(\dot{q}_1, \ldots, \dot{q}_n, \dot{p}_1, \ldots, \dot{p}_n)$. The continuity equation for this current is

$$0 = \frac{\partial \rho}{\partial t} + \vec{\nabla}(\rho\vec{v}), \tag{2.4.11}$$

stating that the total number of particles in the beam is constant. Equation 2.4.11 gives

$$0 = \frac{\partial \rho}{\partial t} + \sum_i \frac{\partial(\rho \dot{q}_i)}{\partial q_i} + \sum_i \frac{\partial(\rho \dot{p}_i)}{\partial p_i}, \tag{2.4.12}$$

$$0 = \frac{\partial \rho}{\partial t} + \sum_i \frac{\partial \rho}{\partial q_i}\dot{q}_i + \rho \sum_i \frac{\partial \dot{q}_i}{\partial q_i} + \sum_i \frac{\partial \rho}{\partial p_i}\dot{p}_i + \rho \sum_i \frac{\partial \dot{p}_i}{\partial p_i}. \tag{2.4.13}$$

Inserting Eq. 2.4.10 yields

$$0 = \frac{d\rho}{dt} + \rho \sum_i \left(\frac{\partial \dot{q}_i}{\partial q_i} + \frac{\partial \dot{p}_i}{\partial p_i} \right), \tag{2.4.14}$$

$$0 = \frac{d\rho}{dt} + \rho \sum_i \underbrace{\left(\frac{\partial^2 H}{\partial q_i \partial p_i} - \frac{\partial^2 H}{\partial p_i \partial q_i} \right)}_{=0}, \tag{2.4.15}$$

$$0 = \frac{d\rho}{dt}, \tag{2.4.16}$$

which proves the invariance of the phase space density.

3. Causes for Emittance Blow-Up

For the luminosity of a collider, it is important to produce and preserve small emittances. Contrary to Liouville's Theorem, the emittance can blow up in an accelerator. There are effects that cause the transverse beam size to increase or decrease. The total allowed emittance increase in the LHC is 7 % [4]. Each effect that increases the emittance has to be studied thoroughly and kept at minimum. In this chapter some effects leading to measurable emittance growth in the LHC are discussed. Other diffusion and scattering processes are explained in [9].

3.1. Injection Mismatch

One of the import effects of emittance growth is injection mismatch. During the transfer and injection to the LHC, errors can occur that lead to emittance growth. Steering errors, injection oscillations and the complementary transverse damper system will be discussed. A full list of possible LHC injection errors can be found in [10].

To preserve the beam quality from the injectors to the LHC, it is necessary to match the beam trajectory, amplitude functions and dispersion functions at the transfer from one accelerator to the next. Amplitude function mismatch is caused by focusing errors while the displacement from the design orbit at injection is caused by steering errors that create injection oscillations [9].

3.1.1. Focusing Errors

A beam has a mismatched amplitude function when the twiss parameters of the beam, α, β and γ, are not the same as the lattice functions, α_0, β_0 and γ_0, at the injection point to the LHC. Errors in the SPS, the transfer line or the LHC can lead to such betatron mismatch. Then the emittance increase due to focusing errors is

$$\frac{\varepsilon}{\varepsilon_0} = \frac{1}{2}\left(\beta\gamma_0 + \beta_0\gamma - \alpha\alpha_0\right), \tag{3.1.1}$$

where ε_0 is the beam emittance with perfectly matched lattice functions and ε the beam emittance with betatron function mismatch. This emittance blow-up depends on the incoming emittance. If the initial beam distribution is Gaussian, the mismatched distribution will still be Gaussian, but with a larger phase space ellipse.

The amplitude function must be severely mismatched to increase the emittance significantly [9].

3.1.2. Steering Errors and Transverse Damper

If the particle phase space distribution is transferred mismatched with a displacement from the ideal orbit the phase space area increases. With non-linear magnetic field components the betatron oscillation frequency depends on the oscillation amplitude. As a result of the incoherent particle motion, the beam distribution filaments and over time the emittance increases. Injection with an offset from the ideal orbit causes injection oscillations. These injection oscillations blow up the transverse emittance by

$$\frac{\varepsilon}{\varepsilon_0} = 1 + \frac{1}{2}\frac{\Delta x^2 + (\beta\Delta x' + \alpha\Delta x)^2}{\beta\varepsilon_0} \equiv 1 + \frac{1}{2}\Delta e^2, \tag{3.1.2}$$

where Δx and $\Delta x'$ are the displacements in phase space from the ideal orbit at the injection point, α and β are the twiss parameters of the emittance ε after filamentation, and ε_0 is the emittance of the incoming beam. The filamentation time τ_f in the LHC is 68 ms [11]. The emittance increase is independent of the initial emittance. Assuming incoming beams with a Gaussian distribution, the emittance growth from steering errors afflicts the phase space ellipse. The particle distribution can be disturbed severely so that it is no longer Gaussian [9].

The LHC has to allow a certain margin for injection oscillations due to shot-by-shot variations and drifts of the transfer lines, and SPS extraction and LHC injection kicker ripples [1] [12]. Injection oscillation amplitudes of up to $\pm$ 1.5 mm occur before correction. To guarantee emittance preservation at injection, the steering errors are compensated by damping the injection oscillation through an external system that provides a damping time τ_d much smaller than the filamentation time, $\tau_d \ll \tau_f$. At the presence of a damping system, the emittance blow-up due to steering errors is

$$\frac{\varepsilon}{\varepsilon_0} = 1 + \frac{1}{2}\Delta e^2 \left(\frac{1}{1 + \tau_f/\tau_d}\right). \tag{3.1.3}$$

The LHC transverse damper system (ADT) can damp oscillations of up to 4 mm in less than 50 turns. The transverse damper gain can be adjusted to vary the damping time if needed [12].

In the LHC there are four independent ADT systems for each beam and plane. The four ADT pick-ups measure the bunch position and kick the bunches back onto the ideal orbit on the next turn [13].

An example measurement of injection oscillations damped by the ADT is shown in Fig. 3.1. At injection of Fill 1268 the transverse injection oscillations are measured

[1] For SPS extraction and LHC injection fast pulsed kicker magnets are used.

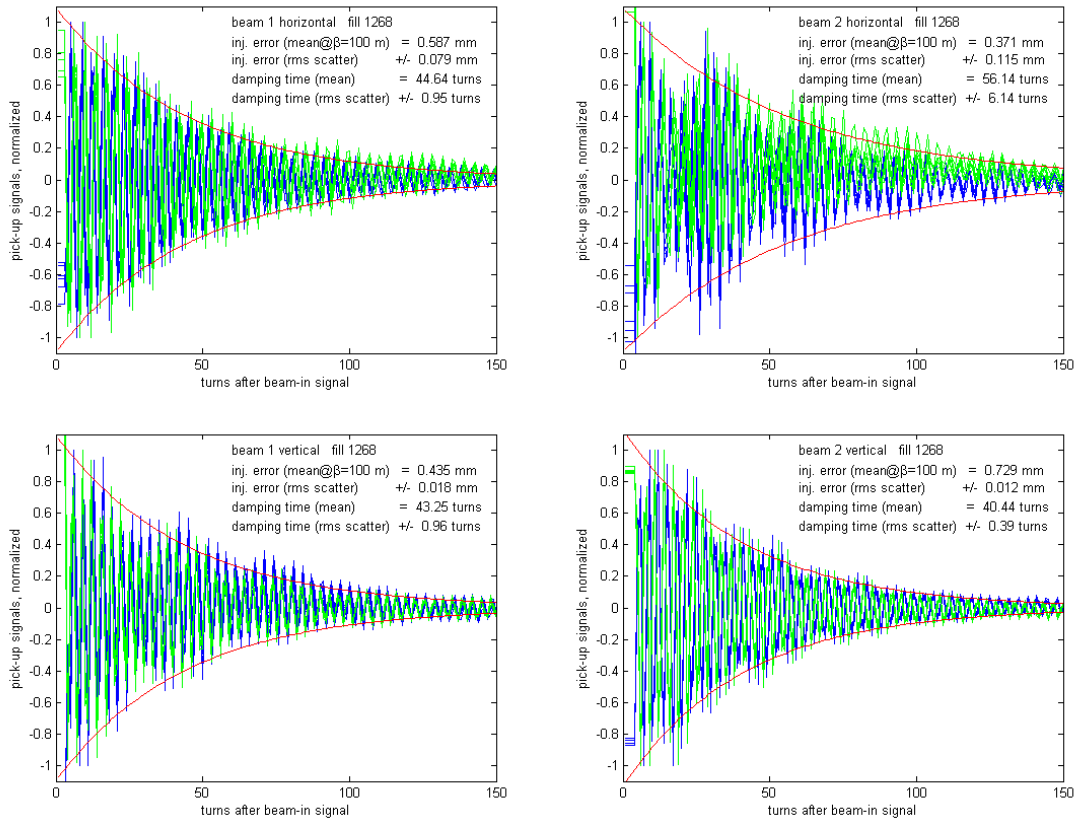

Figure 3.1.: LHC injection oscillations of beam 1 and beam 2, horizontal and vertical, damped by the ADT, Fill 1268 [12]. The images show the measurement of the ADT pick-ups located at the quadrupoles Q7 (green) and Q9 (blue), which are located on the left or right side of IP4 in the LHC, and an exponential fit of the data.

with ADT pick-ups. The oscillation amplitude is decreasing quickly due to the damper.

The damper has to be able to deal with bunch-by-bunch differences of trajectory oscillations. Due to various kicker ripples the injection oscillations can vary significantly between different bunches, see Fig. 3.2. The LHC transverse damper has a bandwidth of 20 MHz with the kick strength varying according to a first order low pass filter (-3 dB at 1 MHz) [14], see Fig. 3.3.

The damping time applied for physics fills at injection in 2012 was 20 to 25 turns. For the ramp the gain was reduced. The damping time at the start of the ramp was about 100 turns for physics fills in 2012.

3.1.3. Dispersion Errors

Similar to the treatment of steering errors, the dispersion function of the transfer line can be mismatched at injection to the LHC. This produces trajectory mismatch for off-momentum particles. For a beam with relative momentum spread $\frac{\Delta p}{p}$, the

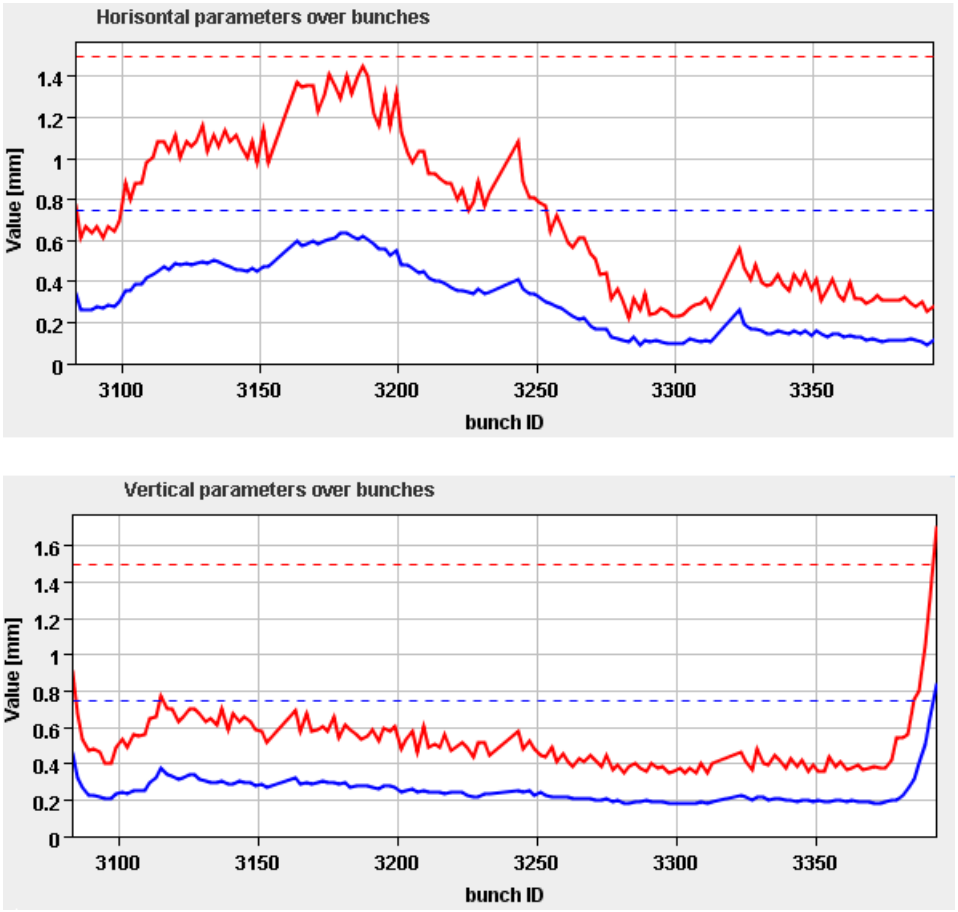

Figure 3.2.: Bunch-by-bunch injection oscillation amplitudes for beam 2 horizontal and vertical. *Courtesy L. Drosdal, CERN, Geneva, Switzerland.*

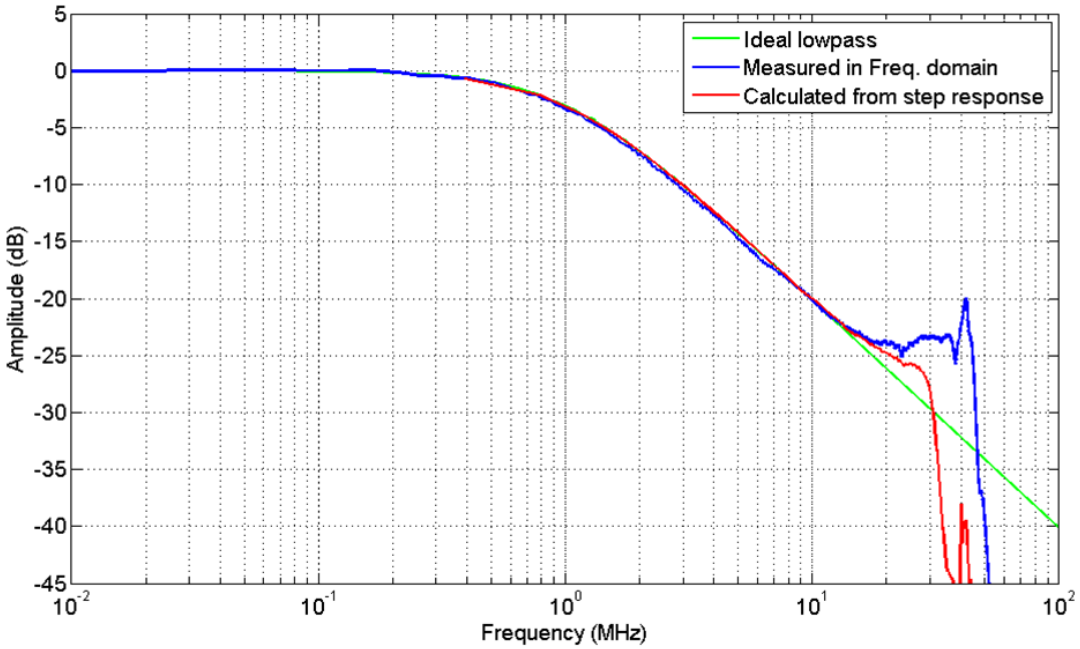

Figure 3.3.: ADT bandwidth [14]. ADT signal chain frequency response calculated from the step response (via the HOM (higher order mode) port).

emittance increase is

$$\frac{\varepsilon}{\varepsilon_0} = 1 + \frac{1}{2}\frac{\Delta D^2 + (\beta\Delta D' + \alpha\Delta D)^2)}{\beta\varepsilon_0}\left(\frac{\Delta p}{p}\right)^2. \tag{3.1.4}$$

Again ε_0 is the emittance of the matched beam and ε is the emittance with the twiss parameters α and β and the dispersion errors ΔD and $\Delta D'$. Any small deviation from the ideal dispersion function can blow up the emittance, if the momentum spread of the beam at injection is large enough [9].

3.2. Intra-Beam Scattering (IBS)

There are various diffusion and scattering processes that afflict the beam. The particles in the beam can interact with the residual gas in the vacuum chamber which can lead to increasing emittance and beam losses. Also scattering among the particles in a bunch can cause the beam sizes to grow. This is called intra-beam scattering (IBS) and will be explained in more detail.

Intra-Beam Scattering is multiple Coulomb scattering of the particles within a bunch [15]. The collisions change the momenta of the particles. Due to dispersion, a change in energy will cause a change in the betatron amplitude and thus, a coupling between betatron and synchrotron oscillations. Above transition, transverse and longitudinal emittances will grow. The IBS growth times for the transverse and longitudinal planes scale like [16]:

$$\frac{1}{\tau_{x,y,\Delta p}} \propto \frac{r_0^2 cN}{\gamma^4 \varepsilon_x \varepsilon_y \varepsilon_L}\left\langle f_{x,y,\Delta p}\left(\beta_x, \beta_y, \varepsilon_x, \varepsilon_y, \frac{\Delta p}{p}, \eta_x\right)\right\rangle. \tag{3.2.1}$$

This formula gives the emittance growth times due to IBS effects for the transverse planes (x, y) and the momentum spread Δp. The classical particle radius is r_0, c is the speed of light, and N is the number of particles in the bunch. The longitudinal emittance is ε_L. The functions $f_{x,y,\Delta p}$ are averaged over the magnetic lattice and depend on the optics parameter, for instance beta function, emittance, relative momentum deviation and periodic dispersion function[2] η_x.

IBS is more important for proton accelerators than electron machines which have radiation damping that counteracts IBS. In a hadron collider, IBS can limit the luminosity lifetime.

In the LHC the dispersion is large in the horizontal plane (design maximum horizontal dispersion in the arc is 2.018 m [1]) and negligible in the vertical plane. Thus IBS emittance growth is only expected in the horizontal plane. In case of coupling the vertical emittance can also be increased by IBS.

[2]If the magnetic lattice is periodic, the dispersion function has a periodic solution.

IBS becomes less import at higher energies. Higher beam intensities and smaller transverse and longitudinal emittances increase IBS growth rates [17]. For transverse emittance preservation of protons at the LHC, IBS plays a role only in the horizontal plane during the injection plateau. However, the longitudinal plane is also affected.

At the LHC design stage the following IBS emittance growth rates for IBS in regions with non-zero dispersion in the ring were assumed [1]:

	Injection	**Collision**
RMS beam size in arc [mm]	1.19	0.3
RMS energy spread $\Delta E/E$ [10^{-4}]	3.06	1.129
Horizontal emittance growth time [hours]	38	80
Longitudinal emittance growth time [hours]	30	61

Table 3.1.: IBS growth times at injection energy of 450 GeV and collision energy of 7 TeV with LHC design values.

3.3. Noise

Another emittance blow-up source is noise. Random power supply noise and ground motion can introduce random energy changes and therefore also increase the emittance in the presence of dispersion [16]. For instance, dipole magnets can produce field noise that gives small random kicks to the beam. Ground motion can kick the beam angularly when the quadrupoles are misaligned. These kicks, averaged over many turns, cause the betatron oscillation amplitude and, hence, the emittance to grow, proportional to the square of the kick angle θ:

$$\frac{d\left\langle r^2\right\rangle}{dn} = \beta\left\langle\theta^2\right\rangle, \tag{3.3.1}$$

where n is the number of turns and r is the amplitude in phase space. For the random dipole noise $\langle(\Delta B)^2\rangle$, the averaged kick over many turns yields:

$$\left\langle\theta^2\right\rangle = \frac{\langle(\Delta B)^2 l^2\rangle}{(B_0 R)^2} \tag{3.3.2}$$

over the length of the dipole l with bending radius R and magnetic field B_0. This yields an emittance growth rate of

$$\frac{d\varepsilon}{dt} = \frac{1}{2}\beta f_{rev}\frac{\langle(\Delta B)^2 l^2\rangle}{(B_0 R)^2}, \tag{3.3.3}$$

where f_{rev} is the revolution frequency of the circular accelerator.

The angular kicks from the quadrupoles with a ground motion amplitude of $\langle(\Delta x)^2\rangle$ are given by

$$\left\langle \theta^2 \right\rangle = \frac{\langle(\Delta x)^2\rangle}{f^2}, \tag{3.3.4}$$

with f being the quadrupole focal length. Considering this effect, the emittance increases over time with a growth rate of

$$\frac{d\varepsilon}{dt} = \frac{1}{2}\beta f_{rev}\frac{\langle(\Delta x)^2\rangle}{f^2}. \tag{3.3.5}$$

4. The LHC: Cycle, Parameters and 2011 Emittance Preservation

This thesis investigates emittance preservation through the LHC cycle from SPS extraction to LHC collisions. The LHC cycle with its different phases is described in the following. The LHC proton run configurations in 2011, 2012 and for the nominal case will be introduced and the results of the emittance preservation studies in 2011 are summarized.

4.1. The LHC Cycle

The operation of the LHC is divided into distinct phases linked to the main accelerator activities. They are called operational modes. The operational LHC modes with beam during proton physics are "injection", "prepare ramp", "ramp", "flattop", "squeeze", "adjust" and "stable beams" [18], see Fig. 4.1.

For the most commonly used filling scheme in 2011 and 2012, 12 injections with up to 144 bunches per injection were required per ring. The total LHC filling time takes about 30 minutes. When the injection process is finished the machine enters the mode "prepare ramp". In this mode the transverse damper gain is reduced to allow a good tune signal during the ramp, as all LHC ramps are run with a tune feedback system. The tune is measured by the Base-Band-Tune (BBQ) system [19]. In preparation for the ramp different machine components are loaded with the ramp functions. Then the beam energy is increased. The ramp from injection energy of 450 GeV to collision energy in 2011 (3.5 TeV) and 2012 (4 TeV) takes about 15 minutes. Once the flattop energy is reached and the pre-squeeze checks are completed, the β^* squeeze is initiated. The beta function at the collision points (β^*) is minimized to achieve high luminosities. The squeeze takes about 15 minutes. In 2012 the β^* at IP1 (ATLAS) and IP5 (CMS) was squeezed from 11 m to 0.6 m. In IP2 (ALICE) and IP8 (LHCb) the β^* was squeezed to 3 m. The squeeze is followed by the mode "adjust" where the beams are brought into collision. The experiments switch on their detectors as soon as the mode "stable beams" is declared. In general, the machine stays in "stable beams" as long as possible. Each pass through the cycle with its different modes is allocated a number, the fillnumber. The record time in "stable beams" in 2012 was 22.8 hours (Fill 2692).

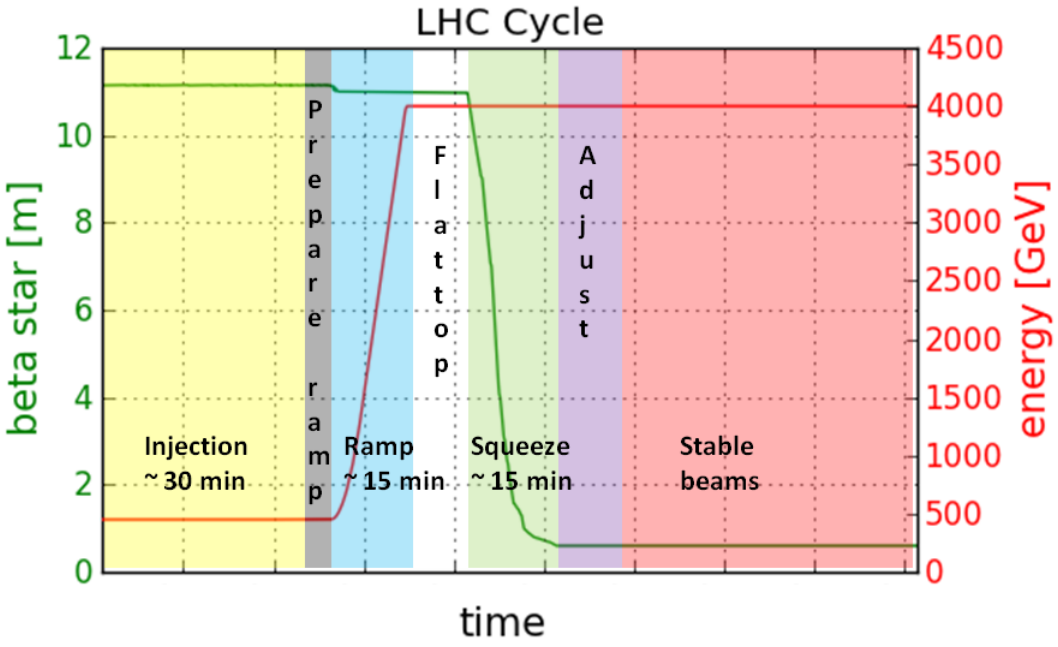

Figure 4.1.: The LHC cycle. The injection process from the SPS to the LHC takes about 30 minutes. The injection plateau is followed by the energy ramp (approximately 15 minutes). After reaching the flattop energy, the β^* is squeezed from 11 m to 0.6 m at ATLAS and CMS (approximately 15 minutes) and, finally in "adjust", the beams are brought into collision. In "stable beams" the experiments take data.

To pin down possible sources of emittance growth, it is necessary to collect data in every phase of the LHC cycle. Therefore beam instrumentation to measure the transverse emittance needs to be adjustable. A variety of instruments is installed in the LHC. Their operation is explained in chapter 5.

4.2. LHC Parameters

To achieve high luminosities in the LHC, the injectors have to produce high brightness beams which are conserved through the LHC cycle. The brightness B is the ratio of bunch intensity N over transverse normalized emittance ε [20]:

$$B = \frac{N}{\varepsilon}. \tag{4.2.1}$$

One of the reasons for the remarkable achievements of the LHC in its first running years was the excellent performance of the LHC injector chain. Beams beyond the design brightness could be produced. The injectors delivered beams with bunch intensities of 1.7×10^{11} protons and a transverse emittance of 1.5 μm. Despite the lower collision energy of 4 TeV per beam instead of the design value of 7 TeV,

	Nominal	**2011**	**2012**
Beam injection energy [TeV]	0.45	0.45	0.45
Collision energy per beam [TeV]	7	3.5	4
Total number of bunches per beam	2808	1380	1374
Maximum number of bunches injected	288	144	144
Number of injections per fill and beam	12 (+1 pilot)	12 (+1 pilot)	12 (+1 pilot)
Bunch spacing [ns]	25	50	50
Number of protons per bunch	1.15×10^{11}	1.1 - 1.5×10^{11}	1.1 - 1.7×10^{11}
Normalized transverse emittance at collision [μm]	3.75	2.4	2.4
β* at IP1/IP5 [m]	0.55	1.0	0.6
Number of collisions (IP1+IP5/IP2/IP8)	2808/2736/2622	1331/0/1320	1368/0/1262
Maximum luminosity achieved [cm^{-2}s^{-1}]	10^{34}	3.65×10^{33}	7.7×10^{33}

Table 4.1.: LHC proton run configuration in 2011, 2012 and for nominal LHC parameters.

peak luminosities of 7.7×10^{33} cm^{-2}s^{-1} were reached in the LHC. The LHC design luminosity is 10^{34} cm^{-2}s^{-1}. Table 4.1 summarizes the LHC run conditions in 2011 and 2012 and compares them to the design run configuration [1]. In the 2011 and 2012 proton run the bunch spacing was limited to 50 ns due to electron cloud effects [5]. The main differences in run configurations from 2011 to 2012 are the increased flattop energy from 3.5 TeV to 4 TeV and the smaller beta function at the IPs. The β* is squeezed to 0.6 m instead of 1 m in 2012. The peak luminosity could therefore be increased from 3.65×10^{33} cm^{-2}s^{-1} in 2011 to 7.7×10^{33} cm^{-2}s^{-1} in 2012.

4.3. Emittance Blow-Up during the 2011 LHC Cycle

The challenge for the LHC is to preserve the high brightness beams coming from the injectors through the cycle. That means maximizing transmission and minimizing emittance blow-up. The largest fraction of the brightness reduction in the LHC in

2011 and 2012 runs comes from emittance growth [21]. The emittances were blowing up significantly in 2011. The main results are summarized in the following [22]:

- No emittance blow-up from the injection process, the transfer from SPS to LHC, within measurement accuracy.
- During the LHC injection plateau the emittances grow in the horizontal plane, consistent with intra-beam scattering (IBS).
- The emittance blow-up during the LHC ramp was more than 20 % for initial emittances of 1.6 μm.
- During the LHC squeeze only beam 1 horizontal was indicating a large emittance blow-up of more than 20 %.

Towards the end of the LHC proton run in 2011 the bunch intensity was increased further and further to push peak luminosity. The data from the summer period and the last month of proton operation in 2011 were combined to obtain the dependence of emittance growth on bunch intensity, see Fig. 4.2. The absolute emittance growth seems to be independent of bunch intensity [23].

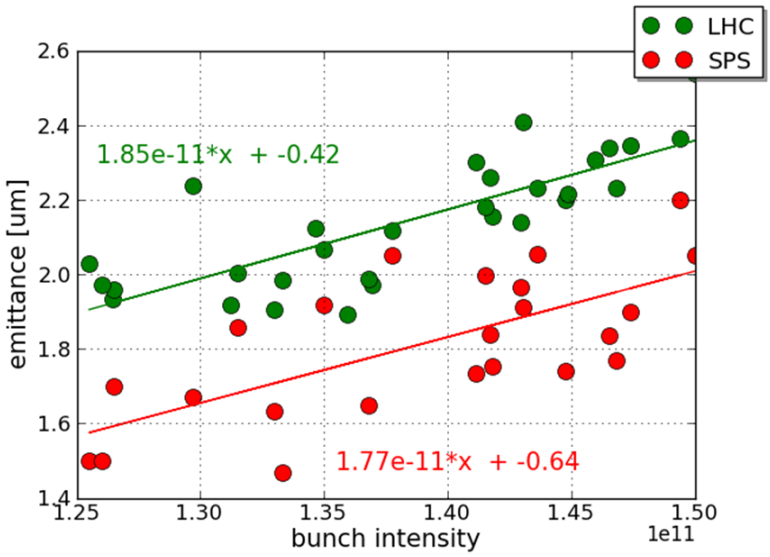

Figure 4.2.: Bunch intensity versus emittance. Comparison of emittance from LHC luminosity and emittance of 144 bunch wire scans in the SPS as function of bunch intensity. The absolute growth between SPS extraction and LHC start of collisions seems to be roughly independent of bunch intensity.

5. Beam Instruments for Emittance Measurements

Emittance cannot be measured directly. It is determined from the transverse beam size through transverse profile measurements. This chapter discusses the different transverse profile measurement systems in the LHC and presents the advantages and disadvantages of the various instruments.

5.1. Transverse Profile Monitors

Three main types of profile monitors are installed in the LHC [1]:

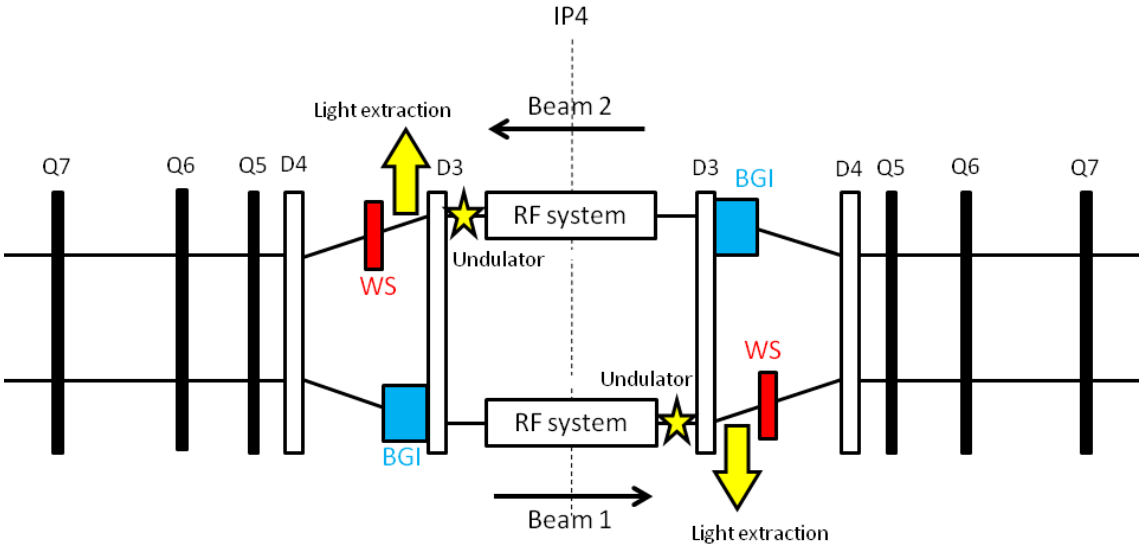

Figure 5.1.: Schematic outline of IP4 (figure not to scale). The beam line in point 4 with RF cavities, quadrupoles Q4, Q5, Q6 and Q7, dipoles D3 and beam instruments is presented. There are four wire scanners (WS) for each beam, two for each plane, including a spare wire system. The Beam-Gas Ionization Profile Monitor (BGI) also has a horizontal and a vertical component for each beam. The Beam Synchrotron Radiation Telescope (BSRT) works with a superconducting undulator at injection energy and the dipole D3 at flattop energy.

- wire scanners,
- Beam Synchrotron Radiation Telescopes (BSRT) and
- Beam-Gas Ionization Profile Monitors (BGI).

Transverse profile monitors are typically located at places with large beta functions. The profile monitors in the LHC are positioned in interaction region 4 (IR4). A schematic overview is given in Fig. 5.1.

There are also matching monitors for both rings positioned in the LHC in point 4 [1]. They are based on the principle of Optical Transition Radiation (OTR) screens. In the LHC they can measure several beam profiles during a few turns for injection mismatch studies. In the transfer line from the SPS to the LHC OTR monitors and luminescence screens can be used to measure the transverse beam profile [1]. The analysis with matching monitors and transfer line screens will not be further discussed in this thesis.

Transverse Profiles and Fitting

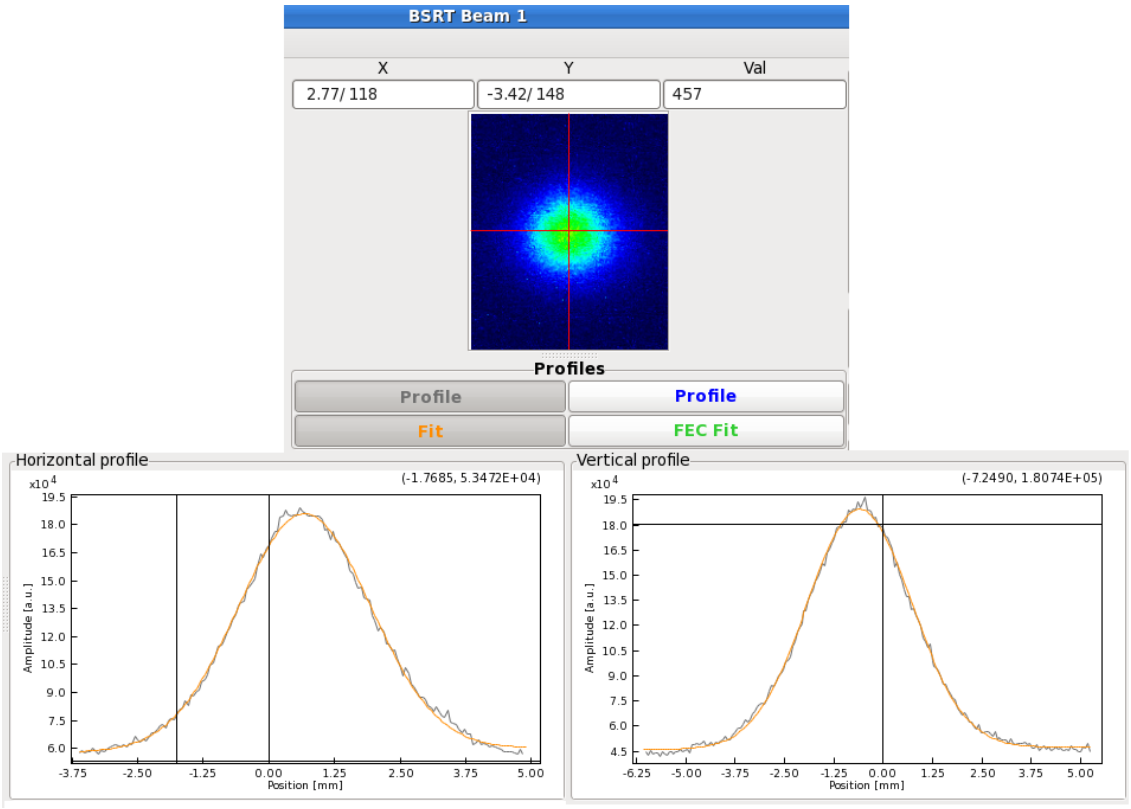

Figure 5.2.: BSRT application transverse profiles. Two-dimensional transverse image of beam 1 measured with the BSRT (top) with the reconstructed horizontal and vertical profile (bottom). A Gaussian fit (orange curve) is applied to the profiles (black curve).

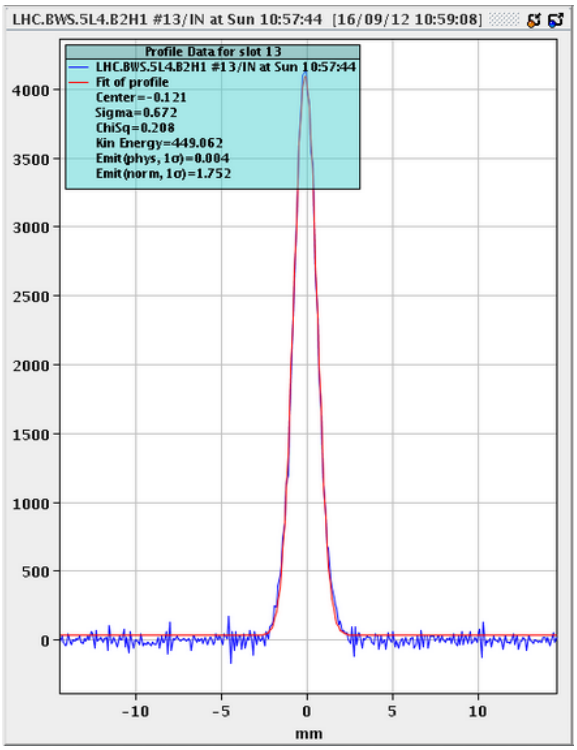

Figure 5.3.: Wire scanner application transverse profile. A horizontal profile (blue curve) of one bunch in beam 2 obtained from the wire scan is shown. A Gaussian fit (red curve) is applied to the profile. On the x-axis the position in [mm] is plotted. The y-axis displays the amplitude of the signal in [a.u.].

The transverse beam size can be obtained either from a two-dimensional or a one-dimensional image of the transverse beam profile. The BSRT camera measures a two-dimensional distribution of the synchrotron light which is projected onto the horizontal and the vertical axis to obtain the transverse profiles, see Fig. 5.2.

Wire scanners and BGI measure only one-dimensional profiles. Therefore an instrument for every plane is needed. An example of a horizontal beam profile from a wire scanner measurement is shown in Fig. 5.3. In most cases the transverse beam distribution is Gaussian.

Once the transverse beam profile is obtained it is fitted with a 5 parameter Gauss function to obtain the beam size σ:

$$f(x) = d + k \cdot x + a \cdot \exp\left(-\frac{x-b}{2 \cdot \sigma^2}\right) \tag{5.1.1}$$

where d is the offset, k is the slope of the baseline, a is the amplitude, and b is the mean of the Gaussian distribution. A horizontal beam profile measured with the wire scanner and fitted off-line with a Gauss function is shown in Fig. 5.4.

The calculated σ is the beam size value of the entire proton bunch intensity. In dispersion free regions the emittance is obtained from the beam size and the beta

function at that point:

$$\varepsilon = \frac{\sigma^2}{\beta}. \tag{5.1.2}$$

To minimize the influence of the sometimes large bunch tails only data points above a certain signal level (typically 20 % of maximum) are used. Thus merely the core of the profile, which contains all data points above the line of the intensity cut, is fitted with a Gaussian to determine the beam size, see Fig. 5.5. In this way the core emittance is calculated.

Another way to avoid fitting the bunch tails is to only fit data points within $\pm\, 2\sigma$. The procedure is: first fitting the whole transverse profile with a 5 parameter Gauss function, and second taking only the measurement points in the region $\pm\, 2\sigma$ to fit this part of the profile again with a Gaussian, see Fig. 5.5.

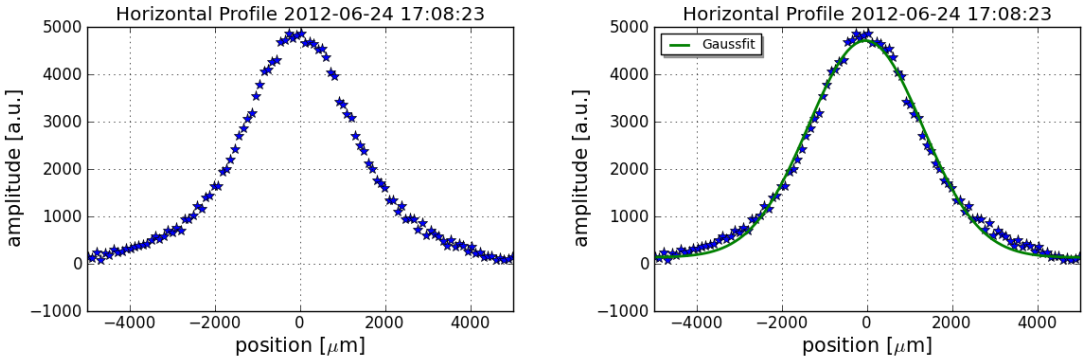

Figure 5.4.: Transverse beam profile (left) with Gauss fit (right), measured with wire scanner. The measurement points (blue) are fitted with a 5 parameter Gauss (green).

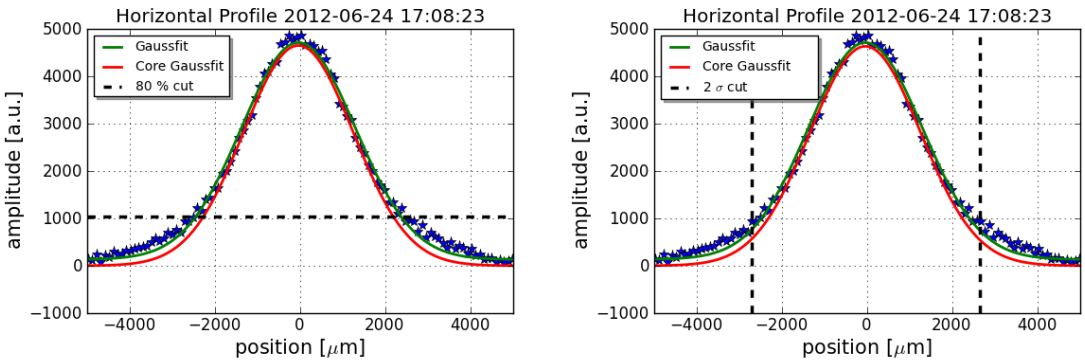

Figure 5.5.: Transverse beam profile with core Gauss fit (left) and a double Gaussian fit (right). The measurement points (blue) are fitted with a 5 parameter Gauss (green) and after a cut of the bunch tails (black) fitted again with a Gauss function (red).

5.1.1. Wire Scanner

Two sets of four wire scanners are installed in the LHC, one wire scanner for each beam and plane and in addition a spare set of wire scanners [1]. The second pair is used as a backup in case of damages of the operational instrument. The wires are used to measure low intensity beams and serve as a calibration instrument for other profile monitors. They are located downstream of the D3 magnet. Wire scanners in the LHC are routinely operated in the "bunch mode" which gives one transverse profile for each bunch.

The wire scanners are equipped with a 36 μm thick carbon wires attached to a moving fork [24]. The transverse beam profile is scanned by moving the wire with a linear motion through the beam. One wire scanner for the horizontal plane and one wire scanner for the vertical plane are needed. In the LHC the wire crosses the beam at a constant speed of 1 m/s. The general layout of a wire scanner is shown in Fig. 5.6. The wire interacts with the proton beam and secondary particles are produced. Their signal is measured outside the beam pipe with a scintillator. Through optical filters the signal is transported to a photomultiplier (PM). The transverse profile is reconstructed from the PM current and the position of the wire fork, see Fig. 5.3. The wire scanner position is measured with a high precision potentiometer. The potentiometer is also used for controlling the position of the wire.

The wire scanner actually records two images per scan. It makes an "in" and an "out" movement. That means the wire passes through the beam twice per measurement. The obtained beam size is averaged over the in and the out scan. Thus the error on the emittance contains the error from the fit, the error from averaging of in and out scan and the error on the beta function. In addition, if the emittance is averaged over several bunches in one batch, the error also includes uncertainties from averaging.

The choice of wire material, wire thickness and scanning speed depends on the beam current and the desired amount of secondary particle production. The wire interacts with the beam several times per passage. Studies showed that the emittance blow-up with commonly used wire parameters is negligible and does not perturb the measurements [25]. A thin and fast wire will produce fewer secondary particles than a slow and thick wire. The wire speed defines the precision of the measurement. For a more accurate measurement a slower moving wire is preferred. For maximum wire lifetime the energy deposition should be small and the material robust against high temperatures. Typically carbon wires are chosen.

Wire heating limits the beam intensity with which the wire scanners can be used in the LHC. In theory the carbon wire should be able to take 2 - 3 $\times$ 10^{13} charges/mm before sublimating. There is also another reason for limited intensity in the LHC.

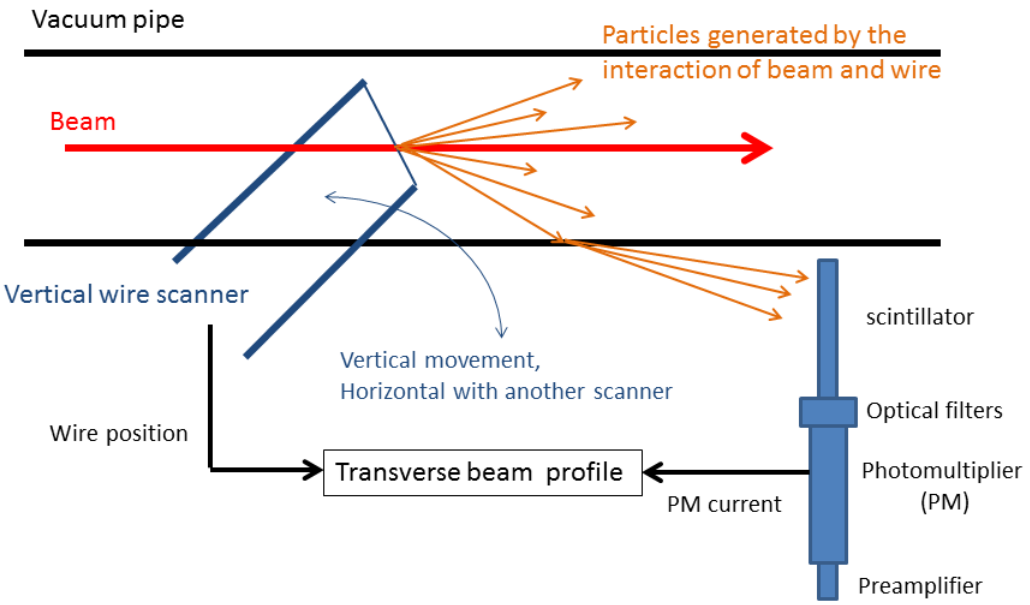

Figure 5.6.: Schematic drawing of the different components of a wire scanner. The basic operational principle of a vertical wire scanner is displayed. The wire scanner consists of a fork with a wire that moves through the beam and produces secondary particles which are measured with a scintillator.

The LHC magnets are superconducting. The particle showers produced by the wires passing through the beam can introduce a magnet quench, a sudden transition from superconducting to normal conducting [6].

All things considered the theoretical wire scanner intensity limit should be 1/4 of the nominal intensity at injection energy and 1/8 of the nominal intensity at 7 TeV [25].

In reality these limits had to be adjusted. Including scan safety margins the limit is 5×10^{12} charges/mm in the LHC calculated from the number of charges in the ring, wire diameter, wire speed, revolution frequency and transverse beam size. [26] Thus at 450 GeV injection energy it is possible to scan the first 50 ns 144 bunch batch coming from the SPS with an intensity of about 1.5×10^{11} protons per bunch. At 4 TeV flattop energy the total measurable bunch number with wire scanners is reduced to about 30 with this bunch intensity.

Due to a broken wire in September 2012 the wire scanners were changed to the spare system. The new wires are still thicker. Thus the secondary particle production is higher and some beam dumps occurred due to increased beam losses. The intensity limit for the wire scanners had to be reduced even further. For safety reasons wire scans of the first 50 ns 144 bunch batch were not possible anymore and the 4 TeV flattop energy wire scan limit was about 20 bunches with bunch intensities of about 1.5×10^{11} ppb and 50 ns bunch spacing.

5.1.2. Beam Synchrotron Radiation Telescope (BSRT)

Upstream of the D3 superconducting dipole magnet, on each side of the IP, a synchrotron light monitor is installed; one for beam 1 and one for beam 2. BSRT measurements are continuous, automatic, passive and compatible with high intensity operation.

The synchrotron light is produced by a superconducting undulator or the D3 dipole itself depending on the energy. The light is extracted 26 m downstream of the entrance of the D3 dipole giving a two-dimensional transverse image of the beam [1]. As shown in Fig. 5.1 a magnetic chicane, between the D3 and D4 magnets, widens the beam separation to have enough space for RF cavities. The D3 dipole deflects the beam by an angle of 1.57 mrad with a maximum field of 3.9 T that gives an orbit radius of $R = 6$ km for 7 TeV protons. In the drift space to dipole D4 the light diverges from the proton beam. The photons are collected by an extraction mirror and pass through a vacuum viewport to the optics outside the beam line where the actual telescope is located. The optical system is adjustable to the radiation source, undulator or dipole. Finally, an image-intensified camera measures the transverse beam profile by counting the photo-electrons emitted from a photocathode. The schematic outline of the optical system is given in Fig. 5.7.

The BSRT produces useful transverse profiles at 450 GeV injection energy and up to 7 TeV flattop energy. Beam images are taken continuously. At 450 GeV the synchrotron radiation has to be intensified by a superconducting undulator placed 1 m from the dipole. At collision energy the light is extracted from the bent proton beam at the dipole.

At injection energy, the dipole provides far too little visible light for measurements (the critical wavelength of the dipole spectrum at 450 GeV is $\lambda_c = 0.23$ mm). A short superconducting undulator with 2 periods of $\lambda_u = 28$ cm is installed before the D3 magnet [27]. The peak of the light spectrum from the protons is at 610 nm. The BSRT camera can only measure the visible wavelength spectrum from 400 to 700 nm. If the undulator is kept as the light source during the ramp and at flattop energy, the photon wavelength does not peak in the visible wavelength range anymore and the BSRT detector would not be able to function. Thus the light source has to be changed to the D3 dipole. At flattop energy of 7 TeV, the critical wavelength of the dipole spectrum is $\lambda_c = 61$ nm.

During the ramp the light source switches from undulator to dipole. Then the longitudinal radiation extraction position shifts by 2.8 m so the optical focus changes. It is impossible to maintain focus and alignment while moving the mirrors. Instead an optical delay line lengthens the photon trajectory to keep the entering optical path constant [27]. Yet, at intermediate energies where both light sources produce visible light, image blurring is a concern, since the image system cannot be focused

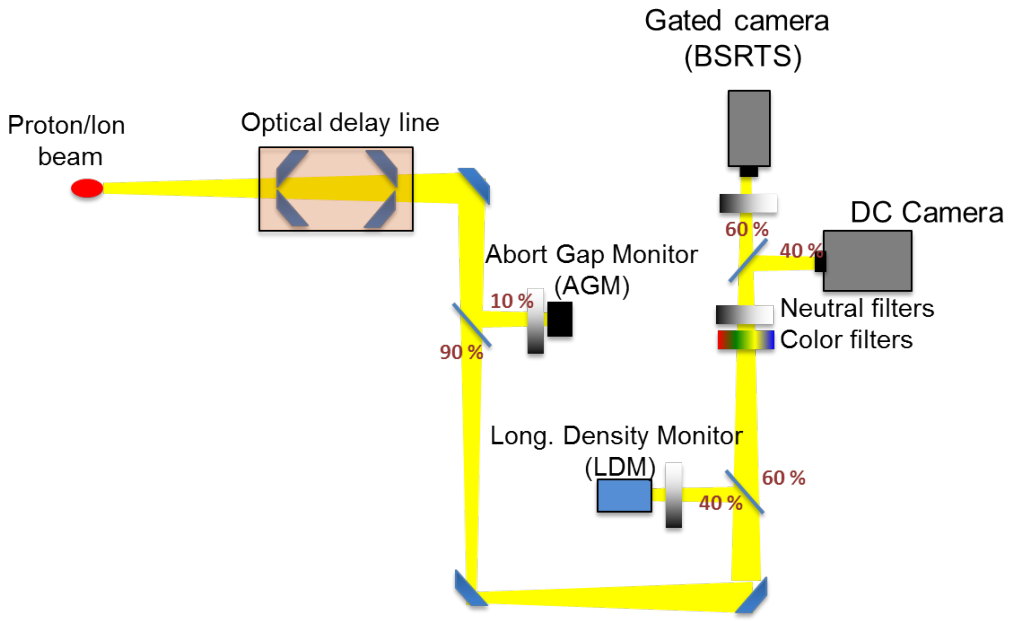

Figure 5.7.: Schematic drawing of the BSRT. The basic outline of the BSRT optical system is shown. The synchrotron light from the particle beam passes through an optional optical delay line and continues to the BSRT camera. Part of the light is used for the Abort Gap Monitor (AGM) [24], a Longitudinal Density Monitor (LDM) [28] and a DC camera. These devices will not be explained further. *Courtesy G. Trad, CERN, Geneva, Switzerland.*

on both. Meaningful beam size measurements from the BSRTs can only be obtained at 450 GeV and flattop energy, not in between.

The LHC BSRTs measure bunch-by-bunch transverse profiles and are calibrated with wire scanners. Even though the BSRT system gives several degrees of freedom for optimization of resolution and accuracy for different beam intensities and energies, there are intrinsic calibration limitations, for instance, diffraction, possible misalignment and focusing errors. Therefore the measured beam size at the BSRT σ_{meas} has to be corrected with a calibration factor σ_{corr} to agree with the wire scanner measurement [29]:

$$\sigma = \sqrt{\sigma_{meas}^2 - \sigma_{corr}^2}. \tag{5.1.3}$$

The errors on the beam size from the BSRT measurement include systematic errors from optical magnification and energy dependent systematic errors from imaging.

Originally a scan took about 5 s per bunch. A physics beam with 1374 bunches was fully scanned in $\sim$ 2 hours, which is obviously not practical. Since May 2012, after a software update, fast scans were available. Transverse beam profiles of 3 to 4 bunches per second could be obtained in this way. The total physics beam can

therefore be scanned in about 7 minutes.

Since September 2012 only BSRT for beam 1 is working. No beam profiles for beam 2 were available until the end of the 2012 proton run.

5.1.3. Beam-Gas Ionization Monitor (BGI)

The Beam-Gas Ionization Profile Monitor (BGI) also provides transverse profiles in a non-destructive way. It can measure the transverse beam profile in the LHC in all four planes continuously over the whole energy range from 450 GeV to 7 TeV for physics beams, including the ramp [30]. Thus the BGI complements the BSRT. The transverse beam size is obtained from the velocity spectrum of the electrons which are created and accelerated when the beam ionizes the residual gas. An electrical field deflects the electrons to an anode with a Micro Channel Plate (MCP) where the position of the electrons is measured. The electron distribution at the MCP reflects the transverse particle distribution of the beam. Through a phosphor screen the electron distribution is converted to a photon distribution, so that it can be viewed by a CCD camera linked to a prism [31]. The basic principle of the BGI is shown in Fig. 5.8.

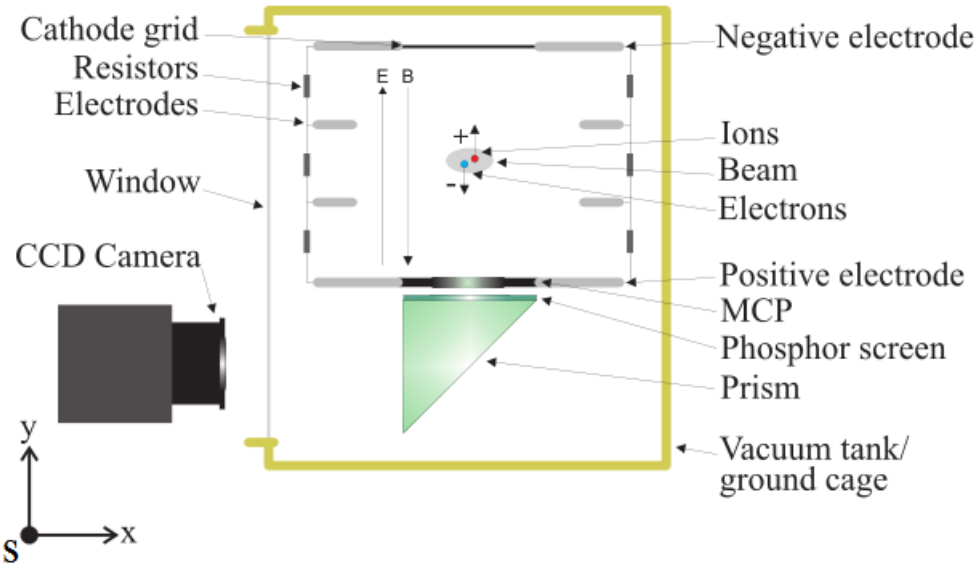

Figure 5.8.: Schematic drawing of the BGI [31]. Electrons ionized from the rest gas through the beam (s-direction) are accelerated up or down (in $\pm$ y-direction) due to the electric field which is created by applying a high voltage at the electrodes. Linked to the anode are a MCP, a phosphor screen, a prism and a CCD camera to measure the transverse profile of the beam.

The ionization rate is proportional to the beam intensity. The BGI only has a lower intensity limit which changes with time of the MCPs in operation. With fresh MCPs the sensitivity for protons can reach a few bunches. But after some years in operation, the LHC BGI cannot measure beams with intensities lower than about 600 bunches. The BGI integration time is about 0.1 seconds and it measures the average beam size for all bunches [32].

Subsystems of the BGI are gas injection, high voltage system, magnets and imaging system. In the past the BGI was not operational due to high voltage instabilities that caused vacuum interlocks and consequently beam dumps. This problem could be solved in the beginning of the 2012 run. The energy dependent calibration of the LHC BGI is not satisfying yet so no data was used for beam size results. Also both BGIs of beam 1 were damaged in 2012. Nevertheless an emittance blow-up during the ramp could be measured with the BGIs in 2012 for beam 2 horizontal and vertical, see Fig. 5.9. The absolute numbers can, however, not be trusted yet. A fully working BGI is foreseen for after the first long LHC maintenance period in 2013/14. It will then monitor continuously on-line the average transverse beam size of the beams [21, 32].

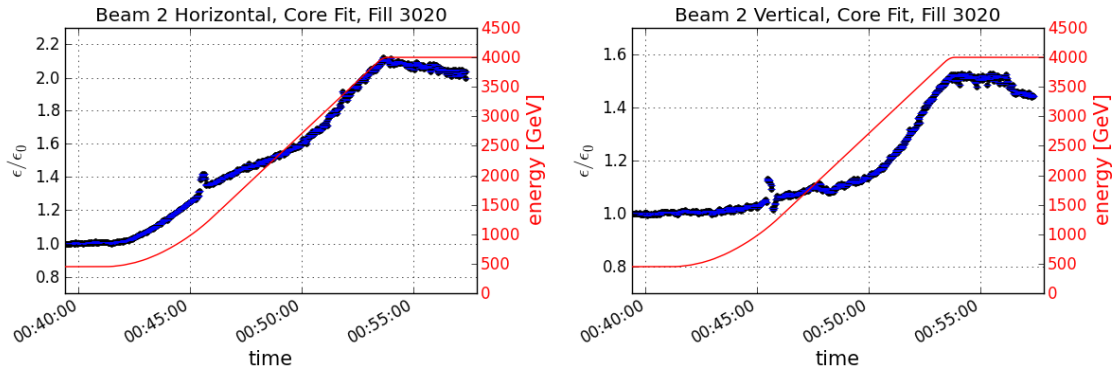

Figure 5.9.: BGI measurement of beam 2 horizontal and vertical during ramp of physics Fill 3020 with 1374 bunches. The cores of the transverse profiles are fitted with a Gaussian.

5.2. Measurement of the Beta Function with K-Modulation

The most commonly used method to measure beta functions in the LHC is the turn-by-turn phase advance measurement with beam position monitors (BPMs) after exciting a transverse oscillation [33]. In point 4 the phase advance between the BPMs is not optimal resulting in a large uncertainty on the β values from this method. Therefore a different method called k-modulation was used to measure the

beta functions at individually powered quadrupoles in IR4. The method will be explained in the following.

K-Modulation

In a circular accelerator the change of the quadrupole focusing strength Δk shifts the tune Q of the machine by [6]:

$$\Delta Q = \frac{1}{4\pi} \int_{s_0}^{s_0+l} \Delta k \beta(s) ds, \tag{5.2.1}$$

where l is the magnetic length of the quadrupole and β is the beta function at the quadrupole. The quadrupole strength is altered by changing the current of the quadrupole. The tune shift is proportional to the mean β-value in the quadrupole and thus:

$$\Delta Q \simeq \frac{\Delta k}{4\pi} \langle \beta \rangle \, l. \tag{5.2.2}$$

After coupling correction, the tune has to be measured as accurately as possible before and after the quadrupole strength change. Then the average beta function in the quadrupole $\langle \beta \rangle$ yields

$$\langle \beta \rangle = \frac{4\pi}{l} \frac{\Delta Q}{\Delta k}. \tag{5.2.3}$$

Typically several points are measured such that the function $\Delta Q\,(\Delta k)$ can be obtained. The slope of the curve is proportional to the beta function, see Fig. 5.10 and Fig. 5.11 as examples.

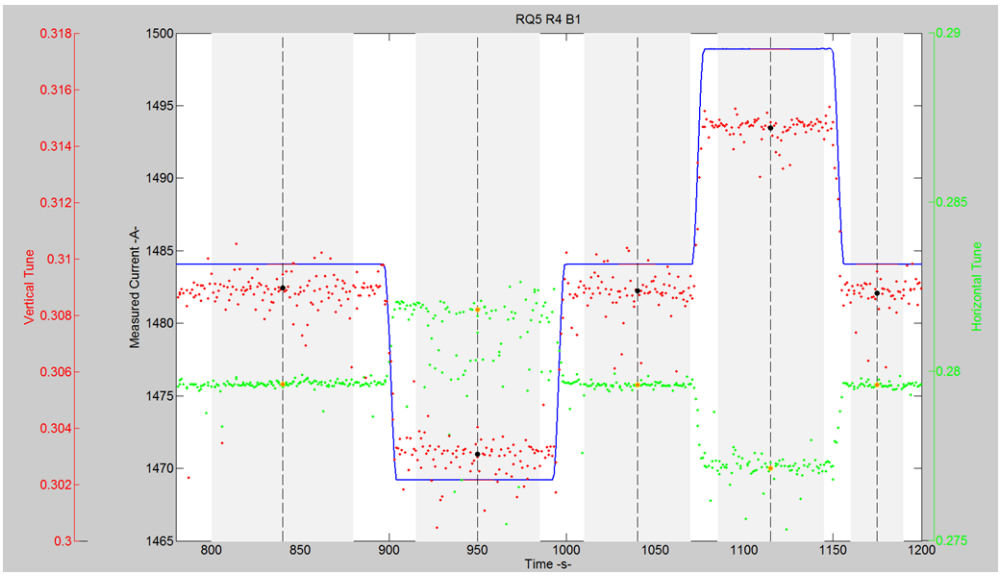

Figure 5.10.: K-modulation results for quadrupole RQ5 R4 B1. The quadrupole current (line) and evolution of the vertical (red dots) and horizontal tune (green dots) are plotted. *Courtesy G. Trad, CERN, Geneva, Switzerland.*

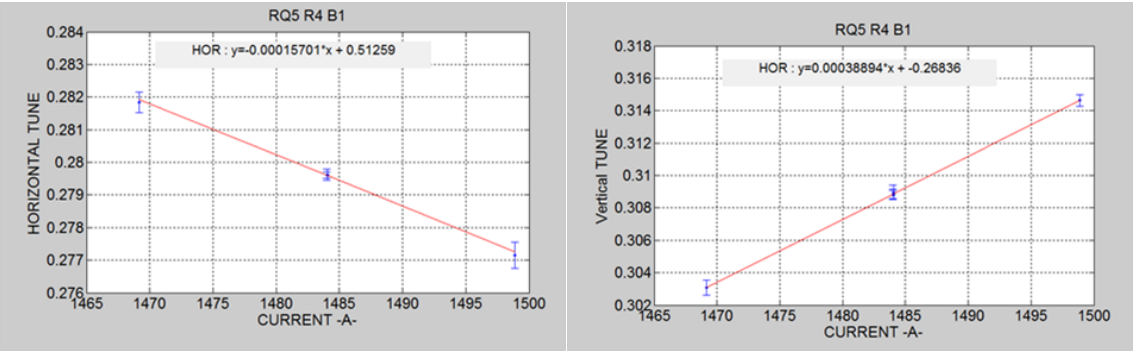

Figure 5.11.: K-modulation results for quadrupole RQ5 R4 B1. The horizontal and vertical tune of beam 1 versus the quadrupole current is plotted. From the slope the horizontal and vertical beta function from k-modulation at RQ5 R4 B1 are obtained. *Courtesy G. Trad, CERN, Geneva, Switzerland.*

Beta function measurement 2012 in IR4

Several individual powered quadrupoles can be found around the transverse profile monitors in point 4. Quadrupoles RQ5 L4 B1, RQ5 R4 B1, RQ6 R4 B1, RQ7 R4 B1, RQ5 R4 B2, RQ5 L4 B2 and RQ6 L4 B2 were k-modulated to measure the beta functions at these quadrupoles. The beta functions were measured for all beams and planes at 450 GeV, 4 TeV and with squeezed optics.

To obtain the β values at the transverse profile monitors, the measured optics functions at the quadrupoles are transported to the instruments using linear transfer matrices. Table 5.1 summarizes the results obtained from k-modulation for wire

β [m]	**Model**	**Injection**	**Model**	**Flattop**	**Squeeze**
WS 1H	165.48	181.2 ± 6.45	165.48	159.2 ± 6.45	161.7 ± 7.50
WS 1V	287.81	287.1 ± 4.22	287.81	288.2 ± 10.90	274.8 ± 5.72
WS 2H	123.51	124.2 ± 2.04	123.51	118.7 ± 4.20	114.3 ± 6.20
WS 2V	404.55	420.7 ± 3.33	404.55	438.7 ± 4.10	410.4 ± 1.33
BSRT 1H	178.14	199.9 ± 9.75	172.97	165.4 ± 5.35	174.5 ± 7.77
BSRT 1V	192.09	189.0 ± 4.94	214.60	207.5 ± 3.10	206.5 ± 4.20
BSRT 2H	127.54	126.5 ± 3.00	127.09	122.1 ± 6.20	126.2 ± 2.70
BSRT 2V	332.83	354.0 ± 2.72	334.61	358.8 ± 3.90	340.0 ± 4.55

Table 5.1.: Beta functions from k-modulation at the wire scanners (WS) and the BSRT light sources (undulator at 450 GeV and dipole at 4 TeV) for every plane at injection energy, flattop energy of 4 TeV and for squeezed optics. The measured beta functions are compared to the LHC design values.

scanners and the BSRT light sources (undulator at 450 GeV and dipole at 4 TeV) and compares them to the nominal beta functions.

5.3. Emittance from Luminosity and Luminous Region

The luminosity is defined as the overlap of the two colliding beams with time dependent beam density distribution functions ρ_1 of beam 1 and ρ_2 of beam 2 [34]:

$$L \propto N_1 N_2 K \cdot \int\int\int\int_{-\infty}^{\infty} \rho_1(x,y,s,-s_0)\rho_2(x,y,s,s_0)dxdydsds_0, \tag{5.3.1}$$

where K is the kinematic factor

$$K = \sqrt{(\vec{v_1}-\vec{v_2})^2 - (\vec{v_1}\times\vec{v_2})^2/c^2}. \tag{5.3.2}$$

For head-on collision at $s_0 = 0$ and same particle velocities $\vec{v_1} = -\vec{v_2} = \vec{v}$, the luminosity can be written as

$$L = 2N_1N_2f_{rev}n_b \cdot \int\int\int\int_{-\infty}^{\infty} \rho_{1x}(x)\rho_{1y}(y)\rho_{1s}(s-s_0)\rho_{2x}(x)\rho_{2y}(y)\rho_{2s}(s+s_0)dxdydsds_0. \tag{5.3.3}$$

For Gaussian particle distributions applies:

$$\rho_{iu}(u) = \frac{1}{\sqrt{2\pi}\sigma_{iu}} \exp\left(-\frac{u^2}{2\sigma_{iu}^2}\right), \tag{5.3.4}$$

$$\rho_s(s \pm s_0) = \frac{1}{\sqrt{2\pi}\sigma_s} \exp\left(-\frac{(s\pm s_0)^2}{2\sigma_s^2}\right), \tag{5.3.5}$$

with i = 1,2 and u = x,y. The deduction can be found in the appendix. If $\sigma_{1x} \neq \sigma_{2x}$ and $\sigma_{1y} \neq \sigma_{2y}$, but still assuming same bunch lengths $\sigma_{1s} \approx \sigma_{2s}$, the luminosity in Eq. 5.3.3 yields

$$L = \frac{f_{rev}n_b}{2\pi} \cdot \frac{N_1N_2}{\sqrt{\sigma_{1x}^2+\sigma_{2x}^2}\sqrt{\sigma_{1y}^2+\sigma_{2y}^2}}. \tag{5.3.6}$$

In the simple case where $\sigma_{1x} = \sigma_{2x} \equiv \sigma_x$, $\sigma_{1y} = \sigma_{2y} \equiv \sigma_y$ and $\sigma_x = \sigma_y \equiv \sigma$, the luminosity can be written as

$$L = \frac{f_{rev}n_b}{4\pi} \cdot \frac{N_1N_2}{\sigma^2} = \frac{f_{rev}n_b}{4\pi} \cdot \frac{N_1N_2}{\beta^*\varepsilon}. \tag{5.3.7}$$

Equation 5.3.7 connects luminosity with emittance. In this way the luminosity measurement together with beam and bunch intensity measurement can be used as an indirect emittance measurement. Usually the emittances of the two beams and

two planes per beam are not the same. The emittance obtained from luminosity is the convolution of the real beam emittances. From Eq. 5.3.6 and Eq. 5.3.7, and assuming β^* is the same for the horizontal and the vertical plane, the convoluted emittance equates as:

$$2\beta^*\varepsilon = \sqrt{\sigma_{1x}^2+\sigma_{2x}^2}\sqrt{\sigma_{1y}^2+\sigma_{2y}^2}, \tag{5.3.8}$$

$$\varepsilon = \frac{1}{2}\sqrt{\varepsilon_{1x}+\varepsilon_{2x}}\sqrt{\varepsilon_{1y}+\varepsilon_{2y}}. \tag{5.3.9}$$

The experiments also measure the luminous region, the horizontal beam size σ_x and the vertical beam size σ_y at the interaction point. The beam size σ_u calculated from the transverse size of the luminous region σ_{LR} is

$$\sigma_u = \sqrt{2}\sigma_{LR}. \tag{5.3.10}$$

The convoluted emittance from the luminous region, again assuming two Gaussian beams with $\sigma_{1x} = \sigma_{2x} \equiv \sigma_x$ and $\sigma_{1y} = \sigma_{2y} \equiv \sigma_y$, and equal β^*, is equal to

$$\sqrt{2}\beta^*\varepsilon_u = \sqrt{\sigma_{1u}^2+\sigma_{2u}^2}, \tag{5.3.11}$$

$$= \frac{1}{\sqrt{2}}\sqrt{\varepsilon_{1u}+\varepsilon_{2u}}. \tag{5.3.12}$$

Luminosity Reduction Factor

If the collisions are not ideally head-on or the particle densities are correlated, the luminosity formula becomes more complicated. This is the case in the presence of a crossing angle, collision offset and the hourglass effect. The strongest luminosity reduction comes from the crossing angle. In this thesis only the crossing angle is considered.

In the LHC there are many circulating bunches with short bunch spacing. To prevent unwanted interactions, the two beams collide at an angle of ϕ =290 μrad. If the beams therefore do not fully overlap the luminosity has to be multiplied by a reduction factor S [34]:

$$L = \frac{f_{rev}n_b}{4\pi}\cdot\frac{N_1N_2}{\beta^*\varepsilon}\cdot S. \tag{5.3.13}$$

For small crossing angles, $\sigma_s \gg \sigma_{x,y}$, and crossing in the horizontal plane, the luminosity reduction factor becomes

$$S \approx \frac{1}{\sqrt{1+\left(\frac{\sigma_s}{\sigma_x}\frac{\phi}{2}\right)^2}}. \tag{5.3.14}$$

An example calculation shows the quantitative influence of this effect. Assuming

that, for ideal head-on collisions of the nominal LHC proton beams, the LHC luminosity is 1.2×10^{34} cm^{-2}s^{-1}. The effect of the crossing angle reduces the luminosity to 0.973×10^{34} cm^{-2}s^{-1} with an estimated factor $S = 0.835$, derived from nominal LHC beam parameters.

Equation 5.3.13 determines the instantaneous luminosity with a reduction factor due to the crossing angle. From that the convoluted emittance can be obtained by knowledge of all other parameters. Nominal values are assumed for crossing angle ϕ, β^* and revolution frequency f_{rev}, see Table 5.2, with approximated uncertainties of 15 % error on β^* and 15 μrad error on the crossing angle.

Crossing angle [μrad]	290
β* in IP1 and IP5 [m]	0.6
Revolution frequency [kHz]	11.245
γ at 4 TeV	4264.392

Table 5.2.: LHC collision parameters in 2012.

In the LHC, bunch intensity, bunch length and luminosity are measured. The bunch intensities are monitored with a Fast Beam Current Transformer (FBCT) [1]. The longitudinal bunch size is measured with the LHC Beam Quality Monitor (BQM) [1] and the luminosity is quantified by ATLAS and CMS.

5.4. The LHCb System for Measuring the Overlap with Gas (SMOG)

At the LHCb experiment, located in IP8 in the LHC, a new method to determine the absolute luminosity has been developed using a beam-gas imaging method. It is based on vertex reconstruction of beam-gas interactions. The beam-gas imaging method at LHCb is called System for Measuring the Overlap with Gas (SMOG). The experiment combines the LHCb vertex locator (VELO) with the gas injection system.

The luminosity is obtained from measuring the beam shapes and overlap. For emittance studies the beam-gas imaging at the LHCb VELO can be used to measure transverse beam profiles. The VELO determines bunch-by-bunch beam sizes in a relatively short time. Bunch profiles can be obtained within minutes with a statistical error of less than 1 % [35]. The beam-gas imaging method is non-destructive. A dedicated gas injection system creates a pressure bump in the VELO which allows fast beam profile measurements. A gas with a high atomic number is chosen (Ne) to achieve higher interaction rates and thus improve the vertex resolution. The vertex

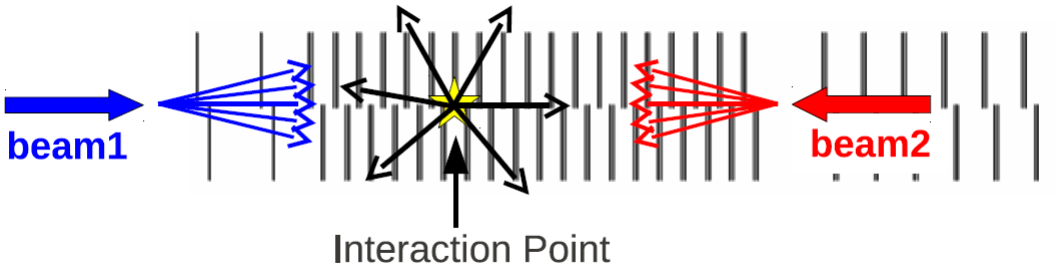

Figure 5.12.: Schematic drawing of the LHCb VELO, [36]. The thick arrows represent the circulating proton beam directions. The thin arrows show example beam-gas and beam-beam interactions.

detector is positioned closely around the interaction point. A schematic overview can be found in Fig. 5.12.

To measure the transverse profiles the vertex position is plotted in the x-s plane and the y-s plane. Single bunch profiles are acquired from the projection of the vertex distribution onto the plane perpendicular to the proton beam trajectory [36]. To determine the emittance from the beam profiles, a Gaussian core fit is used, as explained in section 5.1.1. The nominal beta function at IP8 ($\beta^* = 3$ m) is used to determine the transverse emittance, assuming a β^* error of 15 %.

The SMOG experiment does not need colliding bunches. Through beam-gas interaction all bunch profiles can be obtained, colliding and non-colliding bunches. Currently, the disadvantage of this high precision beam size measurement is that the VELO can only be closed when "stable beams" is declared. The SMOG experiment can only be enabled during collision of proton beams.

6. Emittance Preservation at the LHC in 2012

Emittance preservation studies in 2011 revealed a 20 to 30 % growth of the transverse normalized emittance from LHC injection to collisions. At the LHC design stage the total allowed emittance increase through the cycle was set to 7 %. One of the goals during the 2012 LHC run was therefore to understand and counteract the blow-up. In the frame of this thesis several emittance preservation investigations were performed in 2012. Some of the causes of the emittance growth were found. They are presented in this chapter along with possible solutions for emittance blow-up during the LHC cycle. The results are also published in [21, 23, 37].

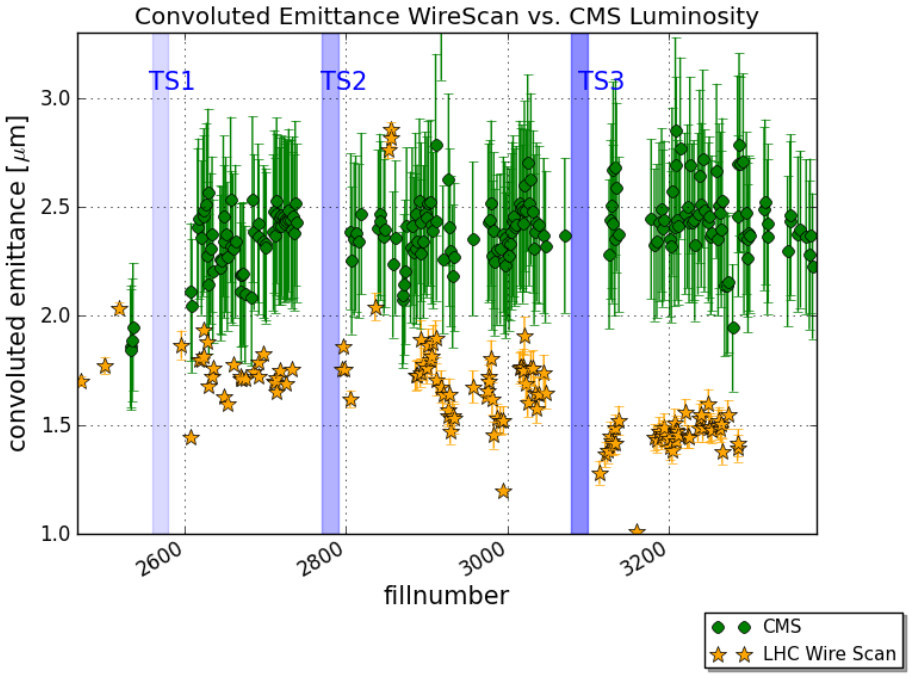

Figure 6.1.: Overview of the emittance evolution in 2012. Convoluted, average emittance of the first 144 bunch batch measured with wire scanners at LHC injection (yellow stars) compared to the emittance calculated from CMS peak luminosity (green dots). The periods of the technical stops are marked with TS. Towards the end of 2012, after Fill 3287, no more wire scans at injection for physics fills were possible due to a broken wire.

A summary of the total emittance blow-up from SPS extraction to LHC collisions for physics fills in 2012 is given in the following. Only fills with 1374 bunches per ring and 50 ns bunch spacing were taken into account. Physics beam emittances are measured at two points of the LHC cycle: wire scans are performed after the first 144 bunch batch injection and indirect measurements of the emittance are obtained through the measurement of luminosity and luminous region at the end of the cycle.

Figure 6.1 shows the evolution of the emittances in collision (green dots) and after injection (yellow stars) for the different physics fills in the 2012 proton run. The injectors managed to produce beams of record brightness, especially with the introduction of the Q20 optics in the SPS after TS3 [1] [38]. Emittances of 1.5 μm with bunch intensities of up to 1.7×10^{11} were injected into the LHC. However, the emittances at collision stayed around 2.3 μm on average, corresponding to a blow-up of up to 40 %.

To find out where the emittances are growing in the LHC cycle and to track down the sources of the blow-up, measurements at all different parts of the cycle were performed:

- at injection into the LHC,
- at the 450 GeV LHC injection plateau,
- during the LHC ramp to 4 TeV flattop energy and
- during the LHC β^* squeeze.

Low intensity test cycles were used to allow wire scanner measurements through the cycle. The LHC BSRTs gave insights into the emittance evolution during the injection plateau and at 4 TeV. Also ATLAS and CMS luminosity and luminous region, as well as LHCb SMOG data were used to shed light on the emittance blow-up in the LHC. The findings are presented in this chapter.

6.1. Emittance Evolution through the Cycle - Overview

Many test cycles with a low number of bunches were carried out. The evolution of the emittances through the different phases was measured with wire scanners at these occasions. A typical example is shown in Fig. 6.2. The emittance growth for all measured cycles in 2012 is similar.

[1] The SPS changed from the so called Q26 optics to Q20 optics to lower the tune and therefore the transition energy in the machine for reasons of longitudinal bunch instabilities. After this change the emittances from the injectors are even smaller, from 1.8 μm to 1.5 μm.

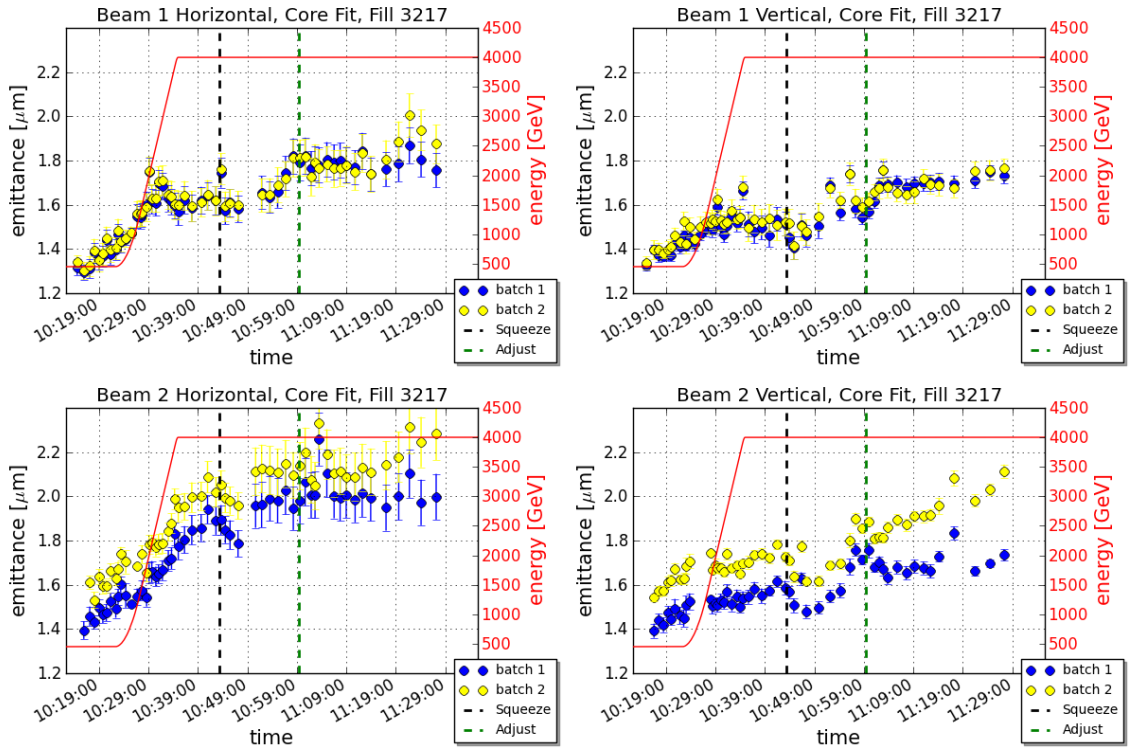

Figure 6.2.: Emittance growth through the LHC cycle for beam 1 and beam 2, horizontal and vertical. The average emittance of six bunches per batch is measured with wire scanners, Fill 3217. Vertical dashed lines indicate the start of the squeeze (black) and the start of "adjust" (green). Batch 1 is colliding in LHCb, batch 2 in ATLAS and CMS.

Figure 6.2 displays the wire scan emittance measurements of the four planes for Fill 3217. Two six bunch batches per ring with bunch intensities of about 1.6×10^{11} ppb and 50 ns bunch spacing were injected, ramped, squeezed and brought into collision. The emittances in the horizontal plane blow up more than the vertical ones. Beam 2 horizontal grows more than beam 1 horizontal. Most of the blow-up seems to come from the injection plateau and the ramp. The total emittance blow-up from injection to collision for all planes is calculated in Table 6.1.

For this particular fill some growth occurs towards the end of the squeeze, which is not negligible for beam 1 horizontal. The measurements in Fig. 6.2 carry on past the beam mode "adjust" where beams are brought into collision. From the point on when "stable beams" is declared, the machine parameters cannot be changed any more to improve emittance preservation. Therefore emittance growth during the period of collisions is not treated further in this thesis. It was tested elsewhere [39].

The rest of the chapter is dedicated to the emittance blow-up during the different phases from SPS extraction to LHC collisions.

		$\varepsilon_{injection}$ [μm]	$\varepsilon_{collision}$ [μm]	$\Delta\varepsilon$ [μm]
B1H	**Batch 1**	1.33 ± 0.04	1.79 ± 0.08	0.46 ± 0.12 (35 %)
	Batch 2	1.34 ± 0.04	1.77 ± 0.08	0.43 ± 0.13 (32 %)
B1V	**Batch 1**	1.37 ± 0.03	1.69 ± 0.03	0.32 ± 0.06 (24 %)
	Batch 2	1.39 ± 0.03	1.66 ± 0.04	0.27 ± 0.07 (20 %)
B2H	**Batch 1**	1.46 ± 0.04	2.12 ± 0.10	0.66 ± 0.14 (45 %)
	Batch 2	1.60 ± 0.03	2.21 ± 0.11	0.60 ± 0.14 (38 %)
B2V	**Batch 1**	1.45 ± 0.03	1.65 ± 0.03	0.21 ± 0.06 (14 %)
	Batch 2	1.60 ± 0.02	1.87 ± 0.03	0.27 ± 0.05 (17 %)

Table 6.1.: Emittance growth through the LHC cycle measured with wire scanners, Fill 3217. Emittances are averaged over six bunches per batch. Wire scans at the end of the cycle are taken at peak luminosity. At the start of collisions beam 1 vertical showed instability. The growth for beam 1 vertical is therefore larger than measured during other test fills.

6.2. Injection into the LHC

The emittances coming from the injectors have bunch-by-bunch variations. Due to the beam production mechanism, the transverse emittances are blowing up more for some bunches in the injector chain. Figure 6.3 shows a wire scan for beam 2 horizontal of the first 144 bunch batch injected into the LHC. The four different PS batches, consisting of 36 bunches each, are injected successively into the SPS. The last batches (PS batch 3 and 4) have smaller emittances than the first batches (PS batch 1 and 2), because they were produced later in time.

The injection process is typically one of the biggest sources of emittance blow-up due to many possible effects of injection mismatch. Special types of screens, inserted into the beam pipe, capable of turn-by-turn profile measurements are normally used to measure the injection mismatch. These monitors are called “matching monitors”. The LHC matching monitors installed in point 4 could not be made operational in the 2011 and 2012 runs. Instead, the wire scan measurements of 144 bunch batches before extraction in the SPS are simply compared to wire scan measurements of the first 144 bunch batch in the LHC.

The SPS is equipped with the same type of linear wire scanners as the LHC. Even though the SPS wire scanners can do bunch-by-bunch measurements, the routine operational mode is “turn mode” which gives one average profile for all bunches. The SPS wire scanners are at locations with very small beta functions. The beam sizes at the wire scanner locations are typically 0.3 to 0.6 mm. Together with the fact that the speed of the wire passing through the beam cannot be reduced further due to

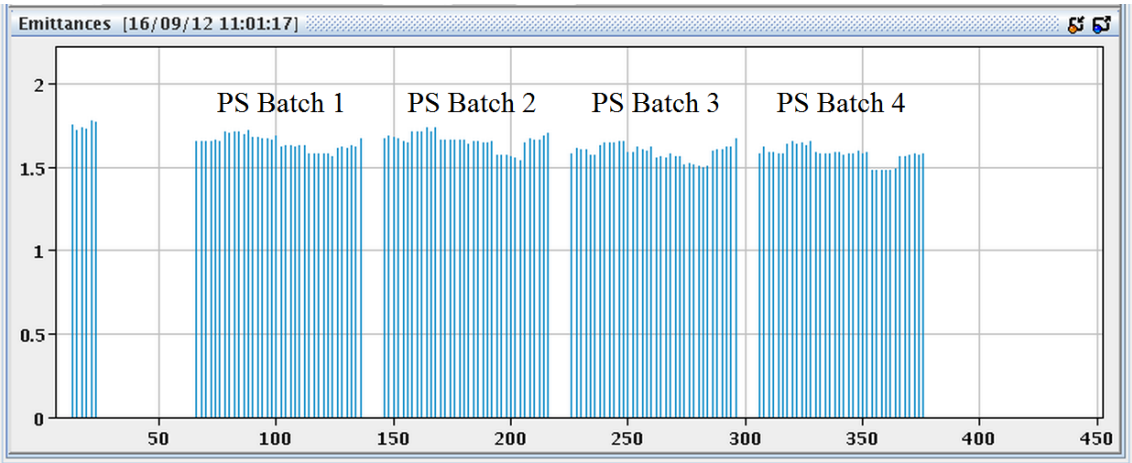

Figure 6.3.: Emittances at LHC injection of the first LHC batch consisting of 144 bunches for beam 2 horizontal. The first six bunches are not counted. The horizontal axes displays the bunch number, the vertical axis the normalized emittance in μm. The emittances measured with wire scanners in the LHC show bunch-by-bunch differences created in the injectors.

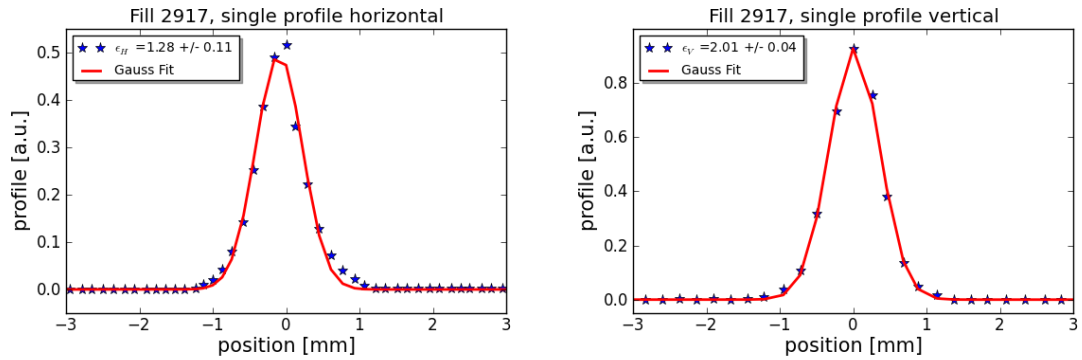

Figure 6.4.: SPS single profile from wire scans of 144 bunches in horizontal and vertical plane at SPS extraction energy of 450 GeV.

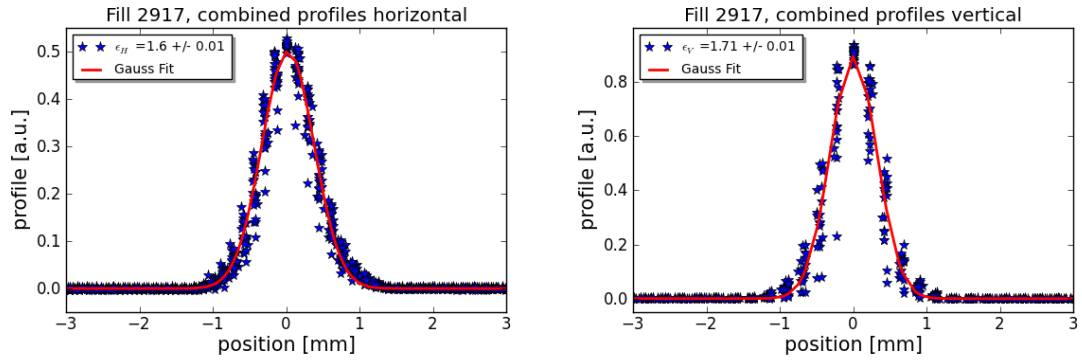

Figure 6.5.: SPS combined profiles from wire scans of 144 bunches in horizontal and vertical plane at SPS extraction energy of 450 GeV.

issues with saturation, only a few points of the profile are available for a single bunch scan. An example is given in Fig. 6.4. Due to a small shot-by-shot beam jitter, the mean of the particle distribution of consecutive scans will be measured at slightly different positions. Overlaying all these profiles and fitting the sum increases the precision of the measurement significantly. Figure 6.5 shows the result of combined profiles in the SPS in the horizontal and vertical plane. This method was also used to obtain the SPS numbers in Fig. 6.6.

Figure 6.6 shows an example of measurements in the SPS (red) and in the LHC (blue). The measurements in the LHC are bunch-by-bunch and filled into a histogram. The LHC emittance values in Fig. 6.6 are obtained from averaging all bunch emittances.

Within the measurement accuracy the emittances at SPS extraction and LHC injection are the same. The measurement error, which includes only the error of the fit, is larger than indicated on the plots of Fig. 6.4, Fig. 6.5 and Fig. 6.6, but difficult to quantify. Typically 10 % accuracy of the emittance measurement is assumed.

Many measurements have been carried out in this way with similar results. As

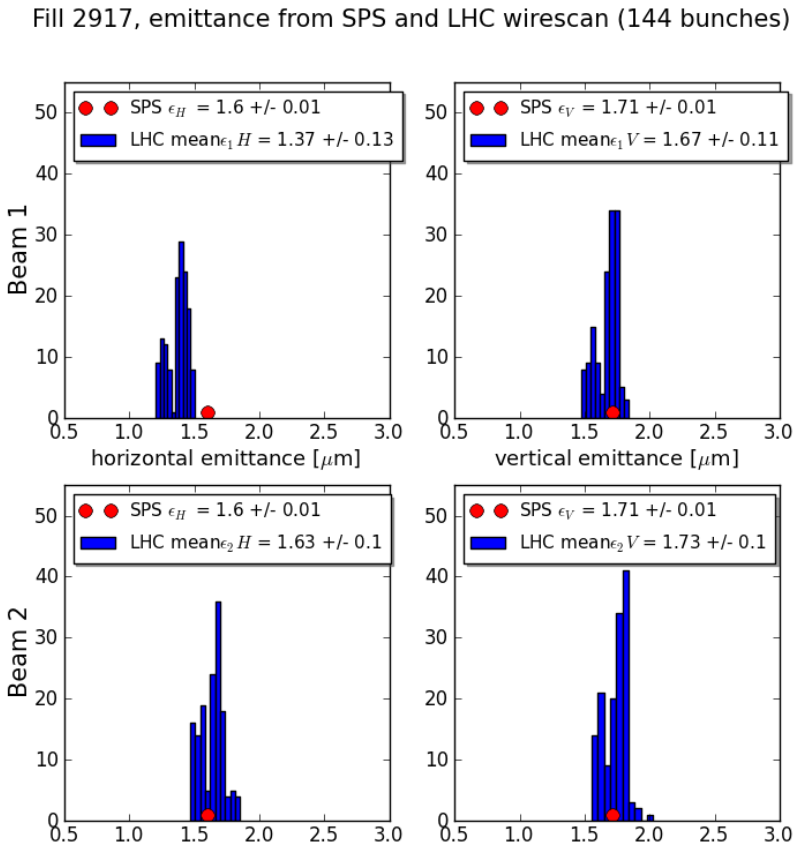

Figure 6.6.: Emittances at SPS and LHC. Wire scan histograms of bunch-by-bunch emittances at LHC injection (blue bars) compared to average emittances of 144 bunches at SPS extraction (red dot).

was already the case in 2011, the emittances in the vertical and horizontal plane are conserved within measurement precision at injection from the SPS into the LHC. This is the result of the excellent matching of the transfer lines to LHC injection point optics and the extremely good performance of the transverse damper system. The effect of the partly large injection oscillations coming from transfer line trajectory instabilities [40] is kept well under control with the LHC transverse damper [13].

6.3. The LHC Injection Plateau

The LHC transverse emittances grow slowly when the beams are circulating at 450 GeV. The growth is stronger in the horizontal plane and does not necessarily manifest itself in the vertical plane. Figure 6.7 displays horizontal emittances of beam 1 as a function of time at the injection plateau for seven individual bunches with different initial emittances. The measured growth rate corresponds to about 10 % growth within 20 minutes. Simulations suggested that the largest fraction of this growth can be attributed to intra-beam scattering (IBS) [41]. Using the measured beam parameters as initial values, the emittances increase by 8 % in 20 minutes in IBS simulations.

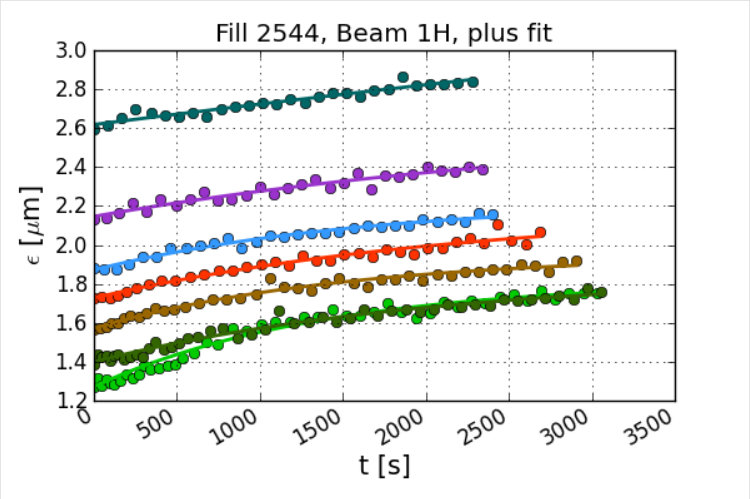

Figure 6.7.: Horizontal emittance growth of beam 1, Fill 2544, at 450 GeV for individual bunches with different initial emittances and bunch intensities. The bunch with the smallest emittance had an intensity of about 0.8×10^{11} ppb, the bunch with the largest emittance had an intensity of about 1.9×10^{11} ppb. For emittances in between, the bunch intensity was increased in steps of 0.2×10^{11} ppb from the smallest to the largest value. Emittances of the seven bunches are measured with the BSRT (dots). An exponential fit (lines) of the emittance blow-up is applied for every bunch.

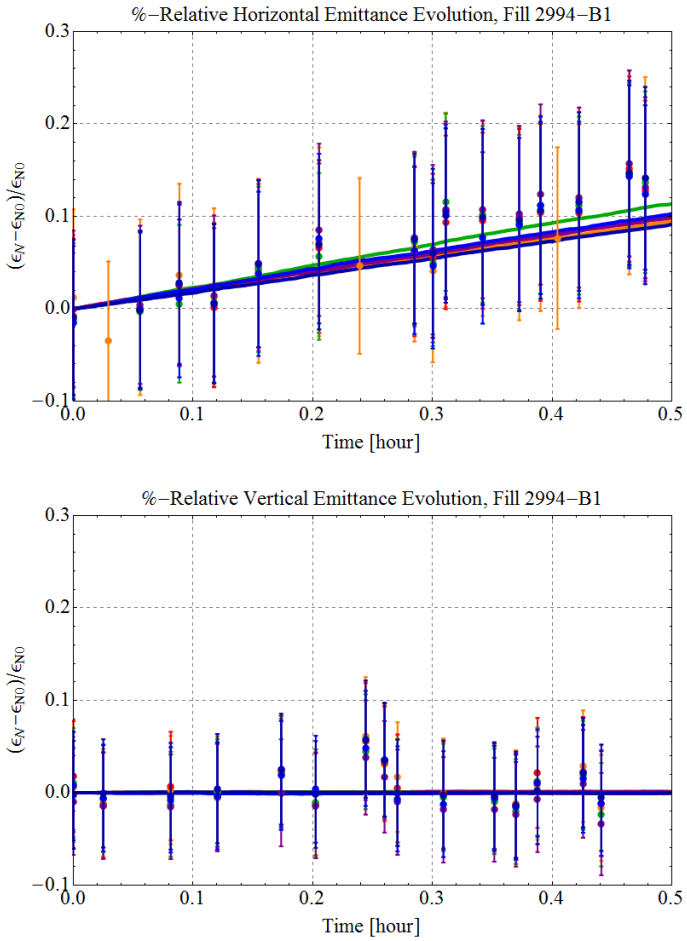

Figure 6.8.: IBS simulations versus measurements of beam 1 horizontal and vertical. Relative emittance growth of beam 1 horizontal and vertical at the injection plateau for six 50 ns bunches with bunch intensities of about about 1.6×10^{11} ppb measured with wire scanner (dots) and compared to IBS simulations with same initial conditions (lines), Fill 2994. *Courtesy M. Schaumann, CERN, Geneva Switzerland.*

In 2012 the emittance evolution of beams with different parameters circulating at 450 GeV was compared to IBS simulations. An example is shown in Fig. 6.8. The horizontal and vertical emittances of six 50 ns bunches with bunch intensities of about 1.6×10^{11} ppb were measured with wire scanners. The results of the IBS simulations are plotted as well. The simulations were performed with the same initial emittance, bunch length and intensity as measured for these bunches. The emittance growth is well predicted with IBS, but slightly faster than the simulation in the horizontal plane. A possible explanation could be noise. The results were cross checked with measurements from BSRT giving similar agreement.

In general, filling for physics takes about 30 minutes for the 12 injections. Because of the emittance growth at injection, batch-by-batch differences of the emittance are expected at the end of the filling. The different batches are injected at different

moments. Therefore they do not all suffer from the same blow-up. This effect introduces batch-by-batch differences in the specific luminosity. The specific bunch luminosity L_{spec} is defined as the bunch luminosity L over the product of the bunch intensities of the two beams, N_1 and N_2:

$$L_{spec} = \frac{L}{N_1 N_2}. \tag{6.3.1}$$

The specific batch luminosity is simply the average specific bunch luminosity of all bunches in one batch.

Batches that stay longer at injection have a larger emittance blow-up and their specific luminosity is smaller than batches that spend less time at the injection plateau, see Fig. 6.9. Averaged over all bunches, emittance blow-up due to IBS is, however, still the smallest contribution to the total observed growth through the cycle.

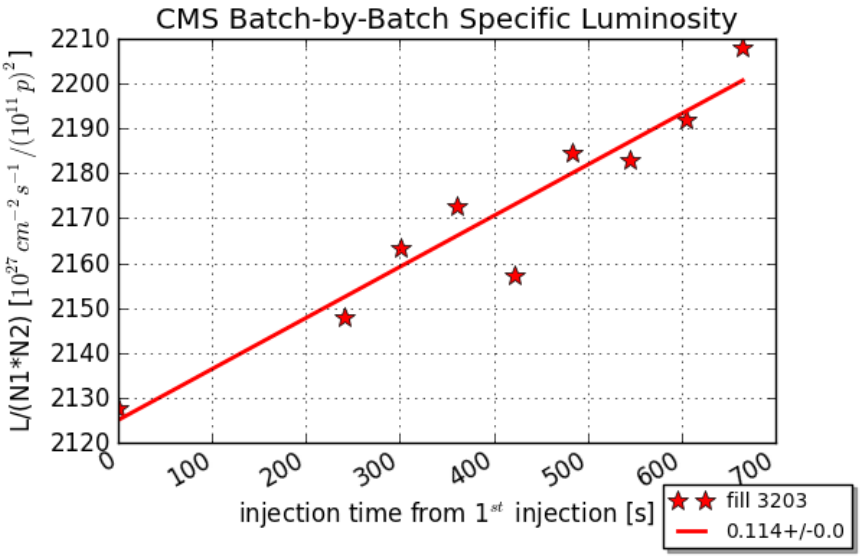

Figure 6.9.: Specific batch-by-batch luminosity of a physics fill (Fill 3203). The specific batch luminosity is plotted as a function of the injection time from the first injection. The data points are fitted with a line, the slope is given in the legend. Last injected batches suffer less from emittance blow-up due to IBS and therefore have a higher specific luminosity.

6.3.1. Possible Cures for Emittance Growth at 450 GeV

A very effective way of reducing the emittance blow-up at the injection plateau would be to shorten the time spent at injection. The LHC filling time could be reduced by at least 30 % by introducing dedicated LHC filling cycles in the injectors. Currently the injectors run several cycles in parallel to LHC beam production. As an example,

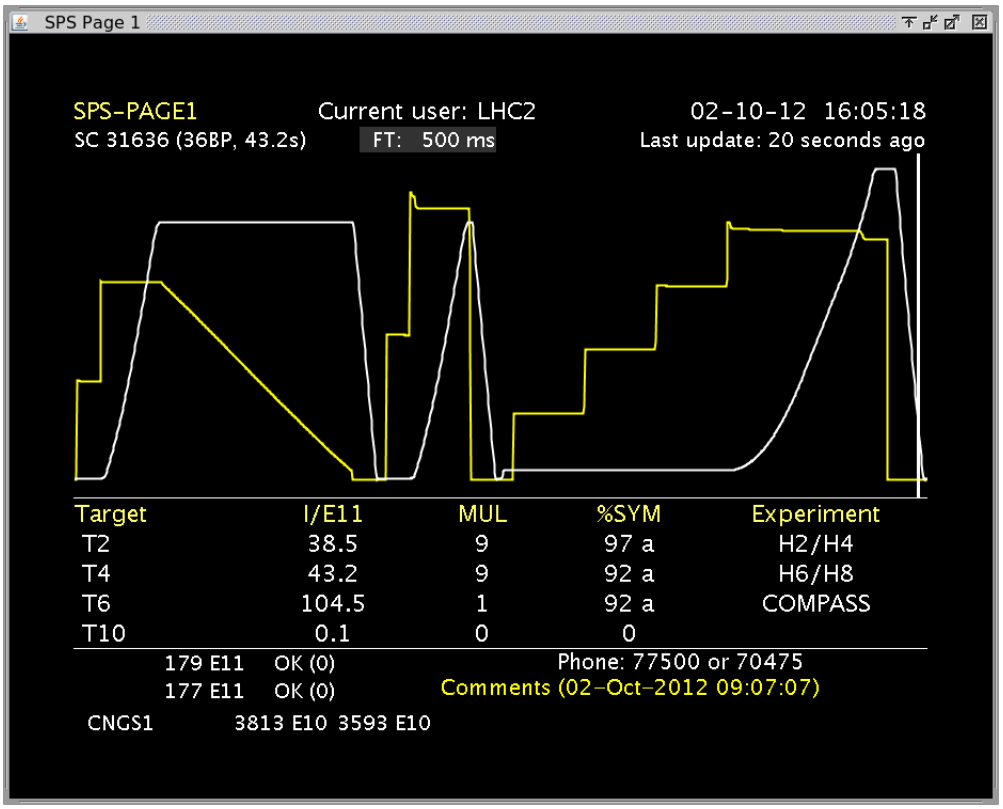

Figure 6.10.: SPS supercycle in 2012 composed of one fixed target cycle for North Area physics, one CNGS (CERN Neutrinos to Gran Sasso) cycle and one LHC cycle with 4 injections of 144 bunches. This was the typical filling cycle of the 2012 LHC run. The total time of the cycle is 43.2 seconds.

Fig. 6.10 shows a picture of the standard SPS supercycle used for LHC filling. A dedicated filling cycle would, however, have significant impact on the physics program in the injectors. The LHC beams in the injectors need namely additional time for preparation outside the filling period as the injector beam parameters are pushed to their stability limits. Currently this would take too much time from other physics programs. Dedicated filling cycles could become an option in case of better reproducibility in the injectors [23].

Fighting IBS: RF Batch-by-Batch Blow-Up

In the LHC a method has been developed to reduce the effects of IBS by decreasing the six-dimensional phase space density of the particle distribution. The so called RF batch-by-batch blow-up increases the bunch length by inducing RF noise which increases the longitudinal emittance. The effects of IBS are stronger for higher densities in six-dimensional phase space. If the longitudinal emittance of each batch at injection from the SPS is blown up, the IBS transverse emittance growth should be reduced.

The longitudinal blow-up only affects newly injected batches, not circulating ones. After each injection, phase noise is injected in the cavities in a periodic time window. The cavity field on the injected RF buckets is modulated with a rise time of 1 μs so that the bunch lengths increase up to a certain target value. The noise spectrum covers a narrow spectral band around the synchrotron frequency suppressing excitation in the tails of the longitudinal distribution and debunching. The excitation is reduced when the average bunch length of the injected batch approaches the target length [42].

RF batch-by-batch blow-up was tested successfully during a machine test period near the beginning of the 2012 run. Figure 6.11 shows a test fill where four batches, consisting of 12 bunches each, were blown up longitudinally and two batches were left to natural growth. The mean bunch length is plotted as a function of the time at injection. Since October 2012 longitudinal blow-up is used for physics fills. To reveal the impact on emittance growth the specific batch-by-batch luminosity of selected physics fills with and without the RF batch-by-batch blow-up is compared, see Fig. 6.12. The average specific luminosity per batch versus time of injection

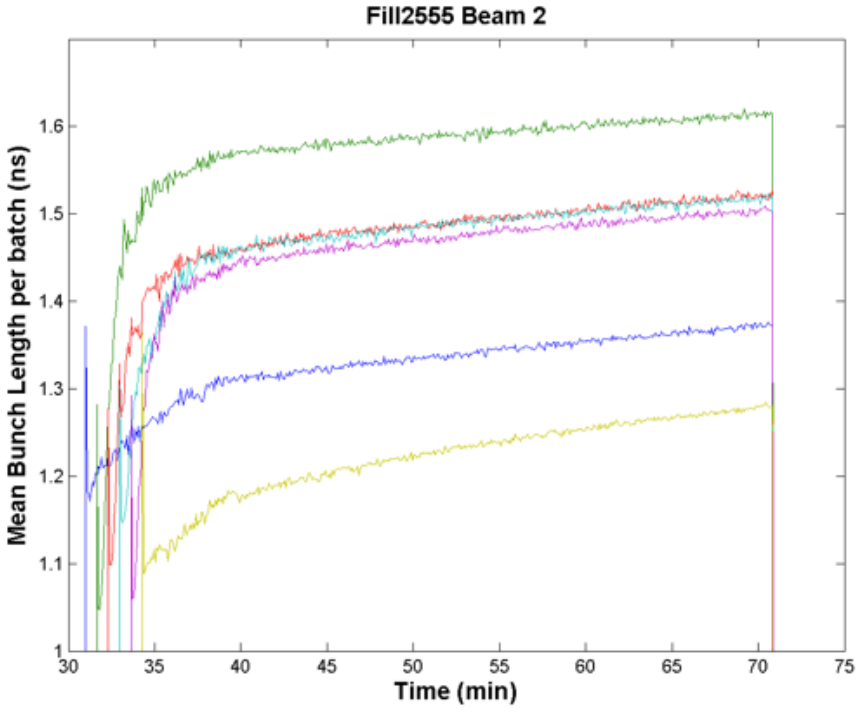

Figure 6.11.: RF batch-by-batch blow-up. Bunch length evolution during batch-by-batch blow-up test: six 12 bunch batches were injected. The first (blue) and last batch (yellow) were left to natural blow-up. The other batches (green, red, cyan and purple) were blown up individually right after injection with a target bunch length of 1.6 ns. *Courtesy T. Mastoridis, CERN, Geneva, Switzerland.*

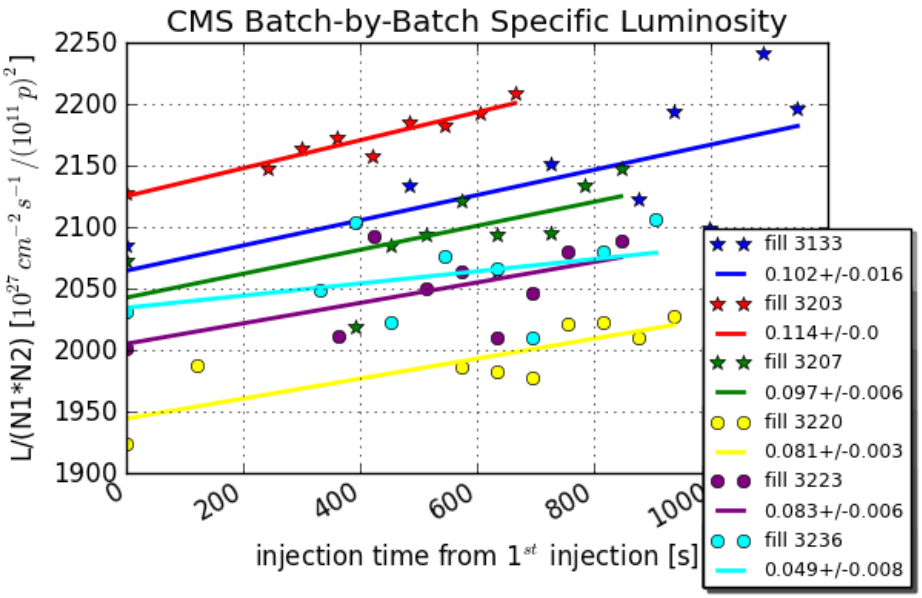

Figure 6.12.: Specific CMS luminosity calculated from CMS peak luminosity and bunch intensity at collision, averaged per batch and plotted as a function of injection time from the first injection for fills with (dots) and without RF batch-by-batch blow-up (stars). Linear fits are plotted as well. The slopes can be found in the legend.

is shown. The slope of the measurement points is a measure for the strength of the emittance blow-up at injection. For fills with RF batch-by-batch blow-up one would expect smaller slopes. Fills 3133, 3203 and 3207 are not blown up. The incoming bunch length is typically 1.2 to 1.3 ns for physics bunches. Fills 3220, 3223 and 3236 have a RF batch-by-batch blow-up with a target bunch length of 1.4 ns. The average slope is slightly smaller for fills with longer bunches but there is no clear improvement. More statistics is needed to make a definite statement. The longitudinal blow-up for physics fills was put into operation only at the end of the 2012 proton run.

6.3.2. Effect of the Transverse Damper Gain at 450 GeV

At injection, the LHC transverse damper is operated with a very high gain to keep emittances small after injection due to injection oscillations and possible other effects. When filling is finished and the mode "prepare ramp" is entered, the gain is reduced to allow for a sufficient tune signal which is measured with LHC Base-Band-Tune (BBQ) monitors [19]. The LHC ramps are run with a tune feedback system which obviously requires a reliable tune signal. The operational damping times in the LHC for physics fills in 2012 are mentioned in section 3.1.2.

The effect of the change in gain on emittance growth was measured in a dedicated test. For Fill 2546 single bunches with an intensity of about 1.4×10^{11} ppb were

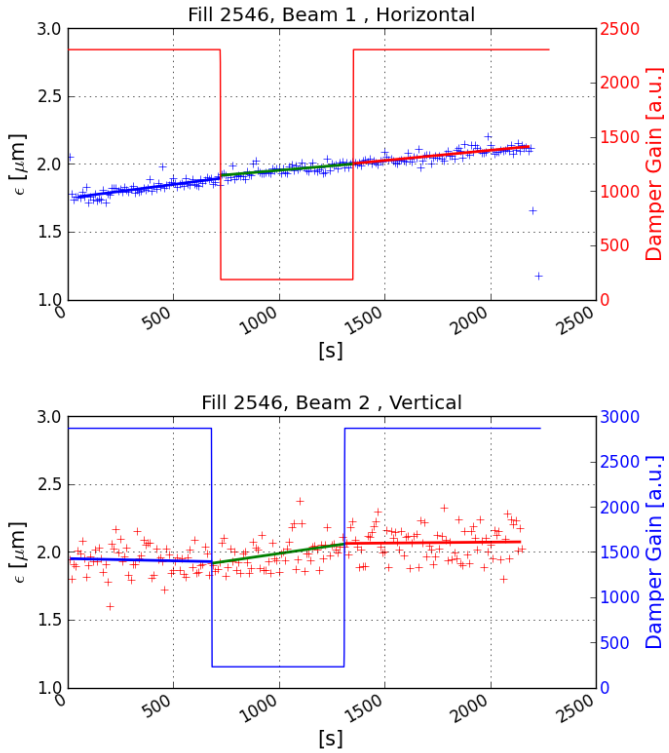

Figure 6.13.: Transverse damper gain effect on emittance growth at 450 GeV, Fill 2546. BSRT measurements of beam 1 horizontal (beam 2 vertical) of one bunch with an intensity of about 1.4×10^{11} protons at injection energy with changing horizontal (vertical) ADT gain from nominal high injection gain to low ramp gain and back to high gain. The emittance growth in the different segments is fitted linearly.

injected. The transverse damper gain was kept at high gain (= injection gain) for 10 minutes while continuously measuring the emittance with the BSRT. Then the gain was lowered to the "prepare ramp" gain for 10 minutes and afterwards increased again for 10 minutes. Figure 6.13 shows the results for beam 1 horizontal and beam 2 vertical. The emittance evolution is displayed as well as the damper gain function. The emittance values are fitted with a linear regression in the different measurement periods to guide the eye. The slope of the fit for the vertical plane clearly increases when moving to lower damper gain. The higher damper gain reduces or even removes the emittance growth. In the horizontal plane the blow-up mainly originates from IBS which the damper has no effect on. The slope of the growth only changes slightly between the different gains.

This result triggered two questions: Could an increased damper gain during the ramp reduce the emittance blow-up, and what causes the blow-up in the vertical plane at 450 GeV, as seen in Fig. 6.13, during the period with lower damper gain? The first question is treated in section 6.4.1. The latter question will be answered in the following.

6.3.3. Influence of 50 Hz Noise

The LHC tune spectrum reveals many noise lines. In Fig. 6.14 a LHC beam spectrum measured with the BBQ system is shown. Some of the noise lines are the 50 Hz main harmonics. The LHC operational tunes [1] are given in Table 6.2. The injection tunes are used from injection to the beginning of the squeeze. With a fractional tune of 0.28 and a revolution frequency of 11.245 kHz, the horizontal tune sits on top of a 50 Hz line ($f_{rev} \times 0.28 = 3148.6$ Hz). Thus the beam is slightly excited by this 50 Hz noise. The LHC equipment responsible for the 50 Hz noise in the beam spectrum has not been identified. Besides magnets or other instruments also field currents in the beam pipe can create noise that disturbs the beam.

The effect of noise on emittance growth was studied during a dedicated experiment, Fill 3159. For this fill 6 + 6 bunches with bunch intensities of 1.3×10^{11} ppb and 50 ns bunch spacing were injected per ring. The transverse damper was switched

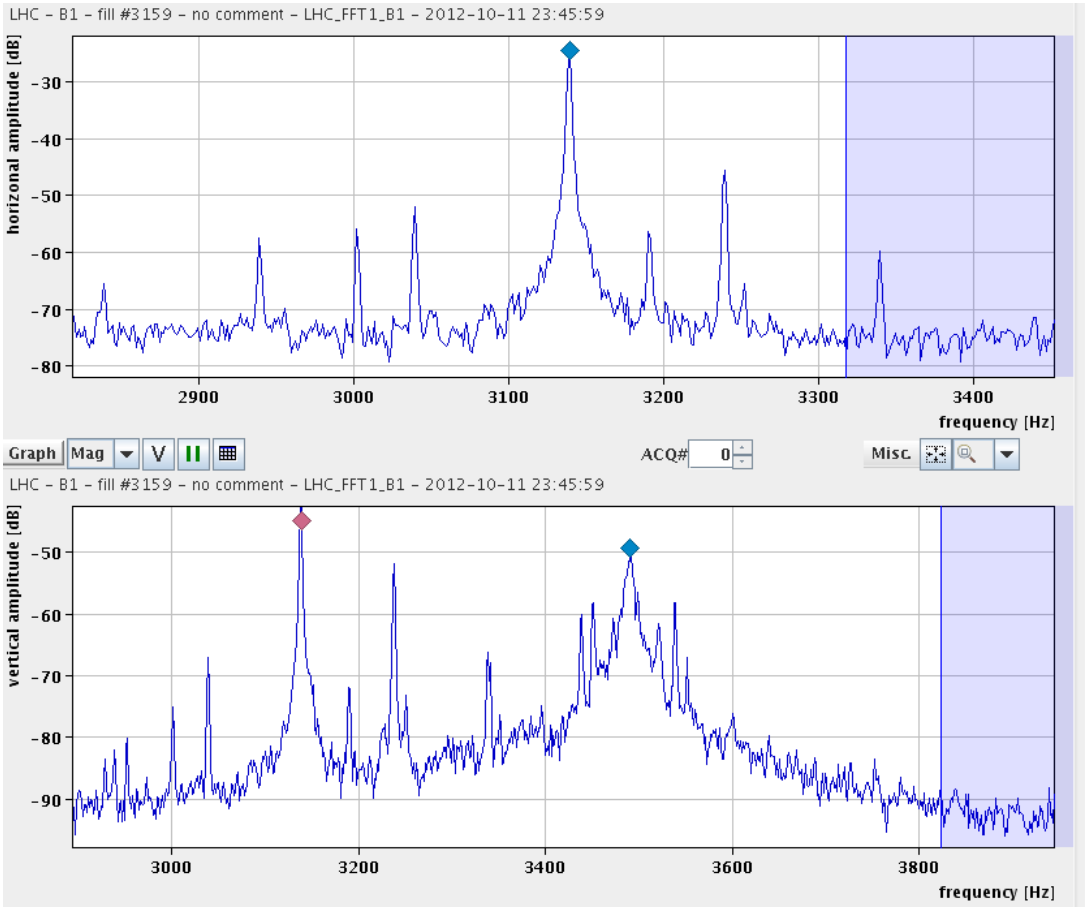

Figure 6.14.: LHC beam spectrum for the nominal tune (0.28 in the horizontal plane) measured with the BBQ for beam 1 horizontal (top) and vertical (bottom). The frequency of the nominal tune is displayed (blue diamond). The horizontal tune sits at 3149 Hz and the signal has a large amplitude due to 50 Hz noise (approximately -20 dB).

off. For a period of 10 minutes the beam was kept at the nominal fractional horizontal tune of 0.28 while the emittances were measured. Then the horizontal tune was moved to 0.283 (f_{rev}· 0.283 = 3182.3 Hz), which should be far enough from a 50 Hz line, see Fig. 6.15. Again the settings were kept for 10 minutes. The series of measurements was finished with another 10 minutes at the nominal horizontal tune. Figure 6.16 summarizes the results. The emittance evolution measured with wire scanners for beam 1 is shown. Not only the emittances in the horizontal plane

	Injection	**Collision**
Horizontal tune	64.28	64.31
Vertical tune	59.31	59.32

Table 6.2.: LHC horizontal and vertical tune at injection (to flattop) and collision (from start of squeeze).

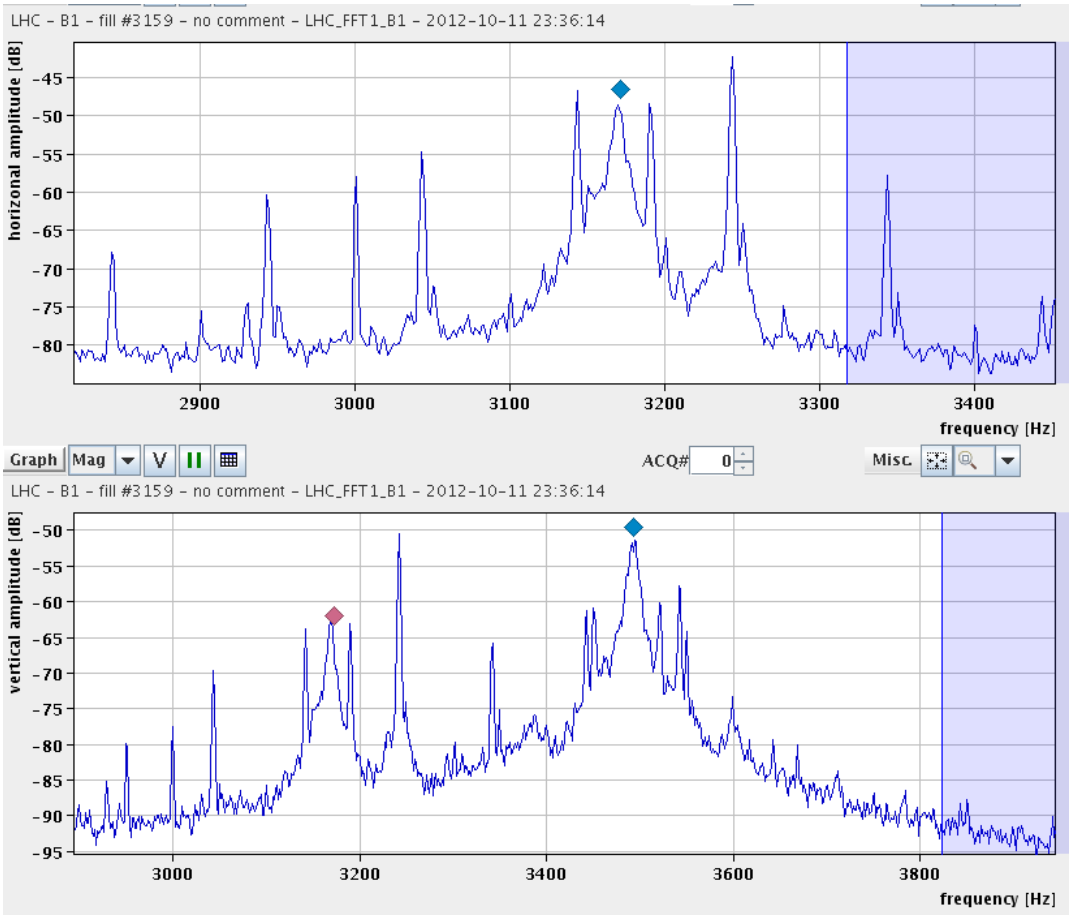

Figure 6.15.: LHC beam spectrum for a different tune (0.283 in the horizontal plane) measured with the BBQ for beam 1 horizontal (top) and vertical (bottom). The frequency of the tune, 3182 Hz, is displayed (blue diamond). The beam is oscillating less, as the amplitude is reduced (approximately -50 dB).

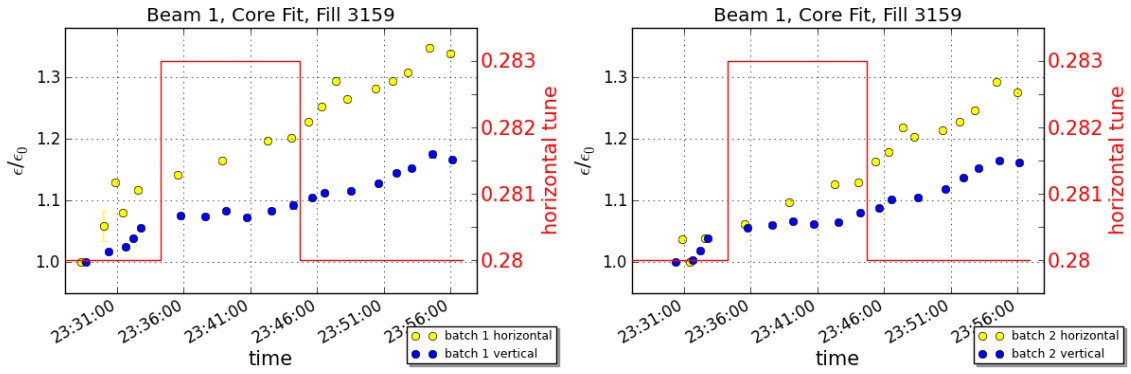

Figure 6.16.: Emittance growth due to 50 Hz noise. Relative average emittance growth of 6 + 6 bunches with bunch intensities of 1.3×10^{11} ppb and 50 ns bunch spacing at injection energy for beam 1 horizontal and vertical measured with wire scanners, Fill 3159. ε_0 is the emittance at injection into the LHC. The horizontal tune is displayed. The left plot displays the results for batch 1 and the right plot for batch 2.

grow faster when at a horizontal tune of 0.28, but also the vertical ones due to the relatively high coupling of $|C^-| \approx 0.005$ during this fill (a factor 2 above the coupling acceptable for physics fills). The emittance blow-up in the vertical plane almost vanishes with a horizontal tune of 0.283. In the horizontal plane, however, IBS keeps the emittances growing also at a tune of 0.283, but more slowly.

The 50 Hz noise and the fact that the horizontal tune sits on top of a 50 Hz line could explain the slightly faster emittance growth in the horizontal plane than predicted in IBS simulations. It could also be an explanation for the observed growth in the vertical plane at 450 GeV at some occasions.

6.4. The LHC Ramp

In an ideal LHC the normalized emittance stays constant during the energy ramp, whereas the geometrical emittance decreases with higher energy following Eq. 2.4.7.

Figure 6.17 shows how the normalized emittances behave in reality in the LHC during the ramp. During a low intensity test fill with 6 + 6 bunches per ring wire scan measurements were taken throughout the ramp. The test ramp is part of Fill 3217 shown earlier when introducing the overall emittance growth during the LHC cycle in section 6.1.

The measurements indicate significant growth of the emittances during the ramp, which is larger in the horizontal plane than in the vertical plane and more pronounced for beam 2 than for beam 1. For Fill 3217 the total average emittance growth during the ramp is about 20 % for beam 2 horizontal, about 15 % for beam 1 horizontal, and approximately 5 % in the vertical plane for both beams. The de-

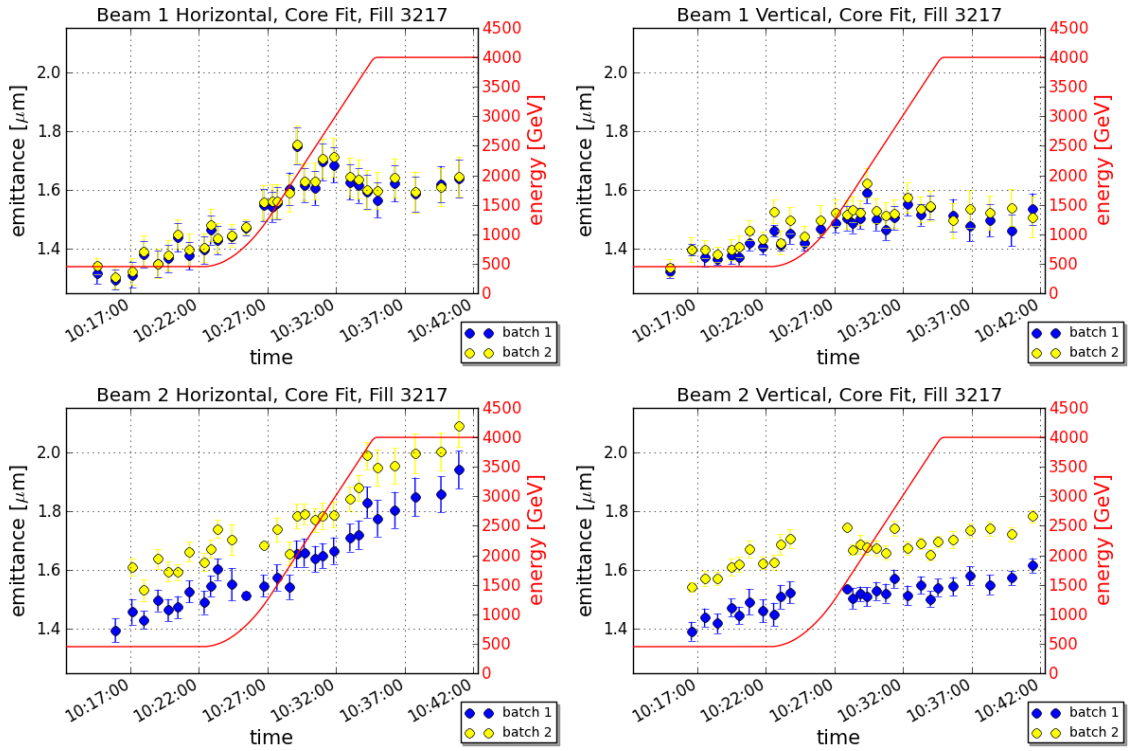

Figure 6.17.: Emittance growth during the ramp for beam 1 and beam 2. Wire scans in the horizontal (left) and vertical (right) plane during the ramp with emittances averaged over six bunches in one batch, Fill 3217.

		$\varepsilon_{injection}$ [μm]	$\varepsilon_{collision}$ [μm]	$\Delta\varepsilon$ [μm]
B1H	**Batch 1**	1.41 ± 0.05	1.59 ± 0.06	0.18 ± 0.10 (13 %)
	Batch 2	1.43 ± 0.05	1.61 ± 0.06	0.18 ± 0.10 (13 %)
B1V	**Batch 1**	1.43 ± 0.02	1.53 ± 0.05	0.10 ± 0.06 (7 %)
	Batch 2	1.46 ± 0.02	1.54 ± 0.05	0.08 ± 0.06 (5 %)
B2H	**Batch 1**	1.52 ± 0.02	1.81 ± 0.05	0.29 ± 0.07 (19 %)
	Batch 2	1.65 ± 0.02	1.97 ± 0.06	0.31 ± 0.08 (19 %)
B2V	**Batch 1**	1.47 ± 0.01	1.56 ± 0.01	0.08 ± 0.01 (6 %)
	Batch 2	1.65 ± 0.01	1.71 ± 0.01	0.07 ± 0.02 (4 %)

Table 6.3.: Emittance growth during the ramp for Fill 3217. The emittances at the start of the ramp and at the end of the ramp are averaged over six bunches per batch.

tailed values of the emittance growth during the ramp can be found in Table 6.3. The observed growth is unlikely to be a measurement artifact. The measured beta functions are used at injection and flattop and a linear interpolation between these values for energies during the ramp is applied. Dispersion is not taken into account

as it has been measured to be small ($\leq$ 10 cm at injection, $\leq$ 30 cm at flattop) [2].

Note that the absolute emittance blow-up through the ramp is roughly the same, independent of the emittance value at the start of the ramp. Beam 2 had two batches with different initial emittances, but their absolute emittance growth during the ramp is similar.

6.4.1. Effect of the Transverse Damper Gain during the Ramp

While the causes of emittance blow-up during the injection plateau have become clear, the sources of emittance growth during the ramp are not revealed yet. Reducing the damper gain to allow for operation of the tune feedback system leads to larger beam oscillation amplitudes which are picked up by the BBQ, see Fig. 6.18. These could potentially lead to emittance increase. Hence a test ramp with larger damper gain was carried out during the third machine development period in 2012.

As the tune feedback has to work for all LHC ramps, the damper gain cannot just be increased across the machine, but for the majority of bunches only. The possibility of a special damper gain modulation around the machine circumference had to be developed, such that a few sacrificial bunches have lower damper gain, whereas for the rest of the bunches the damper gain can be maximized [14].

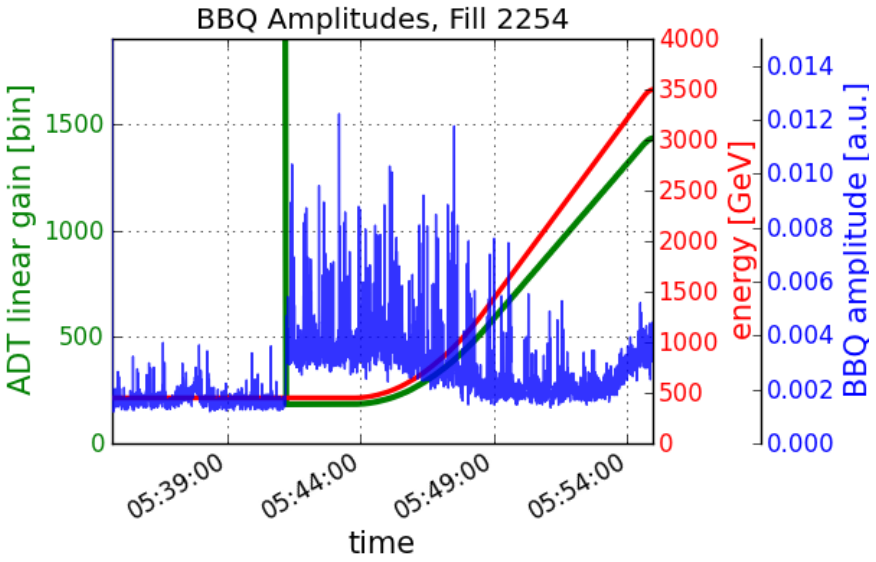

Figure 6.18.: BBQ amplitudes during the ramp (blue) with reduction of the transverse damper gain (green) at the beginning of the ramp. The energy is displayed as well (red).

[2]The beam size contribution from dispersion σ_D to the observed beam size $\sigma_{obs} = \sqrt{\sigma_\beta^2 + \sigma_D^2}$ is $\sigma_D = D \frac{\Delta p}{p}$. With $\frac{\Delta p}{p} \sim 3 \times 10^{-4}$ at injection and $\frac{\Delta p}{p} \sim 1 \times 10^{-4}$ at flattop energy, the beam size from dispersion is $\sigma_D \approx 60$ μm at injection and $\sigma_D \approx 70$ μm at flattop, whereas the beam size from betatron motion is $\sigma_\beta \approx 600$ - 700 μm at injection and $\sigma_\beta \approx 200$ - 300 μm at flattop, in the horizontal plane. The values in the vertical plane look similar.

The behavior of the emittances through the ramp with increased transverse damper gain was investigated during Fill 3160. For this test ramp four six bunch batches with bunch intensities of 1.3×10^{11} ppb and 50 ns bunch spacing were injected per ring. The gain as a function of 40 MHz RF bucket for the ramp looked like depicted in Fig. 6.19. Table 6.4 summarizes the ADT gain for the different batches for this fill. The first batch had a very low damper gain to allow enough signal for the tune feedback. The second batch had the typical low ramp gain which was used during most of the ramps in 2012. Batch 3 and 4 were ramped with a very high transverse damper gain. The gain function through the ramp for this test fill is shown in Fig. 6.20. At low energies it is possible to apply a higher transverse damper gain than at high energies due to saturation of the damper electronics.

For the test ramp the total intensity per ring was low enough to measure the emittances with wire scanners. The results of the ramp of batches with different damper gains are shown in Fig. 6.21. Beam 1 horizontal and vertical are displayed. The emittance blow-up looks similar to previous measurements during the ramp, see

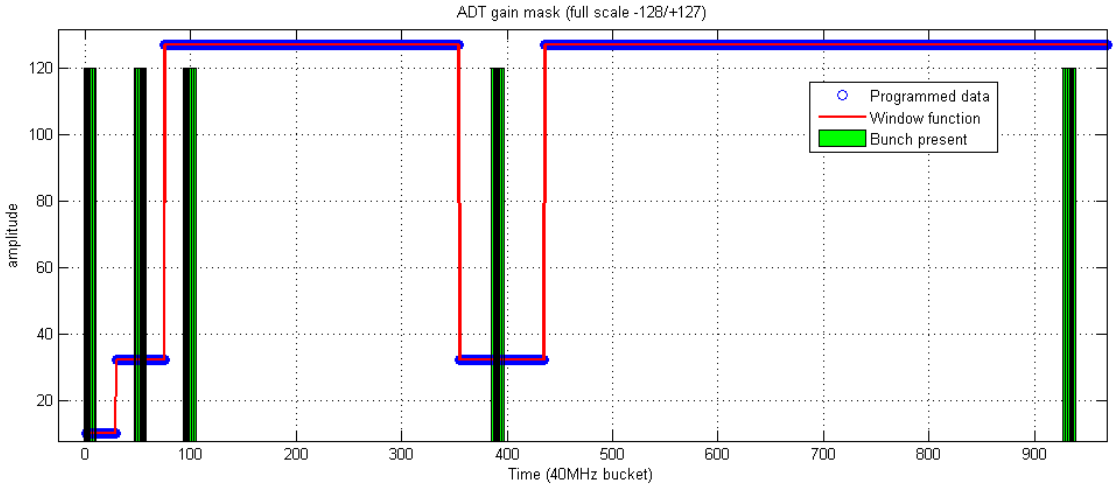

Figure 6.19.: ADT ramp gain modulation for Fill 3160, beam 1. The gain modulation function for beam 2 was identical, see appendix. Batch number 4 was not injected. The function was applied before starting the ramp.

Beam 1 and 2	**Transverse damper gain**
Batch 1	Very low gain bunches: sacrificial, lower than operational gains damping time $\sim$ 300 turns
Batch 2	Low gain bunches: nominal prepare ramp gain damping time $\sim$ 100 turns
Batch 3 and 4	High transverse damper gain damping time $\sim$ 25 turns

Table 6.4.: ADT ramp gain modulation for 4 batches, Fill 3160.

Fig. 6.17. The growth in the vertical plane is smaller than in the horizontal plane. The horizontal emittance blow-up for every batch is compared in Table 6.5. For all batches of beam 1 the average growth in the horizontal plane during the ramp is roughly the same, about 25 % for the very small initial emittances of about 1 μm. There is no significant difference of blow-up for different transverse damper gains. In conclusion the higher transverse damper gain had no measurable influence on the emittance growth during the ramp for this fill.

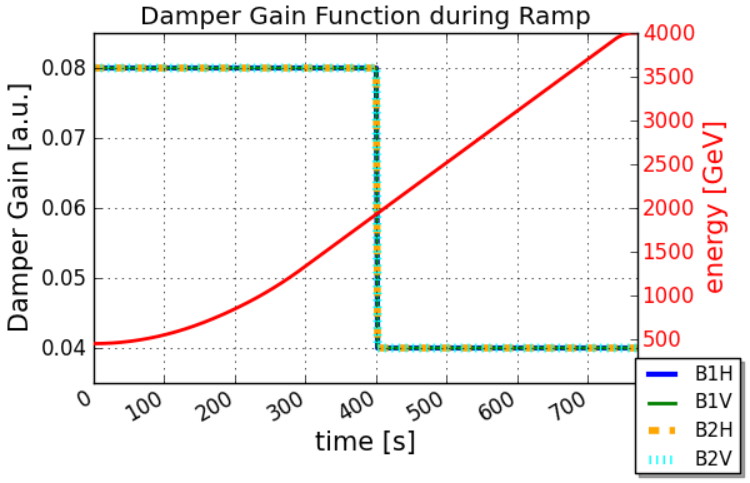

Figure 6.20.: ADT ramp gain functions for all planes, Fill 3160. The normalized ADT gain as a function of the energy is plotted.

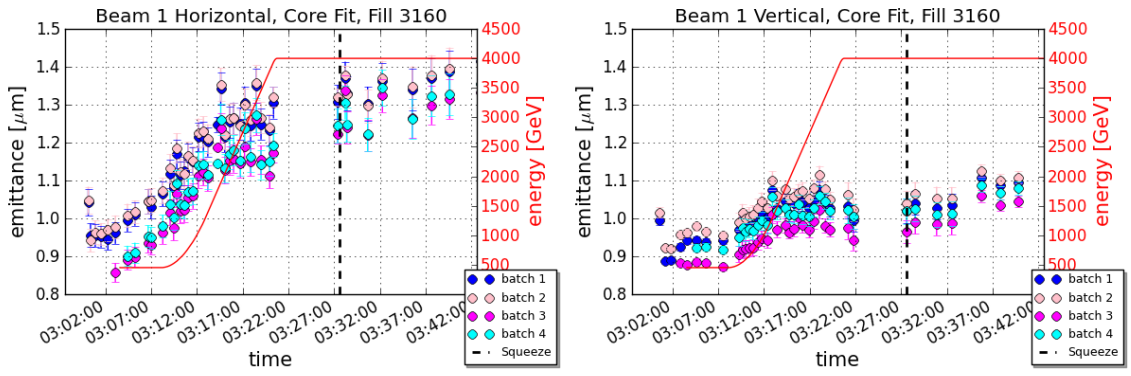

Figure 6.21.: Ramp with different ADT gains. Average emittance of six bunches per batch through the ramp and the squeeze for beam 1 horizontal and vertical measured with wire scanners, Fill 3160. The bunches had different transverse damper gains at the start of the ramp, see Table 6.4.

Beam 1 horizontal	Growth during ramp [μm]
Batch 1	0.24 ± 0.08 (23 %)
Batch 2	0.25 ± 0.06 (23 %)
Batch 3	0.26 ± 0.05 (27 %)
Batch 4	0.27 ± 0.07 (27 %)

Table 6.5.: Emittance growth of beam 1 in the horizontal plane during the ramp for batches with different ADT gains, Fill 3160.

6.5. The LHC Squeeze

The β^* squeeze is a delicate operation, where the optic changes, beta-beat and chromaticity corrections are feed forwarded and the orbit feedback has to work well to keep the beams on the reference trajectory. Nevertheless, unlike to 2011, no significant growth seems to occur during the squeeze in 2012. The emittances stayed constant throughout the squeeze within measurement precision for the largest part of the 2012 run, except when singular bunches went unstable. A typical example of the evolution of the beam sizes during the squeeze is shown in Fig. 6.22. BSRT

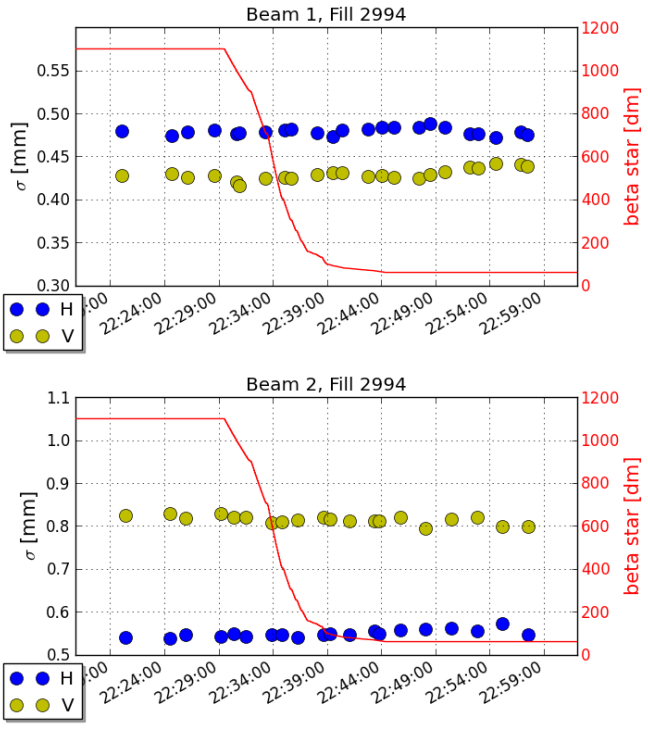

Figure 6.22.: BSRT measurements during squeeze of low intensity Fill 2994 for beam 1 and beam 2, horizontal and vertical. The average transverse beam size of 32 bunches with 50 ns bunch spacing and bunch intensities of 1.1 $\times$ 10^{11} ppb is displayed.

measurements for Fill 2994 are presented. The average beam size of 32 bunches with 50 ns bunch spacing and bunch intensities of 1.1×10^{11} ppb is plotted.

Towards the end of the 2012 proton run a small blow-up at the end of the squeeze for beam 1 horizontal was observed, but not always by the same amount. Figure 6.23 shows wire scanner measurements during the squeeze of beam 1 and beam 2 horizontal for Fill 3217, a fill with 6 + 6 bunches per ring with bunch intensities of 1.6×10^{11} ppb and 50 ns bunch spacing. The beam sizes in the vertical plane are conserved. In the horizontal plane of beam 1 a small blow-up at the end of the squeeze can be seen. This was cross checked with other measurements because of the few data points. The BSRT measurements also confirm an emittance blow-up for beam 1 horizontal, see Fig. 6.24.

Another example of emittance blow-up in the horizontal plane of beam 1 during the squeeze is shown in Fig. 6.25 for a physics fill, Fill 3264. The vertical emittances are also conserved for physics fills. The sources for the emittance growth could have been introduced with the change of LHC run conditions, such as octupole polarity

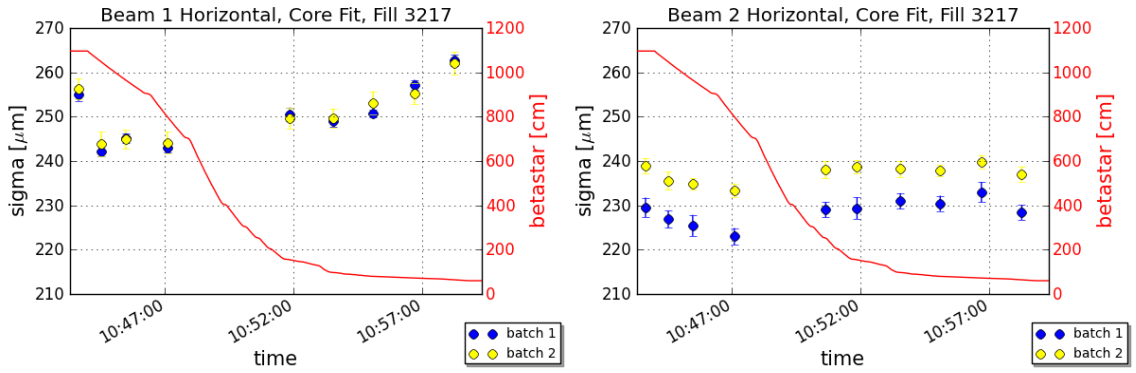

Figure 6.23.: Wire scans during squeeze for beam 1 and beam 2 horizontal. Transverse beam size evolution averaged for 6 + 6 bunches with bunch intensities of 1.6×10^{11} ppb and 50 ns bunch spacing, Fill 3217.

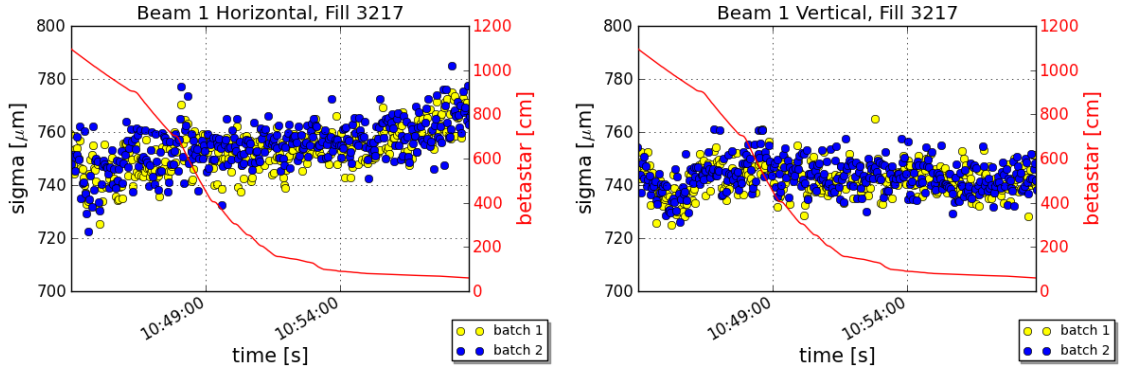

Figure 6.24.: BSRT measurements during squeeze for beam 1 horizontal and vertical. Transverse beam size evolution averaged for 6 + 6 bunches with bunch intensities of 1.6×10^{11} ppb and 50 ns bunch spacing, Fill 3217.

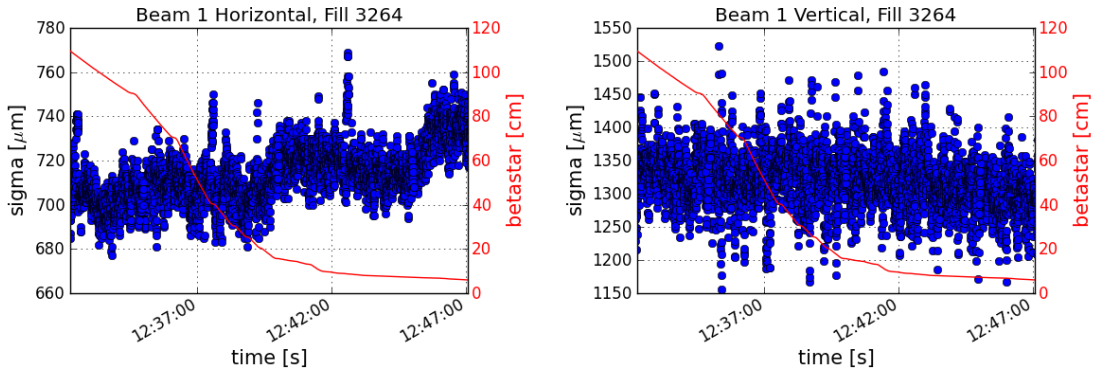

Figure 6.25.: BSRT measurements during squeeze of physics Fill 3264 for beam 1 horizontal and vertical. The bunch-by-bunch transverse beam sizes are displayed.

reversal, higher bunch intensities and chromaticity function adaptations, towards the end of the 2012 proton run.

6.6. Measures against Emittance Growth

Emittance studies in 2011 and 2012 suggested possible solutions for emittance blow-up during the LHC cycle. After technical stop 3 (TS3) several potential measures against emittance growth became operational.

Since Fill 3220 the RF batch-by-batch blow-up is used for physics fills. First the target bunch length of the longitudinal blow-up was set to 1.4 ns. As no improvement in the peak luminosity was observed, the target bunch length was increased to 1.5 ns, which did not lead to improvements in peak luminosity either. The target bunch length (10 to 90 %) is reached in approximately 1 minute.

Because the gated BBQ system [43] became operational after Fill 3286, it was possible to have fills with higher ADT gain for the ramp. The normalized ramp gain as a function of energy is plotted in Fig. 6.26. Also ADT high bandwidth is used from flattop to the start of stable beams. The enhanced bandwidth provides faster damping of high frequency modes, such that ideally damping of every bunch individually is achieved with a bandwidth of 20 MHz [14]. Table 6.6 summarizes details of the measures taken at the end of the 2012 proton run for physics fills.

Figure 6.27 shows the influence of the different measures on the emittance at LHC collision. The emittance at injection is plotted as well, where available, to give an idea about the growth. The emittances at peak luminosity vary slightly. But one can conclude that the way RF batch-by-batch blow-up was used at the end of 2012 did not improve the performance in a measurable way.

In Fig. 6.27 the average emittance from luminosity over all bunches is shown. Towards the end of the period shown in the figure the emittances of more and more

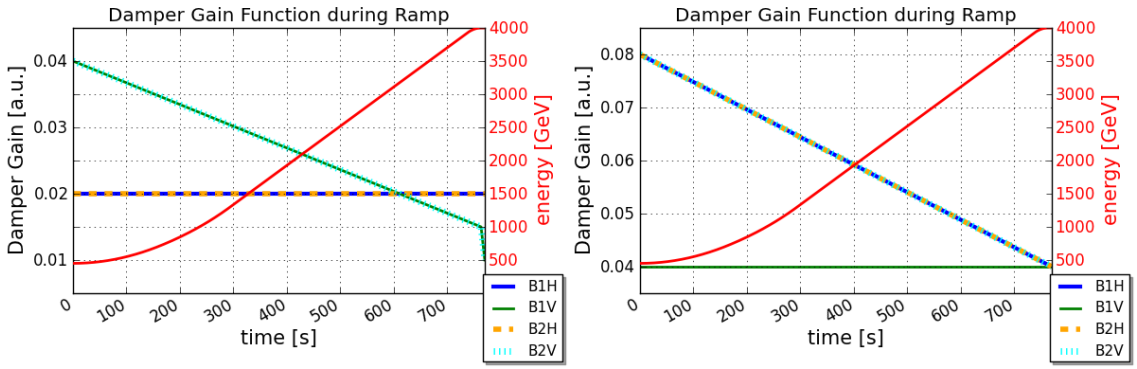

Figure 6.26.: ADT ramp gain functions for all planes. The normalized ADT gain as a function of the energy is plotted. The ADT ramp gain function shown in the left plot was applied for physics fills during the 2012 proton run until the change (11-14-2012) to higher ramp gain towards the end of the 2012 proton run (right plot).

RF batch-by-batch blow-up	Target bunchlength = 1.4 ns in $\sim$ 1 minute Target bunchlength = 1.5 ns in $\sim$ 1 minute
ADT high bandwidth	Measured enhanced frequency response reaches beyond 20 MHz bunch-by-bunch transverse damper
High ADT ramp gain	Damping time $\sim$ 25 turns at the start of the ramp (nominal prepare ramp damper $\sim$ 100 turns)

Table 6.6.: Details of measures against emittance growth: RF batch-by-batch blow-up, high ADT bandwidth and high ADT ramp gain.

singular bunches blew up in the last part of the cycle due to instabilities most likely from an interplay between high machine impedance, beam-beam effects and high chromaticity for high bunch intensities [44–46]. Looking at the specific bunch-by-bunch luminosity is therefore more useful to reveal the influence of the measures taken.

Figure 6.28 depicts a comparison of the specific bunch-by-bunch luminosity of a fill with low damper gain (Fill 3203) and a fill with high damper gain during the ramp (Fill 3299). Indeed, the maximum specific bunch luminosity is higher with higher ramp damper gain. With many bunches slightly unstable in Fill 3299, the average specific luminosity, and thus the emittance, for all bunches is still similar to the values with lower damper gain during the ramp. This increase of specific bunch-by-bunch luminosity has been seen for most fills during the period with higher damper gain in the ramp. In conclusion, the higher ramp damper gain seems to reduce emittance blow-up.

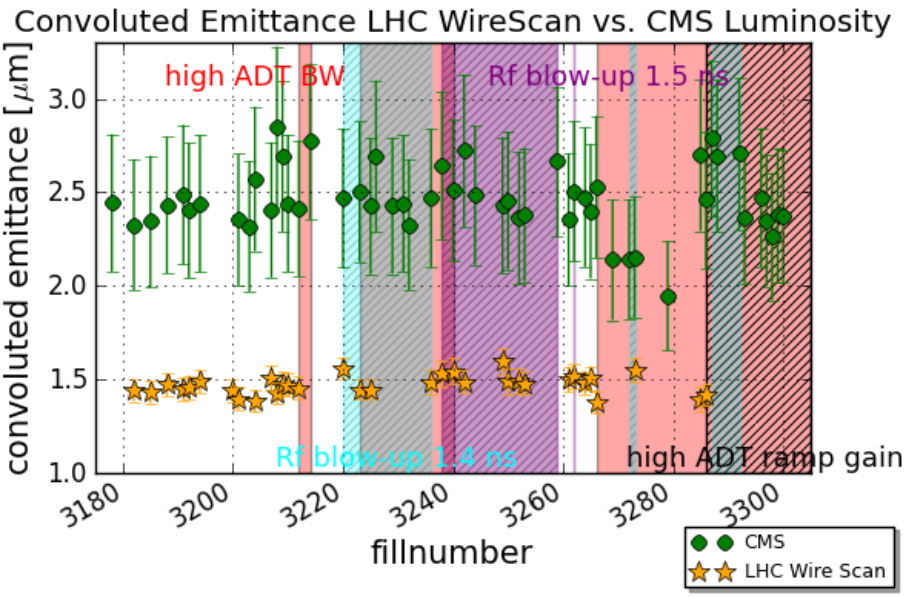

Figure 6.27.: Influence of different measures against emittance growth. Convoluted averaged emittance of the first 144 bunch batch measured with wire scanners at injection into the LHC and compared to the emittance obtained from peak luminosity at CMS. Periods with different measures as RF batch-by-batch blow-up (target bunch length 1.4 ns = blue, target bunch length 1.5 ns = purple), high ADT bandwidth (BW) (red) and high ADT ramp gain (black) are highlighted.

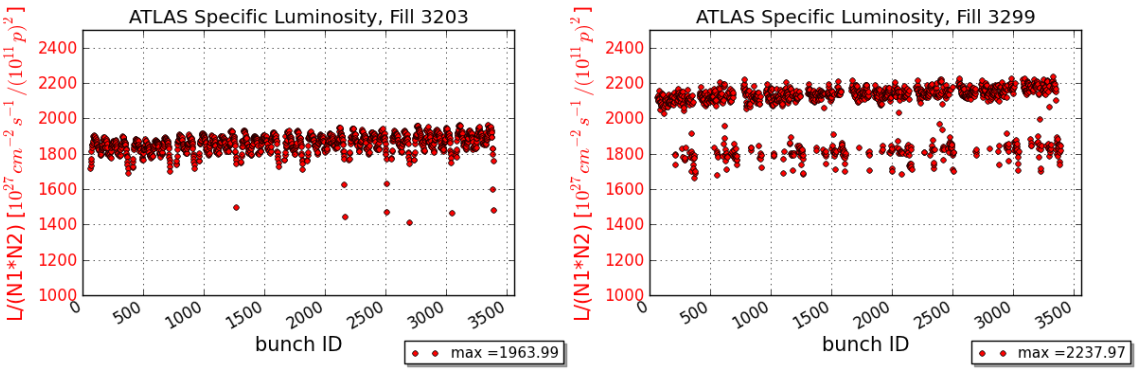

Figure 6.28.: Specific bunch-by-bunch luminosity for higher ADT ramp gain at peak luminosity, plotted for a fill with nominal low ramp gain, Fill 3203 (left), and for a fill with higher ADT ramp gain, Fill 3299 (right). Values for the maximum specific bunch luminosity are given in the legend.

There is a short period around Fill 3280, see Fig. 6.27, where the emittances at collision are reduced. Here only the high ADT bandwidth was used. Due to the small number of fills during this period it is, however, not clear whether this is not just a statistical fluctuation. More fills with these settings will be necessary to

conclude.

In summary, from all possible measures to counteract emittance blow-up through the cycle, only the higher damper gain during the ramp measurably reduces emittance growth.

Summary: 2012 Emittance Preservation at the LHC

- **Injection into the LHC**
  No emittance blow-up from the injection process, the transfer from SPS to LHC, within measurement accuracy.

- **450 GeV LHC injection plateau**
  During the LHC injection plateau the emittances grow in the horizontal plane, consistent with intra-beam scattering (IBS).
  - Possible solutions could be dedicated LHC filling cycles in the injectors.
  - RF batch-by-batch blow-up as a cure against IBS emittance growth did not improve the performance in a measurable way.
  - The higher transverse damper gain has a positive effect on emittance growth at the injection plateau.
  - Additional growth during the injection plateau is caused by 50 Hz noise.

- **LHC ramp to 4 TeV flattop energy**
  The emittance blow-up during the LHC ramp is the largest contribution to the overall growth. The blow-up was stronger for beam 2 than for beam 1 and more pronounced in the horizontal plane than in the vertical plane. The source of the growth during the ramp is not clear.
  - For a test fill higher transverse damper during the ramp had no measurable influence on emittance blow-up.
  - For physics fills higher ADT ramp gain might reduce the emittance growth.

- **LHC β^* squeeze**
  Only towards the end of the 2012 proton run beam 1 horizontal was indicating an emittance blow-up at the end of the squeeze. The emittances in the vertical plane are conserved.
  - Higher ADT bandwidth as used in operation at the end of the 2012 proton run could possibly reduce the total emittance growth through the LHC cycle.

7. Precision of Emittance Measurements with Wire Scanners

The transverse profile monitors have to measure the transverse beam size precisely to be able to determine the emittance correctly. Typically an uncertainty of 10 % on the emittance value is assumed. The wire scanner is the most accurate instrument and the other profile monitors are calibrated against it. However, a complication in choosing the optimum settings for the wire scanners was discovered in 2012.

Shrinking Emittance during the Ramp

Measurements through the ramp with wire scanners in the beginning of 2012 revealed emittances partly shrinking with energy. Examples are shown in Fig. 7.1. The normalized emittance is plotted for different planes and different fills.

This unphysical behavior was observed during several ramps measured with wire scanners. The measured emittances decreased by different amounts for the different beams and planes. In addition, the shrinkage did not occur at the same point during the ramp. No correlation between energy, plane and emittance decrease was found.

Incomplete understanding of the optics as explanation for the shrinking emittances can be excluded. The beta functions were measured specifically. Dispersion was found to be small.

Comparison with Emittance from Experiments

Another indication of the wire scanner issue is the different emittance measurement results from wire scanners and luminosity, luminous region or the LHCb SMOG experiment. During many low intensity test fills the different emittance measurement methods could be compared.

Table 7.1 gives an example of measurements done at the start of collisions for a low intensity fill, Fill 3217. Emittance values are obtained from wire scans and ATLAS and CMS luminosity. They are compared to wire scans at injection. There is a

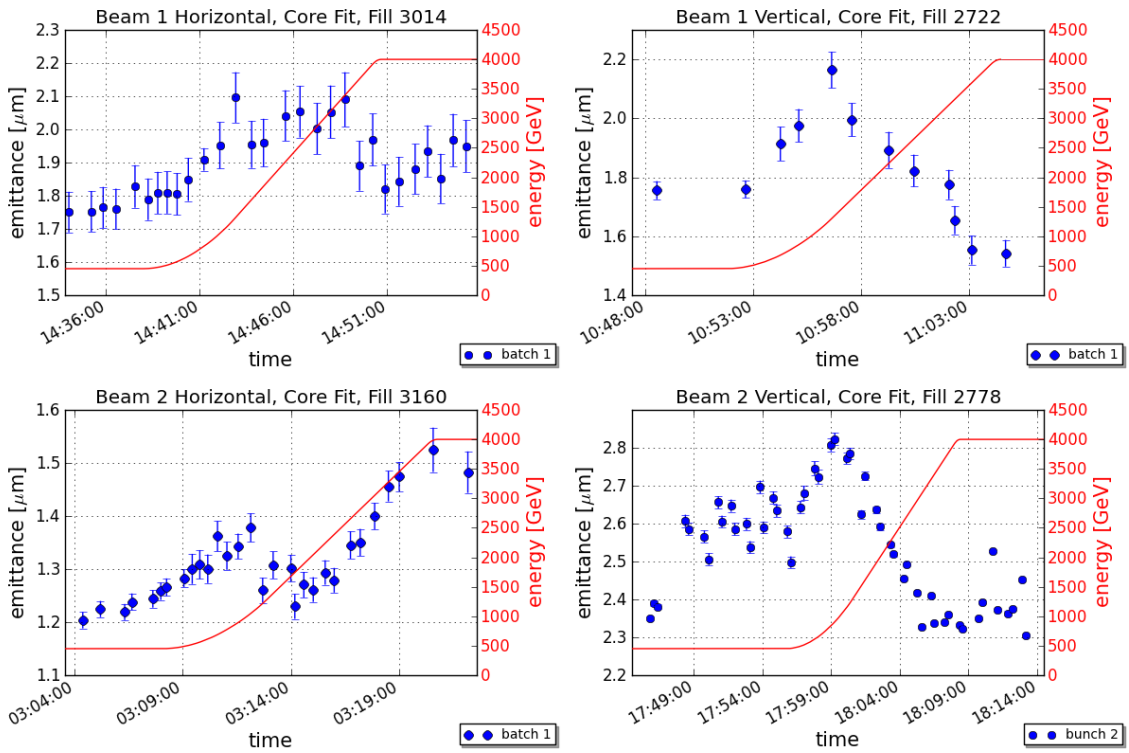

Figure 7.1.: Shrinking emittance during the ramp for different planes and fills. The emittance decreases by different amounts and at different energies. Plots of Fill 3014 and Fill 3160 depict the average emittance of six 50 ns bunches. For Fill 2722 the average emittance of 12 50 ns bunches is shown. During Fill 2778 only individual bunches were ramped.

large discrepancy between the emittance from luminosity and emittance measured with wire scanners. The difference between wire scanner results and emittance from luminosity for Fill 3217 is about 30 % as seen in Table 7.1. There is also a significant disagreement between the ATLAS and CMS emittances for this fill. The errors are, however, large.

During the third machine development period a fill was dedicated to not only compare wire scans with data from luminosity and luminous region but also with SMOG data. For Fill 3160 the emittances were measured with wire scanners and SMOG for all planes, for colliding bunches and also non-colliding bunches. Figure 7.2 summarizes the bunch emittances for two different timestamps.

To calculate emittances from wire scanner measurements the measured beta function from k-modulation for squeezed optics was used. For the emittance from experiments the nominal β^* was taken into account. Beam-beam effects slightly change the optics during collision, but this effect is small and can be neglected [47]. The largest discrepancy between the measurement methods can be found in the vertical plane of beam 1. In general, the wire scanner emittances are smaller than the SMOG emittances.

	ε_{conv} [μm]	growth [μm]
wire scan at injection	1.43 ± 0.03	
wire scan at peak lumi	1.88 ± 0.06	0.45 ± 0.08
ATLAS	2.36 ± 0.35	0.93 ± 0.38
CMS	2.63 ± 0.39	1.20 ± 0.42

Table 7.1.: Emittance at peak luminosity calculated from ATLAS and CMS luminosity compared to the convoluted emittance from wire scanners for Fill 3217 with six colliding bunches in ATLAS and CMS. The absolute average growth during the LHC cycle is given.

The disagreement between the emittances obtained from wire scans and experiments led to investigations of saturation effects of the wire scanner photomultipliers. The results will be discussed in the next section.

7.1. Accuracy of the Wire Scanners

The comparison of various emittance measurement methods indicates that the wire scanners measure too small emittances. First, a bump calibration of the wire scanners in the LHC revealed that the wire scanners overestimate the profile position by about 2 to 4 % for beam 1 and 2 to 3 % for beam 2. Hence the beam size could be slightly underestimated, but the large discrepancy between the emittance measurement methods cannot be fully explained with this result. Therefore the influence of the wire scanner settings on the resulting beam size was examined.

Filter settings and voltage are not automatically chosen by the front end software as a function of intensity and energy, but have to be set by the user. Wrong settings can lead to saturated profiles due to saturation of the read out electronics or saturation of the photomultiplier. Both induce wrong beam size measurements. Saturation of the ADC (Analogue to Digital Converter) is easily detectable, see Fig. 7.3, and avoidable. The maximum accepted profile amplitude is 7500 a.u.. Profiles with higher amplitudes are not taken into account in the off-line fitting routine.

To spot photomultiplier (PM) saturation is less obvious. The front end electronics do not return any PM status signals. This will be provided by an upgraded version of the wire scanner system after the first long maintenance period in 2013/14. Currently, the optimum working range has to be found through measurement campaigns. An example of such a measurement for the Booster is given in the following.

While wire scanners, for example in the Booster, have a predefined saturation curve, for LHC wire scanners there is no PM saturation curve available. Figure 7.4 shows beam sizes of the LHC beam measured with a Booster wire scanner as a function of the wire scanner voltage. In this case, a good wire scanner working point

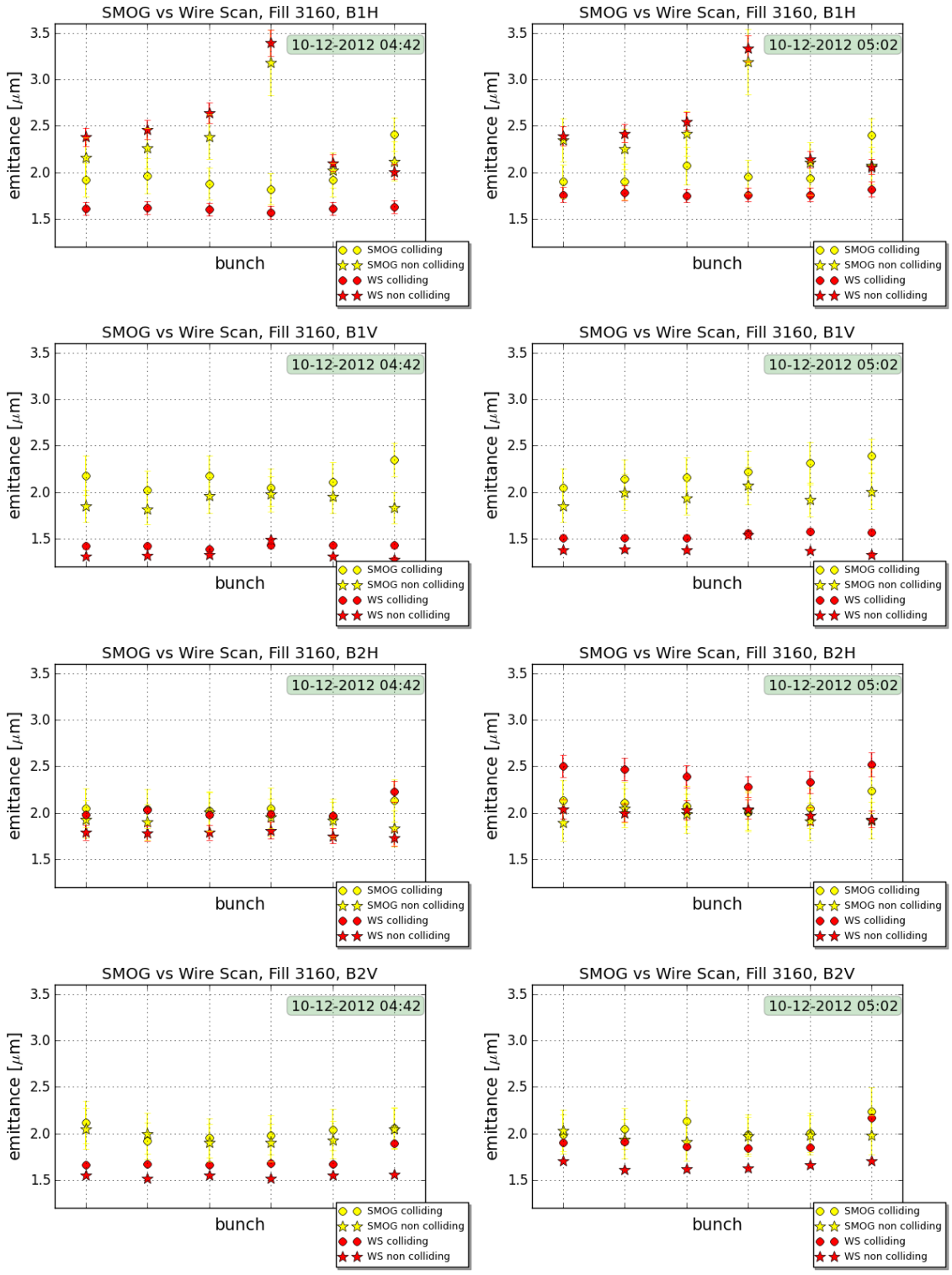

Figure 7.2.: Comparison of emittance from SMOG data and wire scans. Bunch emittances for Fill 3160, with six colliding bunches in ATLAS and CMS and six non-colliding bunches for two different timestamps and wire scanner settings. Left plots: measurement at 10-12-2012 04:42. Right plots: measurements at 10-12-2012 05:02.

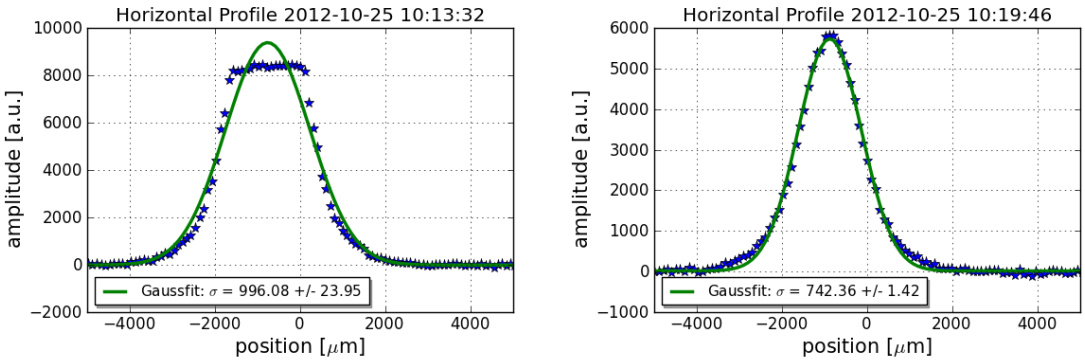

Figure 7.3.: ADC saturated profile (left) and non-saturated profile (right) of the same beam measured with wire scanner during one measurement period. Both profiles are fitted with a Gaussian. The obtained beam sizes, given in the legend, are different.

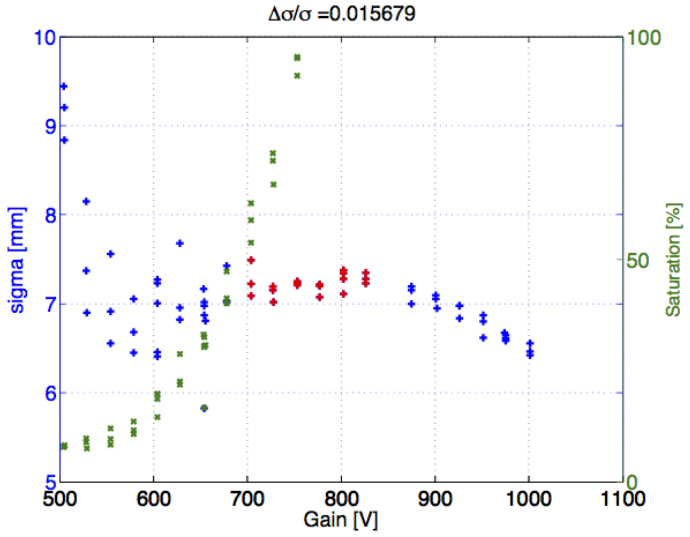

Figure 7.4.: Example of a photomultiplier saturation curve of a wire scanner in the Booster [48]. The beam size is plotted as a function of the wire scanner voltage. The saturation curve given by the wire scanner is shown in green. Beam sizes measured with a good wire scanner working point are red. Beam sizes measured with higher or lower wire scanner gain than optimal are blue. *Courtesy G. Sterbini, CERN, Geneva, Switzerland.*

was found between gains of 700 V to 900 V (red) [48]. If the gain is reduced too much, below 700 V, noise dominates. On the other hand, if the voltage is increased above 900 V, the photomultipliers are saturating and the resulting beam size is too small. The saturation curve given by the wire scanner (green) overestimates the saturation. A good working point is between saturation levels of 65 to 120 %. For optimum PM settings the maximum gain of the PM in the linear region of each amplification stage should be used. In reality, in order to allocate some margin for

the pulse-to-pulse jitter of the beam current, a wire scanner gain between 800 V and 850 V for LHC beams in the Booster is advised.

The technical specifications of the LHC wire scanners advise a gain above 900 V [49]. In the LHC a 20 to 10 % transmission filter and a gain of about 1000 V were assumed to be the optimum wire scanner settings for nominal intensities at injection energy of 450 GeV. Usually the transmission was reduced during the ramp, to avoid ADC saturated profiles, and the PM voltage was lowered in several steps such that at flattop energy of 4 TeV one would typically arrive with settings of 2 to 1 % transmission and about 900 V PM voltage.

After discovering the puzzling results of the measurements discussed in the previous section, investigations were started in the LHC with the aim to define the optimum settings for the LHC wire scanners at all energies, like introduced in the Booster example. For this purpose the beam size was measured with the wire scanners for different settings of PM voltage and transmission filter.

Figure 7.5 shows an example of the measurements at injection and flattop energy for beam 1 horizontal. They were repeated for all beams. In the left plot the constant linear emittance growth at 450 GeV is due to IBS, but clearly gain and filter changes have a significant influence on the emittance. The right plot shows the same dependence of the measured emittance on wire scanner settings. All profiles are Gaussian and not ADC saturated. PM saturation is suspected for certain settings.

Unfortunately, the situation is less clear than in the case of the Booster wire scanners and the optimum settings for LHC wire scanners could not be derived. Including the additional uncertainty on the beam size measurement from the dependence on the wire scanner settings, the error on the emittance measurement is therefore at injection up to 0.5 μm instead of approximately 0.1 μm (only coming from difference between in and out scan, β error and fitting error) and at flattop

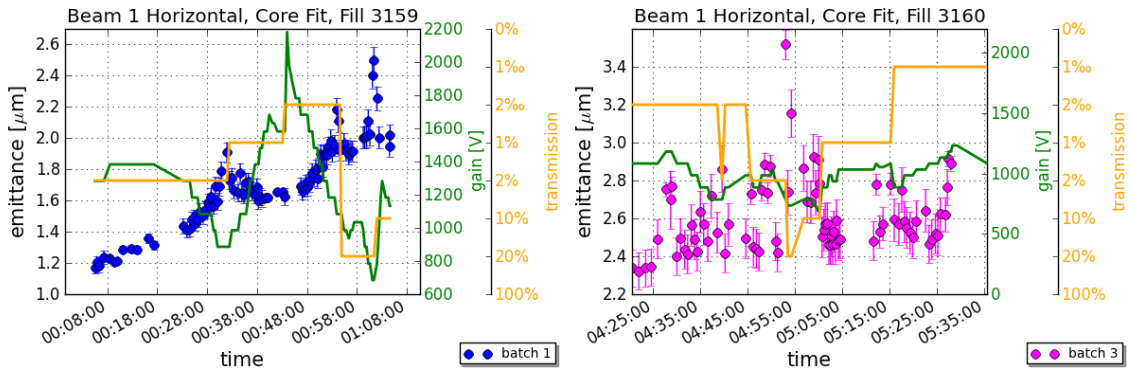

Figure 7.5.: Influence of wire scanner settings for beam 1 horizontal at injection energy of 450 GeV, Fill 3159 (left), and flattop energy of 4 TeV, Fill 3160 (right). Average emittance of six bunches per batch measured with wire scanner with variations of wire scanner filter and voltage.

up to 0.8 μm instead of about 0.1 μm. Because of the fact that the SPS measures similar emittance values at extraction as the LHC at injection, the settings of the wire scanners at 450 GeV are probably in the optimum range. The growth through the ramp is, however, assumable larger. The emittance from luminosity still gives the best indication.

8. Outlook: Future LHC Beams

The remarkable achievements during the first LHC run were partly due to the choice of running with 50 ns beams, which could be produced with a brightness beyond LHC design values. The nominal 25 ns beam with a bunch intensity of 1.15×10^{11} ppb and an emittance of 3.5 μm has a brightness a factor three below the 2012 LHC physics beams.

The LHC injectors have been developing new types of high brightness beams with novel ideas for RF bunch splitting and batch compression in the PS. By reducing the total splitting factor in the PS and injecting 4 + 4 bunches from the Booster, beams with very low emittance (about 1 μm) and bunch intensities of 1 to 1.5×10^{11} ppb can be produced [50]. The proposed parameters for the high brightness 25 ns batch compression beam result in similar brightness values as the 2012 50 ns physics beams.

The 2011 emittance preservation studies indicated constant absolute emittance growth in the LHC independent of initial emittance and bunch intensities. A constant emittance growth would compromise the potential improvement given by the proposed low emittance beams.

Figure 8.1 shows the emittance growth through the LHC cycle as function of bunch intensity for 2012 measurements. From 1.1 to 1.5×10^{11} ppb the growth is indeed constant, about 0.7 μm. For bunch intensities beyond 1.5×10^{11} ppb the growth increases with bunch intensity. It has not been investigated whether the additional growth for higher bunch intensities already occurs during the ramp or is mainly due to instabilities at the end of the squeeze or during the beam mode "adjust".

Two test fills, Fill 2994 and 3372, have been carried out with the new high brightness beams. For Fill 2994 the eight Booster bunches were RF manipulated with two bunch splittings to extract 32 low emittance bunches to the LHC. The bunch intensity was 1.1×10^{11} ppb and the initial emittance about 1 μm. For Fill 3372, the Batch Compression, Merging and Splitting (BCMS) scheme [50] was used resulting in 24 high brightness bunches with a bunch intensity of 1.5×10^{11} ppb and an initial emittance of about 1 μm. The blow-up through the cycle for these two fills is also indicated in Fig. 8.1 (green stars). Whereas for Fill 2994 the overall growth is similar as surrounding points in the plot, the growth for Fill 3372 is below 0.5 μm. Fill 3372 fell in a period where the higher damper gain during the ramp was already operational, which could be an explanation for the lower growth.

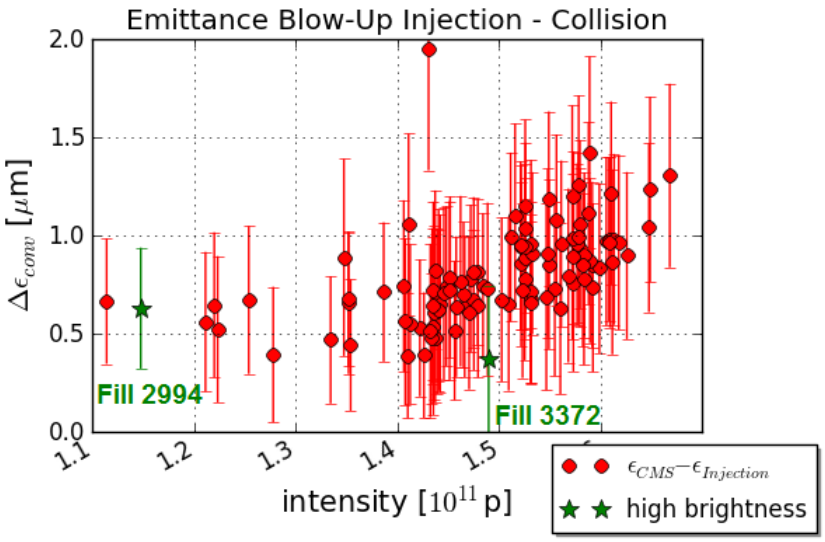

Figure 8.1.: Bunch intensity versus emittance growth in 2012. Emittance growth from injection to collision as a function of bunch intensity at collision. $\Delta\varepsilon$ is calculated from the emittance from CMS peak luminosity and convoluted average emittance of the first 144 bunch batch measured with wire scanners at LHC injection. The high brightness fills (green stars) are highlighted. The intensity is measured with the Fast Beam Current Transformer (FBCT). The last fills of the 2012 proton run are not included due to a broken wire.

Discussion

The proposed parameters for the high brightness 25 ns batch compression beam [50] and the maximum parameters for the LHC Injector Upgrade for the LHC High Luminosity era [51] give a similar brightness as the 2012 50 ns physics beams. The IBS growth rates are therefore expected to be similar to what was observed in the LHC in 2011 and 2012. RF batch-by-batch blow-up could be a solution.

As already suggested from 2011 emittance preservation studies, 2012 studies also show that a good fraction of the observed growth (about 0.7 μm in 2012) is independent of initial emittance and bunch intensity. This effect, if not cured, could spoil the performance of the proposed 1 μm beams obtained by PS batch compression. The largest contribution of the growth occurs during the ramp in the horizontal plane. The origin of this blow-up is not clear. The impact of higher damper gain during the ramp requires further investigation.

9. Summary and Conclusion

The first three-year LHC running period was a major success. With the high brightness 50 ns beams a peak luminosity of 7.7×10^{33} cm^{-2}s^{-1} could be achieved, and in total 29.2 fb^{-1} of integrated luminosity were recorded in ATLAS and CMS. This is a statement for the excellent performance of the LHC and its injector.

Nevertheless, 30 to 40 % of the potential performance of the 50 ns physics beams was lost between injection into the LHC and bringing the beams into collision, mainly due to emittance blow-up. The injectors prepared beams with a bunch intensity of up to 1.7×10^{11} ppb and a normalized emittance as small as 1.5 μm. At collision the beams arrived with about 2.4 μm emittance.

For this thesis the emittance blow-up during the different phases of the LHC cycle was studied, the origins investigated and possible cures tested.

Injection into the LHC does not cause any measurable emittance growth. During the 450 GeV injection plateau the emittances grow slowly due to IBS and 50 Hz noise. Both sources cause the beam to increase mainly in the horizontal plane. The growth rates at injection are about 10 % in 20 minutes. In the presence of coupling significant growth can also occur in the vertical plane.

Longitudinal RF batch-by-batch blow-up as a solution for IBS emittance growth was tested and put into operation towards the end of the 2012 run. The improvement on the difference between specific luminosity of the first batch with respect to the last, and therefore less afflicted by IBS, batch was insignificant. More tests will need to be performed during the second LHC run.

Most of the emittance growth occurs during the ramp. In 2012 the blow-up was mainly observed in the horizontal plane and it was stronger for beam 2 than for beam 1. The emittances in the horizontal plane increased by about 0.2 μm for beam 1 and about 0.3 μm for beam 2. The blow-up mechanism has not yet been identified.

Results from physics fills towards the end of the 2012 proton run showed that higher damper gain during the ramp might reduce the blow-up. The specific bunch-by-bunch luminosity of most fills during the period where higher ramp damper gain was operational, was larger than before.

Towards the end of 2012 occasionally emittance growth was measured at the end the β^* squeeze. The blow-up might have been introduced with the different operational running conditions during that period with inverted LHC octupole polarity,

high chromaticity and high bunch intensity.

Measurements indicate that the emittance blow-up through the LHC cycle is independent of the initial emittance and bunch intensity for bunch intensities up to 1.5×10^{11} ppb and is about 0.7 μm for the 2012 4 TeV cycle. It increases with bunch intensity for bunch intensities larger than 1.5×10^{11} ppb. This result is discouraging for the new very low emittance and high brightness beams from the PS with emittances of about 1 μm. Origin and cures for the blow-up must be found in the LHC to exploit the full potential of these new beams, which were tested for the first time in the LHC in 2012.

In order to understand emittance growth in the LHC, more reliable transverse profile measurement systems are needed. The optimum settings for the LHC wire scanners could unfortunately not be established in 2012, resulting in large uncertainties of about 0.8 μm on the beam size measured at flattop energy of 4 TeV. Only emittance data via luminosity measurement or beam-gas imaging with the LHCb SMOG experiment gives a good indication of the emittance at the end of the LHC cycle. More work is needed before and at the beginning of the second LHC run to establish reliable emittance measurements with the LHC transverse profile monitor systems. The emphasis should be put on passive instruments, which can measure high intensity beams.

Bibliography

[1] O. S. Brüning, P. Collier, P. Lebrun, *et al.*, *LHC Design Report - The LHC Main Ring*, vol. 1. CERN, 2004.

[2] European Organization for Nuclear Research. http://home.web.cern.ch/.

[3] J. Incandela, F. Gianotti, and R. Heuer, "Latest Update in the Search for the Higgs." CERN Scientific Seminar, (Geneva, Switzerland), July 2012.

[4] M. Benedikt, P. Collier, V. Mertens, *et al.*, *LHC Design Report - The LHC Injector Chain*, vol. 3. CERN, 2004.

[5] G. Arduini, H. Bartosik, G. Iadarola, *et al.*, "Electron Cloud and Scrubbing in the LHC," in *Proceedings of the 2012 Evian Workshop on LHC Beam Operation*, (Evian, France), December 2012. (forthcoming).

[6] K. Wille, *The Physics of Particle Accelerators - An Introduction*. Oxford University Press, 2000.

[7] H. Wiedemann, *Particle Accelerator Physics*. Springer-Verlag, 2007.

[8] J. Rossbach and P. Schmüser, "Basic Course on Accelerator Optics," in *CERN European Organisation for Nuclear Research-Reports*, (Geneva, Switzerland), CERN, 1994.

[9] D. A. Edwards and M. J. Syphers, *An Introduction to the Physics of High Energy Accelerators*. John Wiley & Sons, Inc., 1993.

[10] V. Kain, *Machine Protection and Beam Quality during the LHC Injection Process*. PhD thesis, Technische Universität Wien/CERN, October 2005.

[11] D. Boussard, W. Höfle, T. Linnecar, *et al.*, "The LHC Transverse Damper (ADT) Performance Specification," *SL-Note-99-055 HRF*, March 2000.

[12] V. Kain, W. Bartmann, C. Bracco, *et al.*, "Emittance Preservation at Injection into LHC," in *Proceedings of HB2010*, (Morschach, Switzerland), pp. 188–192, September 2010.

[13] W. Höfle, G. Kotzian, M. Schokker, *et al.*, "LHC Damper Beam Commissioning in 2010," in *Proceedings of IPAC2011*, (San Sebastian, Spain), pp. 505–507, September 2011.

[14] D. Valuch, F. Dubouchet, W. Höfle, *et al.*, "What you get - Transverse Damper System," in *Proceedings of the 2012 Evian Workshop on LHC Beam Operation*, (Evian, France), December 2012. (forthcoming).

[15] A. Piwinski, "Intra-Beam Scattering," in *9. International Conference on High Energy Accelerators*, (Stanford, California, USA), pp. 405–409, 1974.

[16] A. Dougan, "Lecture 18: Beam Loss and Beam Emittance Growth," in *USPAS 2002: Introduction to Accelerator Physics*, (Long Beach, California, USA), January 2002.

[17] A. Wolski, "Space Charge, Intrabeam Scattering and Touschek Effects," in *Fourth International Accelerator School for Linear Colliders*, (Beijing, China), September 2009.

[18] R. Alemany, M. Lamont, and S. Page, "Functional Specification LHC Modes," *CERN-LHC-OP-ES-0005*, November 2007.

[19] R. Steinhagen, "Real-Time Beam Control at the LHC," in *Proceedings of 2011 Particle Accelerator Conferences*, (New York, New York, USA), pp. 1399–1403, March 2011.

[20] O. Brüning, H. Burkhardt, and S. Myers, "The Large Hadron Collider," *Progress in Particle and Nuclear Physics 67*, vol. 67, no. 3, pp. 705–734, 2012.

[21] M. Kuhn, G. Arduini, J.-F. Comblin, *et al.*, "Brightness Evolution for LHC Beams during the 2012 Run," in *Proceedings of HB2012*, (Beijing, China), September 2012.

[22] V. Kain, G. Arduini, B. Goddard, *et al.*, "Emittance Preservation in the LHC," in *Proceedings of the 2011 Evian Workshop on LHC Beam Operation*, (Evian, France), pp. 85–92, December 2011.

[23] M. Kuhn, G. Arduini, B. Holzer, *et al.*, "Causes and Solutions for Emittance Blow-Up during the LHC Cycle," in *Proceedings of IPAC2012*, (New Orleans, Louisiana, USA), pp. 160–162, May 2012.

[24] S. Bart Pedersen, A. Boccardi, E. Bravin, *et al.*, "Profile Monitors, Injection Matching Monitor and Synchrotron Light Monitors," in *Proceedings of the 2010 Evian Workshop on LHC Beam Operation*, (Evian, France), pp. 67–70, January 2010.

[25] J. Bosser and C. Bovet, "Wire Scanners for LHC," *CERN-LHC-Project-note-108*, September 1997.

[26] M. Sapinski, "Beam Interaction with Thin Materials: Heat Deposition, Cooling Phenomena and Damage Limits," in *2012 Beam Instrumentation Workshop*, (Newport News, Virginia, USA), April 2012.

[27] A. S. Fisher, A. Goldblatt, and T. Lefevre, "The LHC Synchrotron-Light Monitors," in *Proceedings of DIPAC2009*, (Basel, Switzerland), pp. 164–166, May 2009.

[28] A. Jeff, A. Boccardi, E. Bravin, *et al.*, "First Results of the LHC Longitudinal Density Monitor," *Nuclear Instruments and Methods in Physics Research Section A: Accelerators, Spectrometers, Detectors and Associated Equipment*, vol. 659, no. 1, pp. 549–556, 2011.

[29] F. Roncarolo, S. Bart Pedersen, E. Bravin, *et al.*, "Can We Get Reliable Online Measurements of the Transverse Emittance?," in *Proceedings of the Second 2010 Evian Workshop on LHC Beam Operation*, (Evian, France), pp. 119–123, December 2010.

[30] C. Fischer, J. Koopman, D. Kramer, *et al.*, "Design and Tests of a New Rest Gas Ionisation Profile Monitor Installed in the SPS as a Prototype for the LHC," *AIP Conference Proceedings*, vol. 732, pp. 133–140, May 2004.

[31] H. H. Refsum, *Design, Simulation and Testing of a 2D Electron Source Based Calibrating System for a Proton Beam Ionisation Profile Monitor*. PhD thesis, NTNU Trondheim/CERN, July 2004.

[32] M. Sapinski, "Status of Beam Gas Ionization Monitor (BGI)." Talk at the CERN Machine Studies Working Group (MSWG) Meeting, (Geneva, Switzerland), September 2012.

[33] A. Langner, R. Calaga, R. Miyamoto, *et al.*, "Optics Measurement in the LHC Close to the Half Integer Tune Resonance," *CERN-ATS-Note-2011-095 TECH*, December 2011.

[34] W. Herr and B. Muratori, "Concept of Luminosity," in *CAS - CERN Accelerator School: Intermediate Course on Accelerator Physics*, (Zeuthen, Germany), DESY, September 2003.

[35] M. Ferro-Luzzi, "Proposal for an Absolute Luminosity Determination in Colliding Beam Experiments Using Vertex Detection of Beam-Gas Interactions," *Nuclear Instruments and Methods in Physics Research Section A: Accelerators,*

Spectrometers, Detectors and Associated Equipment, vol. 553, no. 3, pp. 388–399, 2005.

[36] P. Hopchev, "LHCb Beam-Gas Imaging Results," in *LHC Lumi Days: LHC Workshop on LHC Luminosity Calibration*, (Geneva, Switzerland), pp. 64–68, CERN, January 2011.

[37] M. Kuhn, G. Arduini, J. Emery, *et al.*, "LHC Emittance Preservation during the 2012 Run," in *Proceedings of the 2012 Evian Workshop on LHC Beam Operation*, (Evian, France), December 2012. (forthcoming).

[38] H. Bartosik, G. Arduini, and Y. Papaphilippou, "Optics Considerations for Lowering Transition Energy in the SPS," in *Proceedings of IPAC2011*, (San Sebastian, Spain), pp. 619–621, September 2011.

[39] G. Papotti, "Luminosity Analysis," in *Proceedings of the Chamonix 2011 workshop on LHC Performance*, (Chamonix, France), pp. 266–269, January 2011.

[40] L. Drosdal, V. Kain, W. Bartmann, *et al.*, "Sources and Solutions for LHC Transfer Line Stability Issues," in *Proceedings of IPAC2012*, (New Orleans, Louisiana, USA), pp. 2047–2049, May 2012.

[41] V. Kain, G. Arduini, B. Goddard, *et al.*, "Emittance Preservation in the LHC," in *Proceedings of the Chamonix 2012 workshop on LHC Performance*, (Chamonix, France), pp. 81–88, February 2012.

[42] T. Mastoridis, P. Baudrenghien, A. Butterworth, *et al.*, "Batch By Batch Longitudinal Emittance Blowup MD," *CERN ATS-Note-2012-050 MD*, June 2012.

[43] T. Lefevre, M. Andersen, C. Boccard, *et al.*, "What you get - Orbit and Tune Measurement and Feedback," in *Proceedings of the 2012 Evian Workshop on LHC Beam Operation*, (Evian, France), December 2012. (forthcoming).

[44] X. Buffat, W. Herr, M. Lamont, *et al.*, "Squeeze with Colliding Beams," in *Proceedings of the 2012 Evian Workshop on LHC Beam Operation*, (Evian, France), December 2012. (forthcoming).

[45] T. Pieloni, X. Buffat, S. White, *et al.*, "Beam Stability with Colliding Beams at 6.5 TeV," in *Proceedings of the 2012 Evian Workshop on LHC Beam Operation*, (Evian, France), December 2012. (forthcoming).

[46] E. Metral, G. Arduini, R. Assmann, *et al.*, "Review of the Instabilities Observed during the 2012 Run and Actions Taken," in *Proceedings of the 2012 Evian Workshop on LHC Beam Operation*, (Evian, France), December 2012. (forthcoming).

[47] W. Herr, "Observations of Beam-Beam Effects in the LHC in 2011," in *Proceedings of the Chamonix 2012 workshop on LHC Performance*, (Chamonix, France), pp. 99–104, February 2012.

[48] G. Sterbini, B. Mikulec, and V. Raginel, "Calibration Curves for the WS at PSB." Talk at the CERN Emittance Meeting, (Geneva, Switzerland), September 2012.

[49] A. Guerrero, "Saturation in LHC WS PM." Talk at the CERN Emittance Meeting, (Geneva, Switzerland), February 2013.

[50] H. Damerau, H. Bartosik, C. Carli, *et al.*, "Performance Potential of the Injectors after LS1," in *Proceedings of the Chamonix 2012 workshop on LHC Performance*, (Chamonix, France), pp. 268–275, February 2012.

[51] B. Goddard, H. Bartosik, C. Bracco, *et al.*, "Can the Proton Injectors Meet the HL-LHC Requirements after LS2?," in *Proceedings of the Chamonix 2012 workshop on LHC Performance*, (Chamonix, France), pp. 325–331, February 2012.

Appendix A

Deduction of the Luminosity Formula

As derived in section 5.3 the luminosity can be written as

$$L = 2N_1N_2f_{rev}n_b \cdot \int\int\int\int_{-\infty}^{\infty} \rho_{1x}(x)\rho_{1y}(y)\rho_{1s}(s-s_0)\rho_{2x}(x)\rho_{2y}(y)\rho_{2s}(s+s_0)dxdydsds_0. \tag{A.0.1}$$

The integrals are solved for Gaussian beam distribution functions:

$$\rho_{iu}(u) = \frac{1}{\sqrt{2\pi}\sigma_u} e^{-\frac{u^2}{2\sigma_u^2}}, \tag{A.0.2}$$

$$\rho_s(s \pm s_0) = \frac{1}{\sqrt{2\pi}\sigma_s} e^{-\frac{(s\pm s_0)^2}{2\sigma_s^2}}, \tag{A.0.3}$$

with i = 1,2 and u = x,y. Then the luminosity yields

$$L = \frac{2N_1N_2f_{rev}n_b}{(2\pi)^3\sigma_{1x}\sigma_{2x}\sigma_{1y}\sigma_{2y}\sigma_s^2} \int\int\int\int_{-\infty}^{\infty} e^{-\frac{x^2}{2\sigma_{1x}^2}} e^{-\frac{x^2}{2\sigma_{2x}^2}} e^{-\frac{y^2}{2\sigma_{1y}^2}} e^{-\frac{y^2}{2\sigma_{2y}^2}} e^{-\frac{(s-s_0)^2}{2\sigma_s^2}} e^{-\frac{(s+s_0)^2}{2\sigma_s^2}} dxdydsds_0. \tag{A.0.4}$$

The general solution for this integration type is

$$\int_{-\infty}^{\infty} e^{-at^2} dt = \sqrt{\frac{\pi}{a}}. \tag{A.0.5}$$

By summarizing functions with same coordinates the integral transforms to

$$\int\int\int\int_{-\infty}^{\infty} e^{-\frac{x^2(\sigma_{1x}^2+\sigma_{2x}^2)}{2\sigma_{1x}^2\sigma_{2x}^2}} e^{-\frac{y^2(\sigma_{1y}^2+\sigma_{2y}^2)}{2\sigma_{1y}^2\sigma_{2y}^2}} e^{-\frac{(s^2+s_0^2)}{\sigma_s^2}} dxdxdsds_0 = \sqrt{\frac{2\pi\sigma_{1x}^2\sigma_{2x}^2}{\sigma_{1x}^2+\sigma_{2x}^2}} \sqrt{\frac{2\pi\sigma_{1y}^2\sigma_{2y}^2}{\sigma_{1y}^2+\sigma_{2y}^2}} \pi\sigma_s^2. \tag{A.0.6}$$

Inserting this solution into the luminosity equation (A.0.4) finally gives

$$L = \frac{f_{rev}n_b}{2\pi} \cdot \frac{N_1N_2}{\sqrt{\sigma_{1x}^2+\sigma_{2x}^2}\sqrt{\sigma_{1y}^2+\sigma_{2y}^2}}. \tag{A.0.7}$$

Appendix B

Emittance Growth during the LHC Injection Plateau

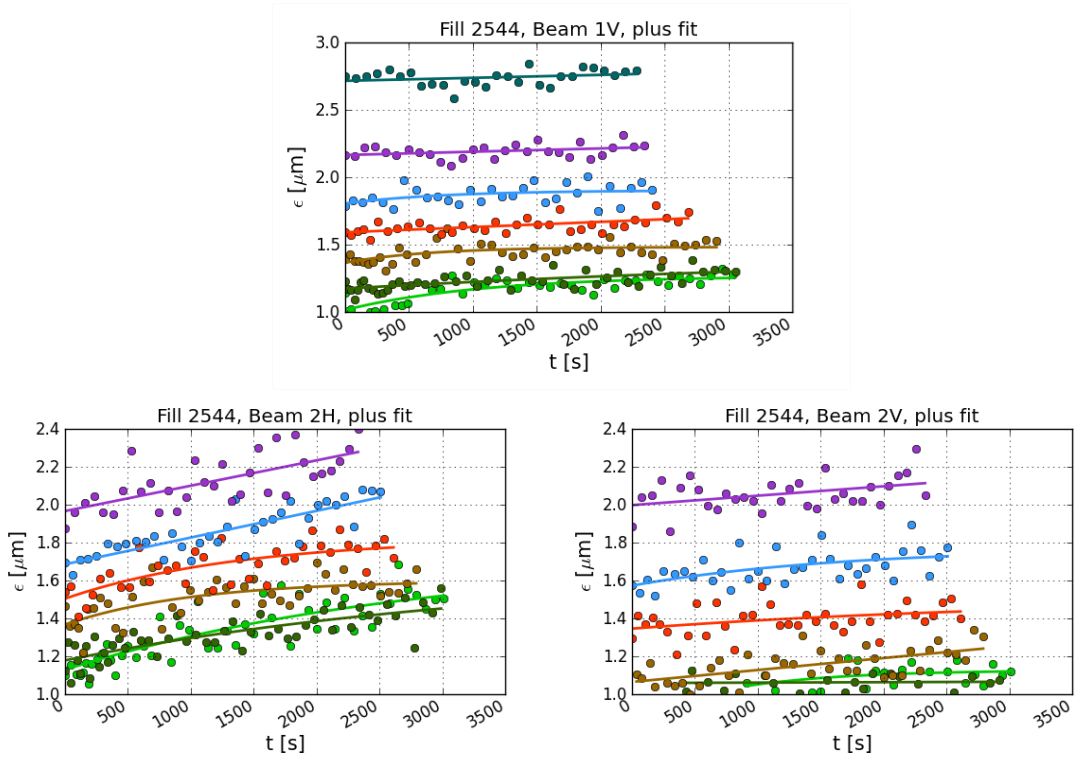

Figure B.1.: Horizontal emittance growth of beam 1 vertical and beam 2 horizontal and vertical, Fill 2544, at 450 GeV for individual bunches with different initial emittances and bunch intensities. The bunch with the smallest emittance had an intensity of about 0.8×10^{11} ppb, the bunch with the largest emittance had an intensity of about 1.9×10^{11} ppb. For emittances in between, the bunch intensity was increased in steps of 0.2×10^{11} ppb from the smallest to the largest value. Emittances of the seven bunches are measured with the BSRTs (dots). An exponential fit (lines) of the emittance blow-up is applied for every bunch.

Appendix C

IBS Simulations

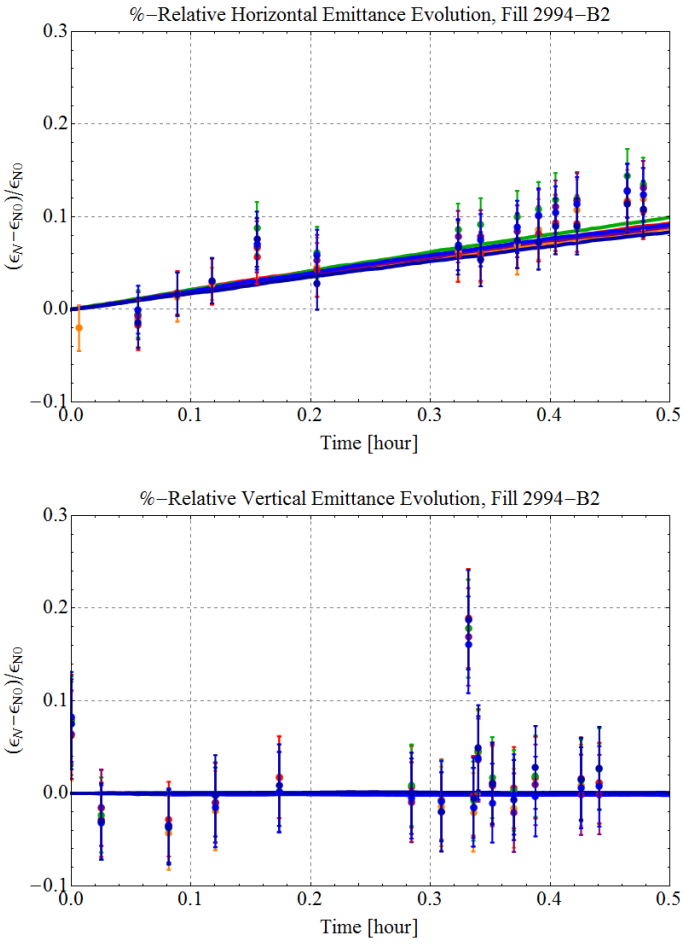

Figure C.1.: IBS simulations versus measurements for beam 2 horizontal and vertical. Relative emittance growth of beam 1 horizontal and vertical at the injection plateau for six 50 ns bunches with bunch intensities of about about 1.6×10^{11} ppb measured with wire scanner (dots) and compared to IBS simulations with same initial conditions (lines), Fill 2994. *Courtesy M. Schaumann, CERN, Geneva Switzerland.*

Appendix D

Effect of the Transverse Damper Gain at 450 GeV

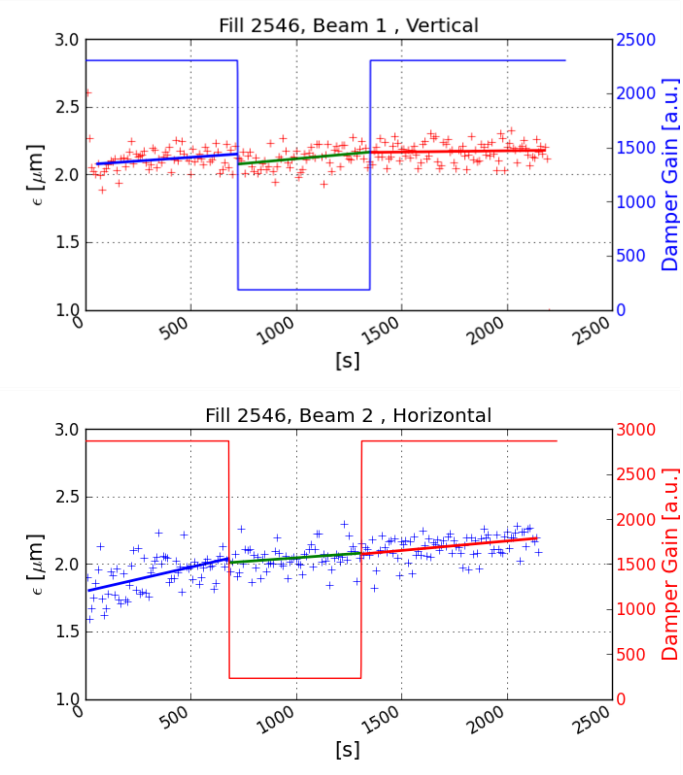

Figure D.1.: Transverse damper gain effect on emittance growth at 450 GeV, Fill 2546. BSRT measurements of beam 1 vertical (beam 2 horizontal) of one bunch with an intensity of about 1.4×10^{11} protons at injection energy with changing horizontal (vertical) ADT gain from nominal high injection gain to low ramp gain and back to high gain. The emittance growth in the different segments is fitted linearly.

Appendix E

Influence of 50 Hz Noise

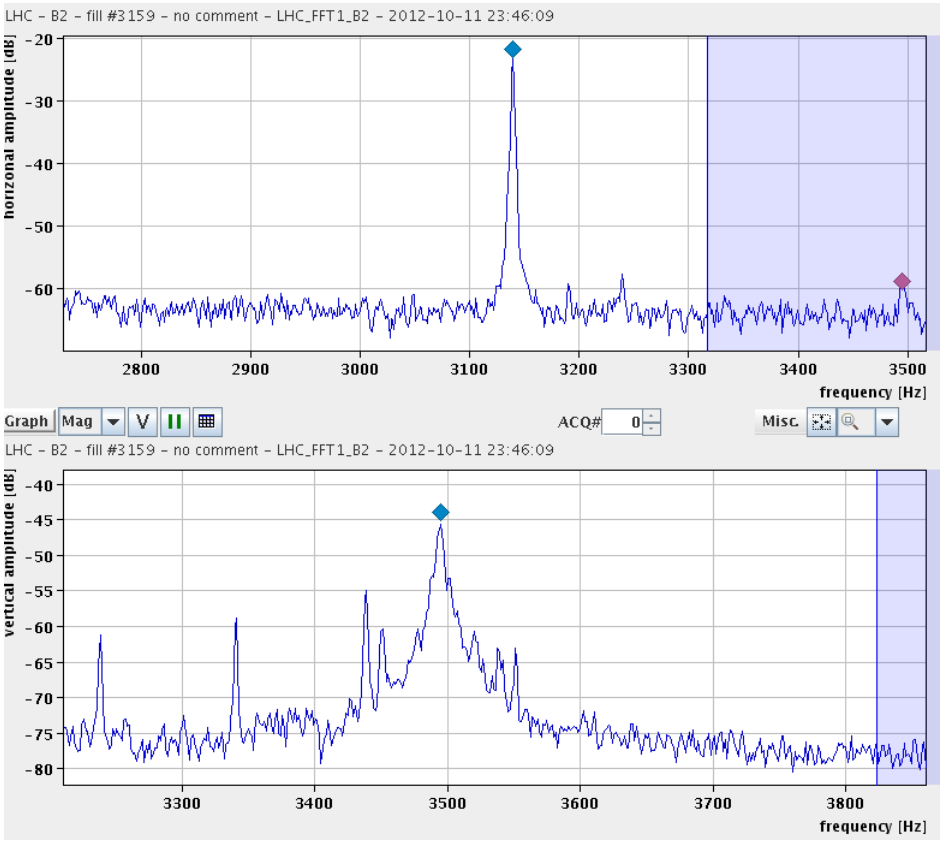

Figure E.1.: LHC beam spectrum for the nominal tune (0.28 in the horizontal plane) measured with the BBQ for beam 2 horizontal (top) and vertical (bottom). The frequency of the nominal tune is displayed (blue diamond). The horizontal tune sits at 3149 Hz and the signal has a large amplitude due to 50 Hz noise (approximately -20 dB).

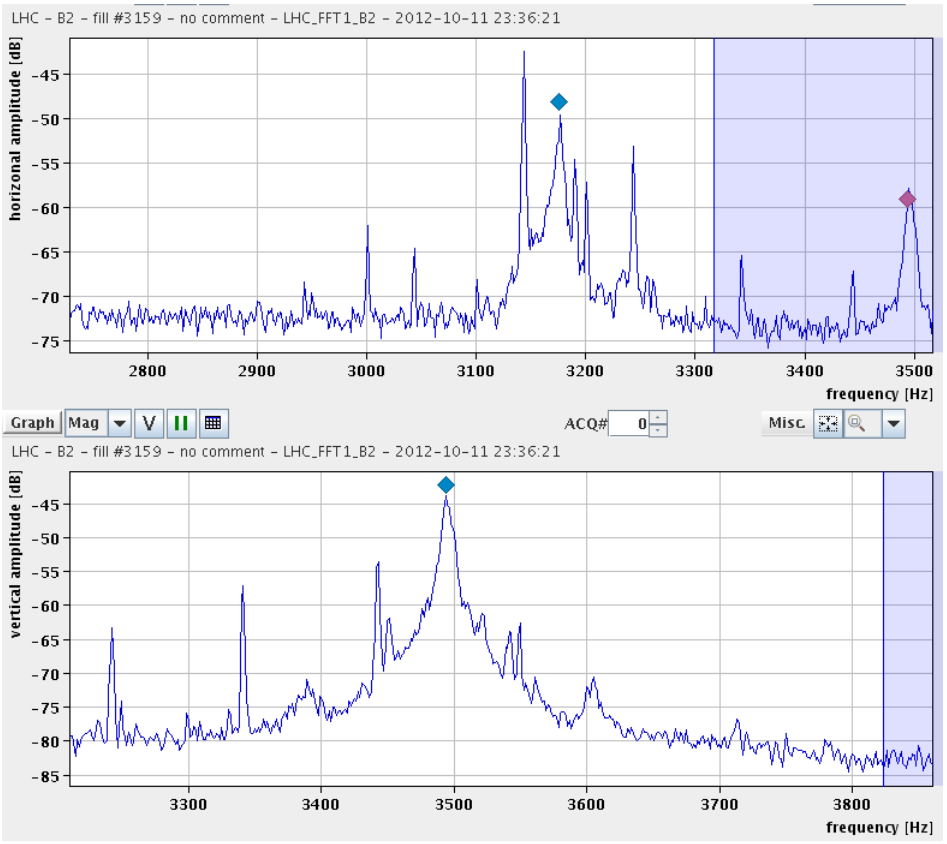

Figure E.2.: LHC beam spectrum for a different tune (0.283 in the horizontal plane) measured with the BBQ for beam 2 horizontal (top) and vertical (bottom). The frequency of the tune, 3182 Hz, is displayed (blue diamond). The beam is oscillating less, as the amplitude is reduced (approximately -50 dB).

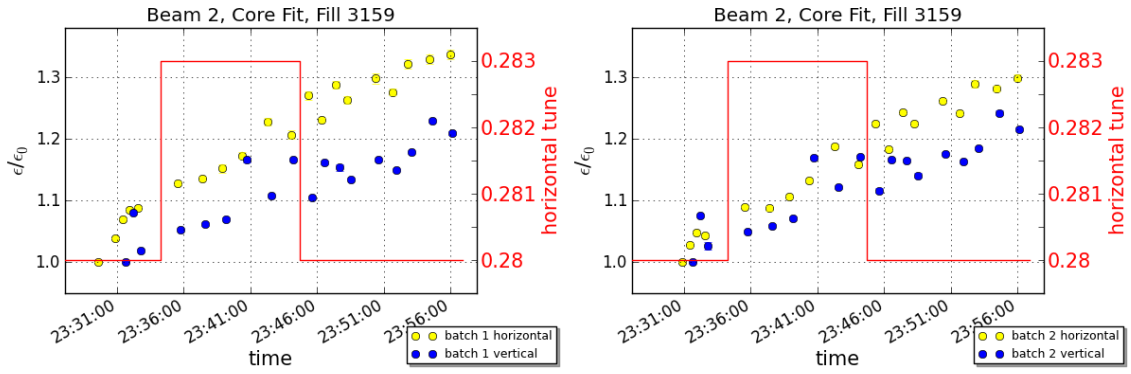

Figure E.3.: Emittance growth due to 50 Hz noise. Relative average emittance growth of 6 + 6 bunches with bunch intensities of 1.3 $\times$ 10^{11} ppb and 50 ns bunch spacing at injection energy for beam 2 horizontal and vertical measured with wire scanners, Fill 3159. ε_0 is the emittance at injection into the LHC. The horizontal tune is displayed. The left plot displays the results for batch 1 and the right plot for batch 2.

Appendix F

Effect of the Transverse Damper Gain during the Ramp

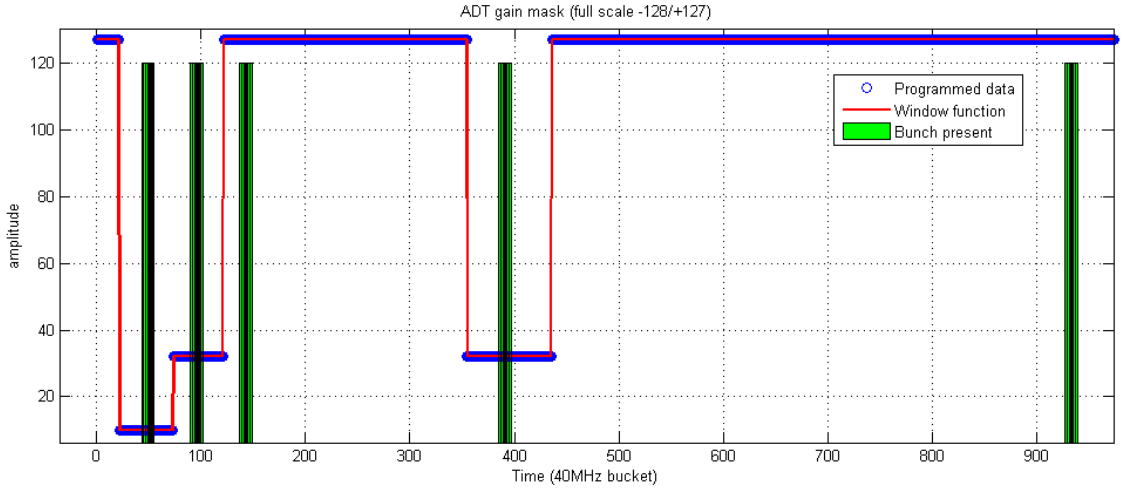

Figure F.1.: ADT ramp gain modulation for Fill 3160, beam 2. Batch number 4 was not injected. The function was applied before starting the ramp.

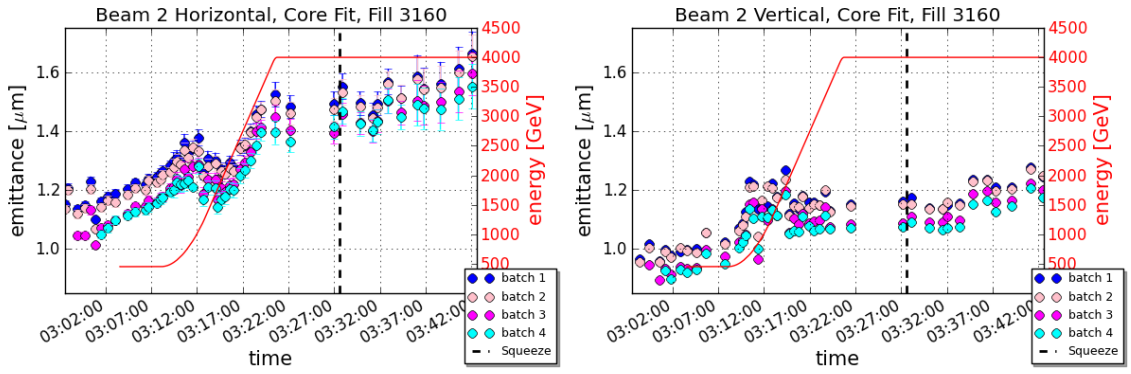

Figure F.2.: Ramp with different ADT gains. Average emittance of six bunches per batch through the ramp and the squeeze for beam 2 horizontal and vertical measured with wire scanners, Fill 3160. The bunches had different transverse damper gains at the start of the ramp, see Table 6.4.

Appendix G

The LHC Squeeze

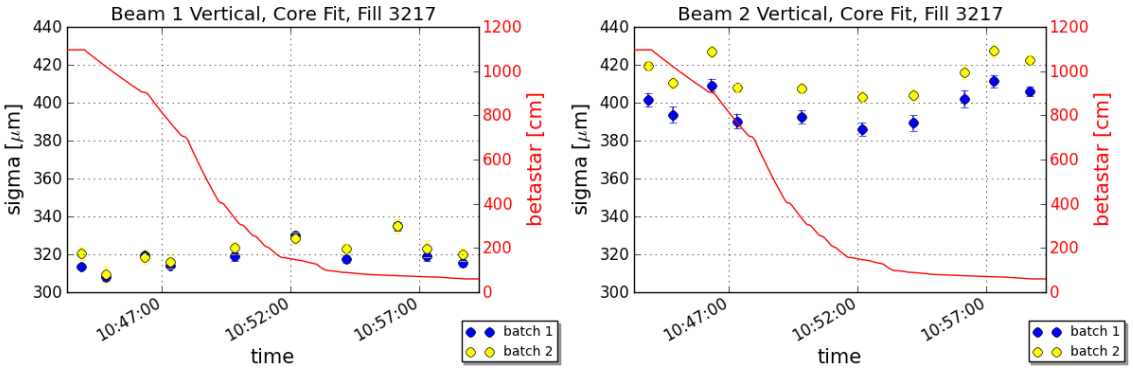

Figure G.1.: Wire scans during squeeze for beam 1 and beam 2 vertical. Transverse beam size evolution averaged for 6 + 6 bunches with bunch intensities of 1.6×10^{11} ppb and 50 ns bunch spacing, Fill 3217.

Erklärung

Hiermit bestätige ich, dass die vorliegende Arbeit von mir selbstständig verfasst wurde und ich keine anderen als die angegebenen Hilfsmittel, insbesondere keine im Quellenverzeichnis nicht benannte Internet-Quellen, benutzt habe und die Arbeit von mir vorher nicht einem anderen Prüfungsverfahren eingereicht wurde. Die eingereichte schriftliche Fassung entspricht der auf dem elektronischen Speichermedium. Ich bin damit einverstanden, dass die Masterarbeit veröffentlicht wird.

Genf, 12. März 2013